THE UNIVERSITY OF
SYDNEY

Ultrafast Mid-infrared Fibre Lasers

A thesis submitted in fulfilment of the requirements for the degree of

Doctor of Philosophy

by

Tomonori Hu

University of Sydney
Faculty of Science
Centre for Ultrahigh bandwidth Devices for Optical Systems
Institute of Photonics and Optical Science
School of Physics

12 August 2015

Abstract

Laser light has enabled the most important scientific discoveries and innovations, and research in new types of lasers still continues to do so. Mid-infrared light, which interacts strongly with naturally occurring molecules, holds many promises in sensing and medical technologies and their applications are now beginning to appear. This surging development will strongly benefit with the availability of field-usable, compact and robust sources of mid-infrared light. The fibre lasers have the extreme potential to achieve this, however their performance in terms of generating ultrafast pulses of mid-infrared light has not yet been demonstrated. Here we explore the potential fluoride fibre lasers have in the ultrafast pulsed regime. We have demonstrated this via the production of nanosecond, to picosecond, and finally femtosecond pulses from fluoride fibre lasers using a variety of methods. These demonstrations reveal that fluoride fibres lasers are strong candidates to be an ultrafast mid-infrared source, with applications ranging from frequency comb based molecular sensing to next generation laser scalpels.

Acknowledgements

I have spent a significant amount of my time and effort to produce the contents of this thesis. That being said, what is more important than this document are the lessons I have learnt, the countless mistakes I have made, and most importantly - the people who I have met. By no means could I have done this alone and I must dedicate the next few pages to those who have allowed me to improve as a scientist and as a person.

First and foremost I must mention Associate Professor Stuart Jackson and Professor Benjamin Eggleton who opened the door for me to begin my PhD. Although I will mention their technical expertise that contributed to this thesis later, I first would like to thank them both for accepting me in working with them. Despite having little to no experience in the field ended up devoting my time to, Stuart assured me that I could do this and took me on board as his PhD student. My relation with Professor Benjamin Eggleton goes back to my undergraduate time where his lectures inspired me to take a career in optics and photonics. His great success is reflected in the quality of research produced by his research group, the Centre for Ultrahigh bandwidth Devices for Optical Systems (CUDOS). Not only has he provided a world-leading research environment, but it is also one that gives students opportunity to become world-leading scientists.

Taking a few steps back now, I thank my parents for bringing me into this world. There are many choices we have in life, but choosing who to be born under is not one of them. I may not have been "blessed" with wealth, but absolutely blessed with great parents. They never forced an academic education on me, but instead were strict on more important things in life such as following my passions, basic mannerisms/courtesy, and respect for all people. They never conformed to societal norms or expectations and did what they believed - which lead to leaving their home country of Japan, away from the stressful education system. Incidentally I ended up taking an academic career, but the difference was that it was a pure decision made by myself. Throughout my PhD studies also, they never asked much from me

but gave me all their support. This extends to my brothers also, Mark and Nathan, who always gave me different perspectives on life. Being the youngest and slightly "odd one", I only got through my education because of the protection from my older brothers. Thank you for all your support, I look forward to repaying this over the coming years.

I must dedicate a section to my partner Karen Chiam. We have been together approximately since the start of my PhD, so Karen had to listen to my winging and whining for the entire time. As Karen had already completed a PhD of hers alone, she always provided words of encouragement that "experiments will work in the end". More important than the conversations was her support for my lifestyle. I cannot measure how much help she gave me - thanks for it all! Thank you for being so strong during our long-distance relationship, I can't wait to be living with you again. And yes, you were right, the experiments did work in the end. It just took some time.

Moving beyond my immediate family, the next person I am most grateful of is my teacher in the martial art of Kendo - Takayama Sensei. I have been practising Kendo for around 6 years but it was only in the last 4 years, after I met Takayama Sensei, that I realised Kendo was more than just some routine activity. When studying something like a PhD in Physics it was quite easy for me to get ahead of myself and think that I was better than others. Though I never expressed this verbally, somewhere inside my heart this was how I felt. During my first year of my PhD Takayama Sensei repeatedly told me without hesitation, that I was below-average and stupid. Of course, it is easy to call somebody stupid, but he was able to make me understand this was the case. As demoralising as it may sound, there was nothing more helpful for me at the time. I respect Takayama Sensei because he always did what he needed to do, and not what he wanted to do. For myself, he knew that I needed to change, and even though it lead to many harsh conversations (which I believe he didn't want to have either) it was for the better. This is why I will continue to practice Kendo almost daily, to find the faults in myself. Though Takayama Sensei would not care a bit about this passage, he would prefer to see more positive change in me than a paragraph of words, I thank him so much.

This also extends to the entire University of Sydney Kendo Club, for providing the environment for me to learn a lot of things, much of which I applied to my studies. A special thanks to those who had to work under me whilst I was in charge of the club. Also a message to Ervin Peng, Kelvin Tran and Walter Chung whom I

joined with to make our club's top team. Many of matches were fought, I remember every single one, and lots of bitter tasting silver medals. Some say its such a small world to be competing in, but I bet they will be jealous of our team spirit. I hope we can keep doing Kendo together for the foreseeable future.

Next comes the people directly involved with my PhD. Of course, the first person is my supervisor Stuart Jackson. It has been an incredible journey of - perform experiments, run into problems, attempt solution, ... and repeat. Stuart always provided the grander scientific directions for my project. Meetings with Stuart came in many varieties; in his office, on the lab white board, over a drink, and who could forget the hour-long spontaneous corridor meetings. Nothing was more enjoyable than trying to crack the problem with our ideas. His expertise on fibre handling and laser design contributed to a majority of my study. I thank Stuart for all his efforts for me, and being a great example. My work was only possible because he built the ground work for my research to build on (the so called, "standing on the shoulders of a giant").

Many thanks to Darren Hudson, also my supervisor. Darren showed me all the details of experimental physics. Coming from a theoretical Masters background I had no experience in free-space and fibre optics at all, so his guidance was essential. From aligning lenses to the design of nonlinear polarisation rotation mode-locked fibre lasers - Darren always was around for help. Most important was Darren's expertise in mode-locked lasers and ultrafast optics. Looking back now, the biggest steps such as using ring cavities and Frequency Resolved Optical Gating measurements, were set in motion by Darren. I remember in the last few months of my PhD, when we were ready to throw in the towel and give up, Darren said we should keep trying for one more week, and surely, we achieved the final result in that last week. Thanks Darren for not giving up on me and the experiments!

For more detailed technical contributions I thank Eric Magi and Phil Dennis for teaching me about basic electronics and helping me to build some of the detectors used in this work. I also acknowledge the work of Sam Chorazy, an undergraduate honours student, whom I was responsible for looking over with Darren. It was a tough year Sam, but your software work made the last measurement of my thesis possible.

Now to the amazing colleagues. Starting from the beginning I thank Alvaro Casas for making me feel welcome as I joined CUDOS and showing me around the

place. Also to Matthew Collins who, along with Alvaro, I made a trio with and had many morning coffee conversations about many things. These were the treasured times of my PhD. More recently to Young Zhang, Neetesh Singh, Fernando Diaz, and Irnis Kubat whom I had many nights of drinking and debating about the way science and the world should be and how we are going to change it. My gratitude goes to the OSA/SPIE Student Chapter for giving me amazing opportunities to explore the world. The leadership meeting at San Diego opened the world for me where I met people like Dr. Jean-luc Doumont, whom even though I only met over a few days, I consider as my mentor in communication skills. Particularly noteworthy are Björn Sturmberg, (John) Scott Brownless and Caitlin Fisher who were always around to help, especially for that KOALA conference we organised.

I know there must be more people I have not included, I apologise if I missed you. This PhD is not a result of my work alone, but the countless people who have helped me. Typically we, as scientists, prefer to think of a cause-and-effect relation (i.e. one person contributed to a certain section), but its absolutely not the case here. My last 3-4 years is a complete mixture of the above people's knowledge and experience, all intertwined, giving result to this thesis, and my growth as a person.

Thank you to everybody from the bottom of my heart.

Declaration of Originality

This thesis presents work done by myself and colleagues at the School of Physics at the University of Sydney. There is no material which has been accepted for award of any other degree or diploma in any university, and contains no previously published material by any person, unless it is explicitly mentioned.

I decclare this to be wholly my own, unless stated otherwise.

Tomonori Hu
Sydney, Australia
2nd April 2015

List of publications included in this thesis

- T. Hu, D. D. Hudson, and S. D. Jackson, "Actively Q-switched 2.9 μm Ho3+Pr3+ doped fluoride fiber laser," *Opt. Lett.*, vol. 37, no. 11, pp. 2145-2147, 2012.

- T. Hu, D. D. Hudson, and S. D. Jackson, "High peak power actively Q-switched Ho3+, Pr3+-co-doped fluoride fibre laser," *Electron. Lett.*, vol. 49, pp. 766-767, 2013.

- T. Hu, D. D. Hudson, and S. D. Jackson, "Stable, self-starting, passively mode-locked fiber ring laser of the 3 μm class.," *Opt. Lett.*, vol. 39, no. 7, pp. 2133-6, 2014.

- T. Hu, S. D. Jackson, and D. D. Hudson, "Ultrafast pulses from a mid-infrared fiber laser.," *Opt. Lett.*, vol. 40, no. 18, pp. 4226-8, 2015.

Contents

Chapter 1

Introduction

Much of our world is enabled by lasers.

The laser is without a doubt one of the most revolutionary inventions science has provided us. Our world today is enabled by lasers, from the optical communication signals that travel transoceanic distances that underpins the internet, to the fabrication of nano-scale devices that drive the modern electronics industry. It would be impossible, and rather meaningless, to list all the countless applications the laser has brought us. Those who doubt this are invited to look at the underlying technologies of a number of the most recent scientific discoveries and innovations, and will surely find the laser to be at the heart. On top of this immense success, research in lasers continues to thrive today, and the work presented in this thesis attempts to take the next steps in the development of future generation lasers.

To provide some intuition regarding how much exploration there remains, we start with a brief history of the laser. Research in this field was triggered with the first demonstration of the Maser (microwave radiation) in 1955 by James Gordon, Herbert Zeiger, and Charles Townes [1]. Then in 1960 the same concept was conducted using visible light, by Theodore Maiman, and the term "Laser" (Light Amplification by Stimulated Emission of Radiation) stuck [2]. This then lead to an arsenal of other lasers coming into fruition, each with their own unique application. Interestingly, the leap from the maser to the first laser completely skipped over a vital section of the electromagnetic spectrum - the infrared wavelengths. History has shown these wavelengths of light (700 nm - 1 mm) yielded astonishing applications. The most disruptive of these has been the development of the erbium-based lasers and amplifiers, at the wavelength of 1.55 μm that accessed the low loss window of optical fibres, underpinning telecommunication technologies globally. In this Chapter I will share the motivation for developing lasers venturing even further into

the infrared region (wavelengths beyond 2 μm) and highlight the promises for the future.

1.1 Mid-infrared light - interacting with molecules

The infrared wavelengths are further categorised into subclasses of near [0.7 - 2 μm], mid [2 - 20 μm] and far [20 μm - 1000 μm] infrared. As mentioned earlier the near-infrared (near-IR) wavelengths have an enormous impact in the telecommunication industry both scientifically and economically, but creating light at longer wavelengths, particularly the mid-infrared (mid-IR), is also an area of growing interest.

What makes the mid-IR wavelengths so interesting is the fact that their corresponding photon energies (approximately 0.06 - 0.6 eV) are degenerate with the fundamental vibrational modes of many molecules. This results in extremely strong

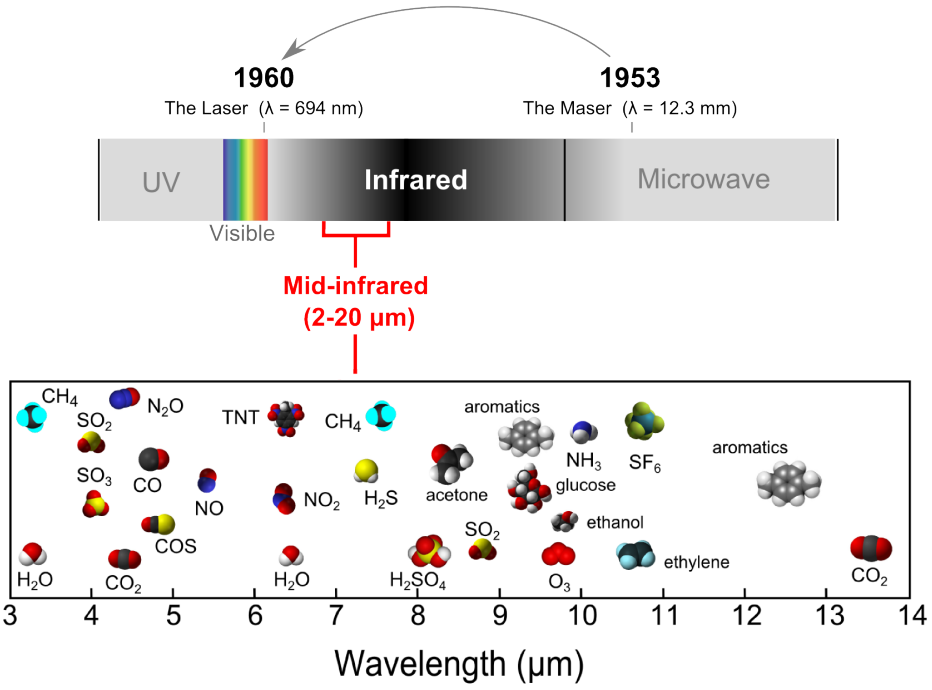

Figure 1.1: (Above) Electromagnetic spectrum showing the leap in wavelength from the first Maser to the first optical laser, skipping the infrared region. (Below) A selection of molecule species with strong vibtrational resonances in the mid-IR spectrum (Image adapted from Daylight Solutions [3])

absorption resonances that can allow the sensitive detection of specific molecules. Fig. 1.1 shows just a handful of molecules that have absorption "fingerprints" at these wavelengths. Mid-IR light therefore hold applications such as hazardous chemical detection, atmospheric monitoring, or health analysis. By taking advantage of these strong absorptions, a recent study used light at 6.2 μm for sensing NO_2 molecules, important for air quality monitoring. Sensitivities as high as 1 part-per-trillion molecules were demonstrated [4]. More advanced systems are pushing these sensitivity limits up to 43-parts-per-*quadrillion* [5]. In comparison to this, modern commercial Raman spectroscopy sensors operating in the near-IR sense on the scale of parts-per-million [6]. These capabilities unlock new high impact applications, particularly in the health sector, such as monitoring diabetes through breath analysis [7] and in-vivo early detection of skin cancer [8].

Although the number of applications may seem endless, I will focus on one specific molecule which is of relevance to the work presented in this thesis - water (H_2O). Water has its strongest absorption due to the asymmetric and symmetric O-H stretching vibrations at wavelengths of 2.662 μm and 2.734 μm respectively [12, 13]. This is highlighted in Fig. 1.2, showing the absorption spectrum of liquid water. Along with these two vibrations there is also the third, the H-O-H bending mode, at 6.269 μm. The broad shoulder feature at approximately 15 μm is related to

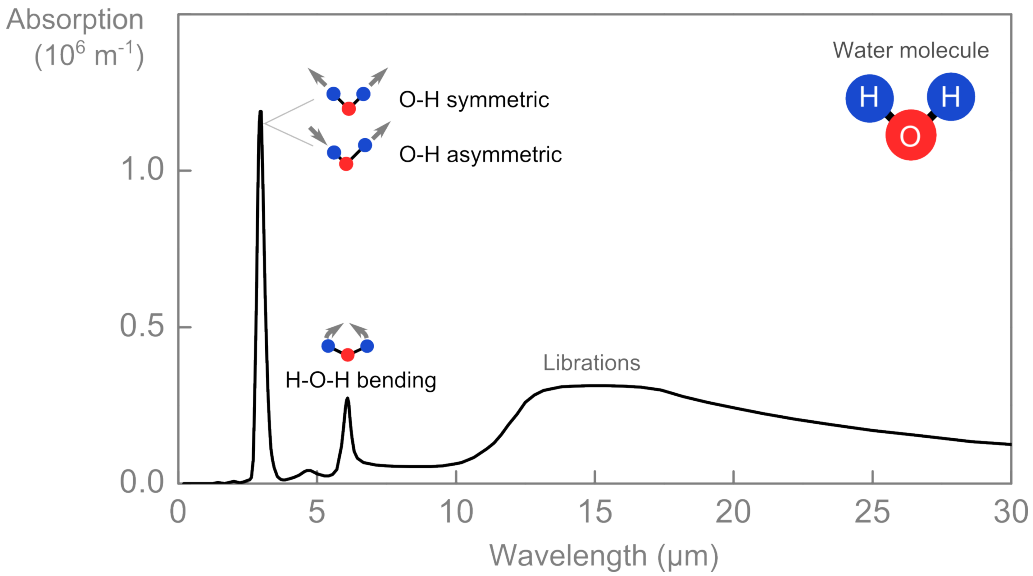

Figure 1.2: The absorption spectrum of liquid water, showing the strongest OH absorption at approximately 2.7 μm (Data provided by references [9–11])

librations which are effects caused by neighbouring water molecules, which vary depending upon environmental conditions [14]. A major application of targeting this water absorption lies in laser microsurgery for minimally invasive ablation of human tissue. In current medical surgery, unintentional tissue damage done during an operation often leads to excessive bleeding of the patient and in some cases the outcomes can lead to death. In a recent study in the United States some 49% of patients undergoing cardiac surgery suffered a bleeding complication of some kind [15]. In the same study the financial impact on the hospital for revision surgery and extended stay of patients was also assessed and found to be detrimental. One of the causes of this excessive bleeding is believed to be related to the tools currently used.

Laser surgery based on tightly focused light pulses has the potential to achieve highly localised ablation of human tissue, on the micron level. CO_2 lasers targeting water in tissue at 10.6 μm are used routinely in the medical field [17], often seen in the cosmetic surgery sector [18], having the advantage of precision control and coagulation (i.e. minimal bleeding). However, high-average power laser beams are also known to inflict unwanted thermal damage to tissue. This extra damage often results in melting and burning of tissue, and thermal injury involves excess collagen deposition resulting in scarring and functional impairment - a significant problem in laryngeal surgery for example. There is a "damage area" associated with CO_2 lasers being on the order of 800 μm, which under-performs against conventional

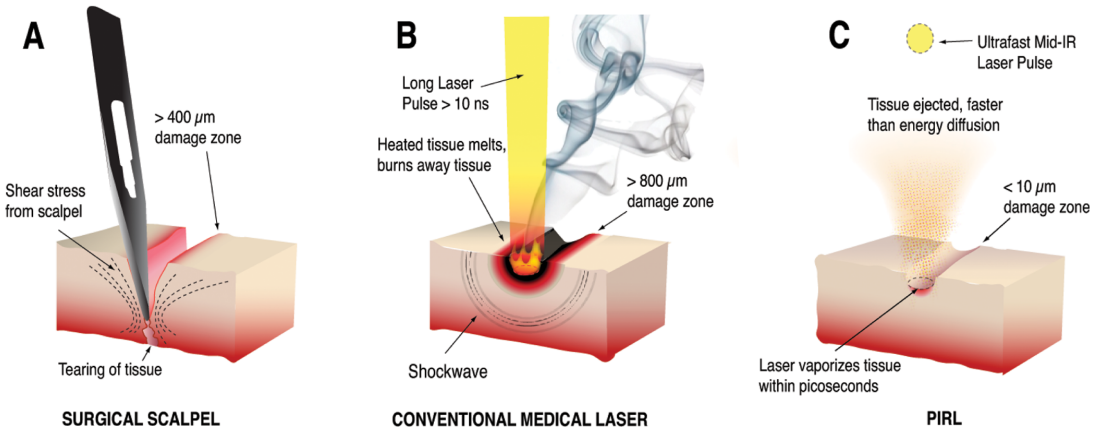

Figure 1.3: Comparison between tissue cutting and laser ablation. a) Surgical scalpel used in current practices b) The conventional quasi-cw laser inflicting collateral thermal damage c) Usage of a picosecond infrared laser, leading to the smallest damage area. Image adapted from Ref. [16].

metal scalpels (400 μm). To overcome the thermal damage issue an *ultrafast* laser pulse can be used where the laser vaporises the tissue within picoseconds, a time scale faster than the thermal diffusion through the tissue. Combining this pulsed operation with the highly absorbing mid-IR wavelengths, damage areas reaching $<$ 10 μm, on the scale of a single cell, are expected [16]. These regimes of tissue cutting are described in Fig. 1.3. Recent tests on biological samples have begun confirming these predictions using pulses at a rate of 1 kHz [19], showing the potential of pulsed mid-IR lasers for next generation medical laser surgery tools.

This specific example relates well to the theme of the work presented in this thesis; the development of ultrafast lasers operating in the mid-IR (near 3 μm) wavelengths. The generation and measurement of light pulses on the scale of picoseconds or less, known as "ultrafast optics" is a well-developed field, giving birth to many scientific discoveries such as the study of chemical reactions at short time scales, resulting in the 1999 Nobel Prize in Chemistry [20]. In Chapter 2, I will discuss the mechanisms behind the generation such ultrafast pulses, and also how to measure them, given they are too fast to be resolved by currently available electronic detectors. Before that, I will first discuss the different laser platforms one can use to achieve this, and focus on fibre lasers which were chosen for this investigation.

1.2 Mid-infrared coherent light sources

As a result of the numerous applications, numerous sources emitting mid-IR radiation have been developed. As there is no such a thing as an all-purpose mid-IR source, we will highlight some of the main platforms. Fig. 1.4 summarises the wavelength coverage of four classes of heavily researched mid-IR sources; the rare-earth-doped solid-sate and fibre devices, solid-state vibronic devices, parametric devices, and semiconductor devices.

1.2.1 Semiconductor lasers

Without a doubt the mid-IR source that has achieved the greatest attention recently has been the semiconductor devices. There are two main types that have been extensively studied for the mid-IR; the interband cascade lasers (ICL) and quantum cascade lasers (QCL). These are both quantum well devices with highly engineered band structures using specific semiconductor materials. Their small descending electron states corresponds to low energy photons and can be made to efficiently generate mid-IR light. Fig. 1.5 shows the typical band structure of ICLs and QCLs.

ICLs generate photons by electron-hole recombination from the conduction band

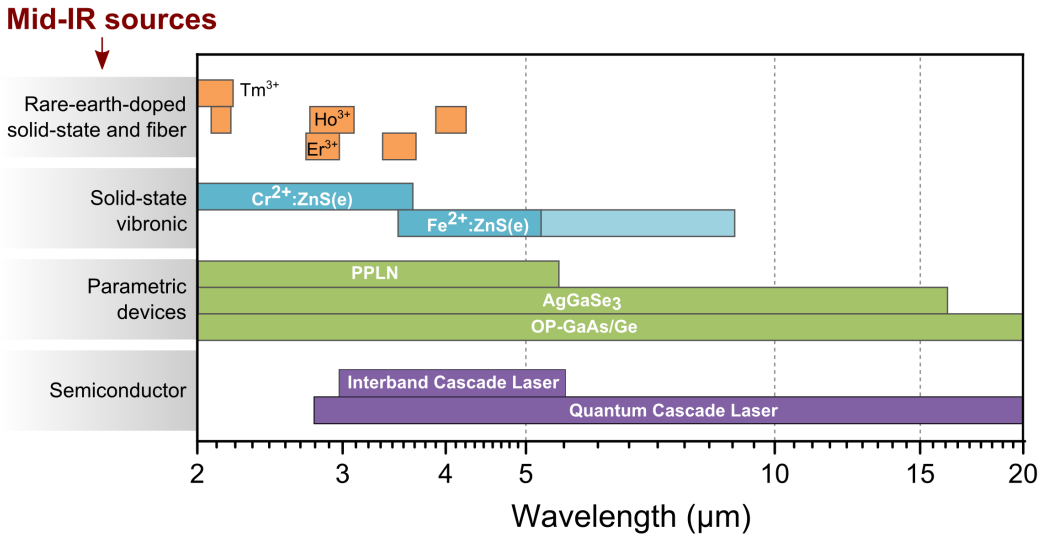

Figure 1.4: Mid-IR wavelength coverage of various categories of lasers. The semi-transparent region for Fe^{2+}:ZnS(e) shows potentially available wavelengths but not yet demonstrated. Data adapted from [21].

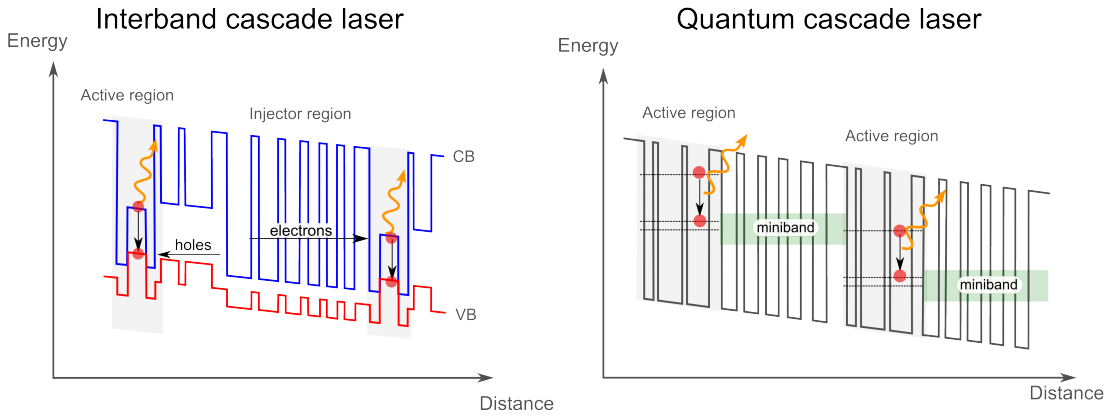

Figure 1.5: Band structure diagrams highlighting the difference between Interband Cascade Lasers (ICL) and Quantum Cascade Lasers (QCL). *Left:* ICLs create light via electron-hole recombination from the conduction band to the valence band in a carefully structured material. *Right:* QCLs generate light within sub-bands created by the electron potential well, which tunnel through a 'miniband' region to be recycled in another active region.

to the valence band in the active region, and a through a carefully structured injector region the electron and holes are separated again to further produce carriers to produce more photons. Typically ICLs have a lower threshold power to achieve lasing, compared to QCLs, but are limited to materials such as GaSb, and operate in the 3-5 μm region [22].

QCLs, on the other hand, use only one carrier (the electron) to generate multiple photons. The transitions instead occur between energy levels of bound electron states in tight quantum wells in the active region, called *sub*-transitions. After radiating a photon, the electron moves across the biased structure via tunnelling effects, through the miniband region, and continues to emit another photon in the next active region. By engineering the band-structure of the material (often layers of AlInAs/InGaAs) the operating wavelength of these lasers can be tuned over the mid-IR, typically emitting 100's of mW. The first demonstration at a wavelength of 4.2 μm in 1994 [23] sparked the field of QCLs. The shortest wavelengths of 2.6-2.9 μm has been achieved [24–26], and a longest wavelength of 161 μm [27]. However achieving these extreme wavelength edges required cryogenic cooling, for room temperature operation the emission is closer to 3-20 μm.

QCLs have achieved incredible performance having a wall-plug efficiency of 50% [28]. They have attracted much attention due to their applications in environmental monitoring, homeland security and medical diagnostics [29]. More recently

the applications have expanded into generating frequency combs (see Section 1.3) for advanced sensing applications [30]. Despite the high cost involved in the intricate fabrication of QCLs, their performance and robustness make them an ideal source for spectroscopy across the mid-IR. In terms of pulsed operation, QCLs can typically can emit nanosecond-level pulses, however recent results have shown mode-locked operation producing 3 ps pulses [31]. This result still operates at the relatively low energies (0.5 pJ, correspodning to a peak power of 1.2 W), it is not yet clear how QCLs will perform at higher energies and peak powers.

1.2.2 Solid state vibronic devices

The class of vibronic lasers refer to those with gain media, often doped with transition metal ions, which have a strong interaction between electronic states and lattice vibrations (phonons). This vibrational-electronic interaction causes a strong homogeneous broadening of the gain bandwidth, and can be advantageous for lasers requiring large tuning ranges. A well-known example of this type of laser is the titanium-sapphire laser with an extremely large bandwidth able to produced pulses as short as 4.3 fs [32]. Fig. 1.6 shows this broad emission spectrum (0.65-1.1 μm), and also its counterpart in the mid-IR based on the host glasses of ZnSe, ZnS and CdSe.

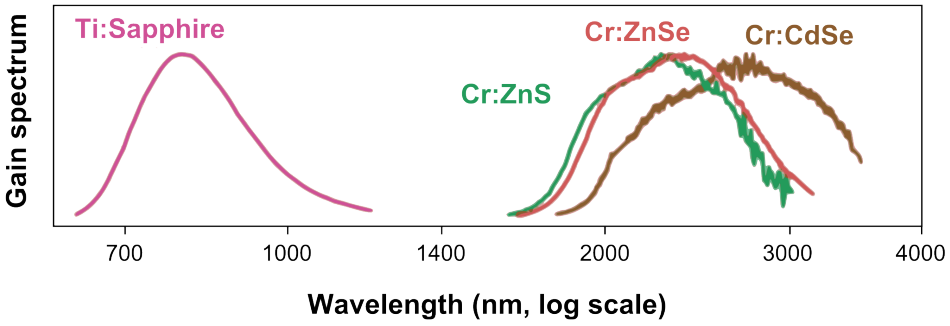

Figure 1.6: Gain spectra of various transition metal based materials. Due to the little shielding provided by the electron orbitals, these dopants experience enormous broadening via interaction with the surrounding lattice. Ti:Sapphire has proven to be an important source in the near-IR, and Cr doped in materials such as ZnSe are an attractive material for the mid-IR. Image adapted from [33].

ZnSe offers optical transmission up to 20 μm and is recently attracting much attention for mid-IR lasers. Doping these glasses with Chromium (making Cr^{2+}:ZnSe) allows emissions across 1.9 μm to 3.3 μm [34,35] with passive mode-locking demonstrated to produce 95 fs pulses [36]. To venture to longer wavelengths the Fe^{2+}:ZnSe gain medium allows an extremely broad emission range from 3.77 μm to 5.05 μm [37]. Gain switched nanosecond-level pulses have been reported [38] but to date no ultrafast performance has been demonstrated. This remains an exciting area to be researched as these vibronic lasers have the extreme bandwidth to support ultrashort pulses, and have the potential to be equivalent Ti:Sapphire lasers of the mid-IR. It is also worth mentioning that planar on-chip Cr^{2+}:ZnSe lasers have also been developed by exploiting the photosensitivity of ZnSe [39]. Though the reported powers were lower (10's of mWs) these platforms realise as a compact source of mid-IR radiation.

1.2.3 Parametric devices

The use of parametric processes such as nonlinear optical effects allows the mixing of one or more pump wavelengths to generate other wavelengths. Mid-IR light can be generated by using the $\chi^{(2)}$ or $\chi^{(3)}$ nonlinearities in certain materials. For example, Fig. 1.7 shows the case of two pump photons annihilating to generate two photons of different energies (the idler and signal photons). Despite the relatively low conversion efficiency of nonlinear effects, with high enough pump powers and suitable resonator design, these processes have proven to be useful for a variety of applications.

The class of lasers known as Optical Parametric Oscillators (OPO) refer to para-

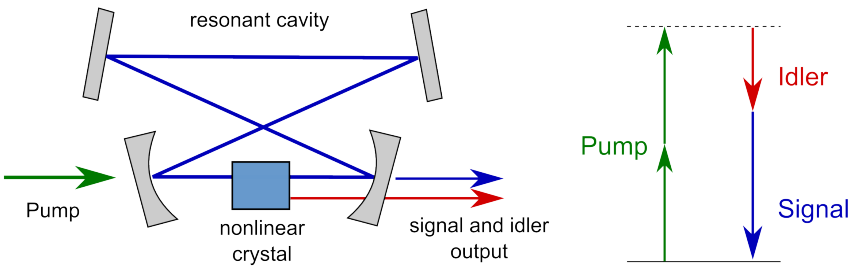

Figure 1.7: Schematic of an Optical Paramatetic Oscillator, a laser based on a parametric process. A nonlinear crystal converts two pump photons into a signal and idler pair (of different frequencies) which can be made to oscillate inside a resonant cavity.

metric processes where an optical cavity is built to resonate signal and/or idler frequencies, as shown in Fig. 1.7. At the mid-IR wavelengths, nonlinear crystals such as GaAs and $AgGaSe_2$ allow transmission and wavelength conversion from 3 to 15 μm. Such an OPO system using a GaAs crystal has shown an enormous spectral emission bandwidth from 2.6 to 6.1 μm, where signatures of molecules in the air become apparent [40]. In another study, pumping a $AgGaSe_2$ crystal with a 1550 nm source resulted in pulsed tuneable emission from 4.1 - 7.9 μm, with pulse widths of approximately 450 fs [41]. In an attempt to simplify the cavity arrangement of an OPO, other systems only operate single-pass through a nonlinear crystal - which are referred to as optical parametric amplifiers (OPA) or Difference Frequency Generation (DFG). Materials such as lithium niobate are favourable due to their strong nonlinear coefficient and ability to be quasi-phase matched. Having a transparency up to 5 μm, near-IR pump light has been converted to 320 fs pulses at 4 μm light in a single pass device [42]. By choosing appropriate crystals (such as AgS and AgSe) tunable emission over 1000 nm at 7.5 μm has also been achieved [43]. The wavelength coverage highly depends upon the pump frequencies used for the mixing, however parametric devices using crystals such as $AgGaS_2$ [44] and AgGaSe [45] allow extremely broadband tuning across the mid-IR, as highlighted in Fig. 1.4. More recently the Orientation-Patterned GaAs (OP-GaAs) has gathered interested due to its wide transparency (0.7 - 17 μm) and ability to be quasi-phase-matched, enabling a high conversion efficiency [46].

1.2.4 Fibre lasers

Fibre lasers have proven to be key sources both across research and in industry. In these lasers the light is confined inside an optical fibre that has been doped to provide gain. The advantage of fibre lasers is that the cavity is compact (inside an optical fibre), efficient, and robust to environmental changes. With the explosive development of optical fibre technology, strongly driven by the telecommunication and manufacturing industries, their performance in the near-IR has been extraordinary. Low-loss silica fibre (<0.5 dB/km at 1550 nm [49]), combined with devices such as wavelength division multiplexers and grating writing, has made the fibre lasers versatile for many applications.

The geometry of the optical fibre, having a high surface area to volume ratio, makes them favourable for high power operation as they have good thermal dissipation. At the near-IR wavelengths fibre lasers have shown incredible power performance, reaching kilowatt average power systems [50]. In terms of pulsed per-

(a) Image adapted from Fiberoptic Components [47]

(b) Image adapted from CALMAR Laser [48]

Figure 1.8: (a) An optical fibre bundle guiding light, showing their flexibility and compactness. (b) An example of a commercial fibre laser system producing 100 fs pulses (mobile phone placed for size comparison).

formance at 1550 nm, pulses as short as 37.4 fs has been reported [51]. On top of this, other benefits include high beam quality, efficiency and low cost of components, make fibre lasers ideal. However as seen from Fig. 1.4, fibre lasers have only just scratched the surface of the mid-IR region. The main reason for this is that standard optical fibres are primarily made from silica (SiO_2), which becomes opaque beyond 2.2 μm due to a multi-phonon edge. Consequently the longest wavelength laser emitted from a silica fibre laser was at 2.21 μm [52]. Nonetheless, performance at 2 μm using thulium-doped silica fibre lasers operating at 1.9 to 2.1 μm have shown high performance with demonstration of kW average power systems [53–55]. However in order to venture further into the mid-IR wavelengths the silica platform inevitably needs to be abandoned and new materials need to be investigated.

The relative transmission of various glasses (of thickness ranging from 2-3 mm [56]) able to be drawn into fibres are shown in Fig. 1.9. As mentioned earlier the transmission of silica glass drops off rapidly for wavelengths longer than $\approx$ 2.1 μm due to the multiphonon edge. Fig. 1.9 shows other glasses with lower phonon energies, allowing transmission to longer wavelengths. The application of these glasses can be divided into two classes; light delivery (transportation) and fibre laser (generation) devices. The passive delivery fibres are often required to be able to support broadband throughput at high powers for applications in defence. Future mid-IR fibre lasers may include the usage of these delivery fibres such as the polycrystalline fibres [57, 58] and the hollow waveguides [59, 60]. In terms of

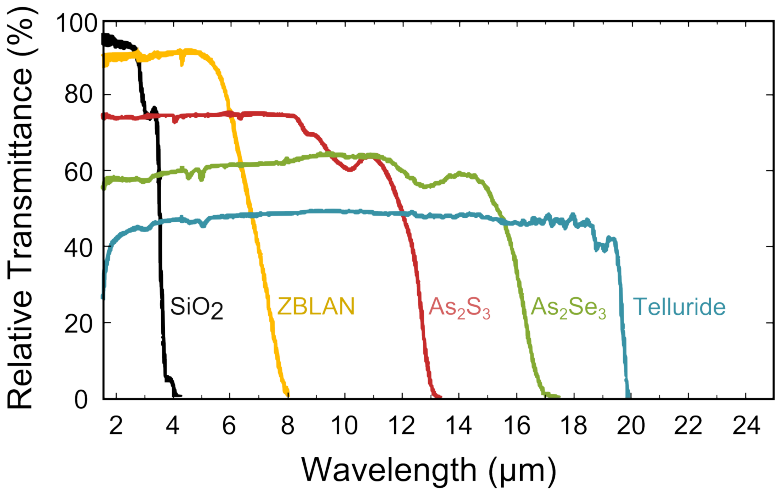

Figure 1.9: Relative transmission of bulk samples of various glasses able to be drawn into optical fibres. SiO_2 has the highest phonon energy and prevents transmission beyond 2 μm, whereas the ZBLAN and chalcogenide glasses can extend deeper into the mid-IR. Figure adapted from Ref. [56].

generating laser light, an exciting alternative are the chalcogenide glasses that are based on the chalcogen group (Group 16 elements) comprising of sulfur, selenium and tellurium, usually combined with other materials to build a glass matrix. Fig. 1.9 shows the transmission of two widely used chalcogenide glasses, As_2S_3 and As_2Se_3, transparent out to 12 μm and 16 μm respectively. The chalcogenide glasses have shown laser performance at a wavelength of 1.06 μm from a neodymium doped gallium-lanthanum-sulfide fibre [61], however no demonstration of lasing at other wavelengths have been demonstrated. Much of the issues have been discussed and are said to be related to glass quality, glass processing routes, and rare-earth-ion clustering resulting in high loss [62]. However upon overcoming these material issues, detailed analysis predicts lasing at wavelengths of 4.6 μm, 4.89 μm and 7.5 μm by using suitable rare earth doping [63].

The type of fibre that has shown best performances at the shorter mid-IR wavelengths are fluoride fibres. These are non-oxide glasses composed of fluorides and various metals, which also have a low phonon energy. In particular the ZrF_4-BrF_2-LaF_3-AlF_3-NaF (ZBLAN) composition is transparent up to 5 μm and has demonstrated high performance for laser generation. Extremely low losses at the near-IR have been measured (0.45 dB/km at 2350 nm [65]) and have been shown to be an excellent host glass for rare-earth-ions. A thorough review of their fabrication

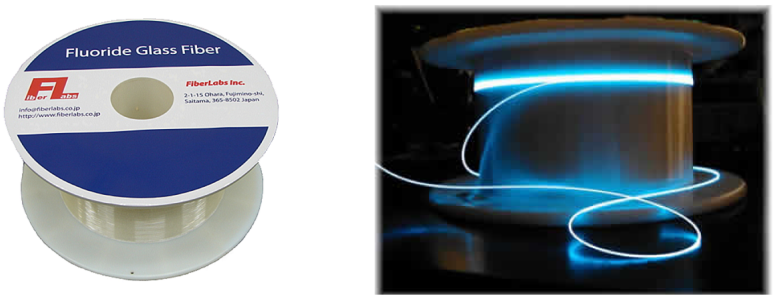

Figure 1.10: Fluoride fibre can be purchased commercially either undoped for mid-IR light delivery or doped to generate mid-IR light (right, doped with Tm). Photo courtesy of FiberLabs Inc. [64].

and performance is summarised by Zhu and Peyghambarian [66]. As a result several commercial companies distributing fluoride fibres have emerged, for example FiberLabs Inc. shown in Fig. 1.10.

By the year 2011, moderate power ZBLAN fibre lasers had already been demonstrated at wavelengths near 3 μm. ZBLAN fibres doped with rare earth ions such as erbium and holmium have allowed efficient lasers emitting up to 24 W of average power [67], with the highest efficiency of 35.4% achieved [68]. The extended mid-IR transmission provided by the ZBLAN fibre has allowed lasers at 3.22 μm [69], 3.5 μm [70] and 3.9 μm [71], with a thorough summary provided by a review by Jackson [72].

Recently there has been a shift towards pulsed laser systems using fluoride fibres. Early demonstrations of pulse production in ZBLAN fibre lasers using gain switching and Q-switching (discussed in Chapter 2) resulted in 307 ns [73] and 90 ns [74] pulses respectively. There is an exciting avenue to explore here whether the fluoride fibre lasers can achieve shorter pulses towards the ultrafast regime (picoseconds and shorter), which will be the topic of this thesis. Together with the benefits offered from the fibre geometry there are some exciting potential applications, one of which we will highlight here.

1.3 Mid-infrared frequency combs

We finally describe a field where these ultrafast mid-IR fibre lasers are expected to have some fundamental scientific application - in the generation of "frequency combs". This has become a heavily researched topic since 2005, when the Nobel Prize was awarded for its discovery to John. L. Hall and Theodor W. Hänsch. An optical frequency comb is a light source that has an spectrum containing equidistant, well defined, spectral lines - shown in Fig. 1.11. If the precise position of these comb lines is known it can be used as an extremely sensitive spectral measurement system, i.e. a spectral "ruler". These combs have shown immense potential in metrology by revolutionising precision measurement of frequencies (and hence, time). Frequency uncertainties as low as 10^{-18} Hz have been shown [75], surpassing the measurements from the caesium atomic clock (the current standard used to define the second).

Much interest has grown in generating these frequency combs at the mid-IR wavelengths [76]. The reason, as we have established, is due to the resonant molecular absorption lines for sensing applications. On top of multiple line spectroscopy [77], the fundamental theories of molecular chemistry can be studied in detail. For example, accurate measurements of infrared frequencies of chiral molecules are expected to provide evidence on the parity violation due to the weak interaction [78], and hint of the formation process of certain chiral molecules, which remains a highly debated

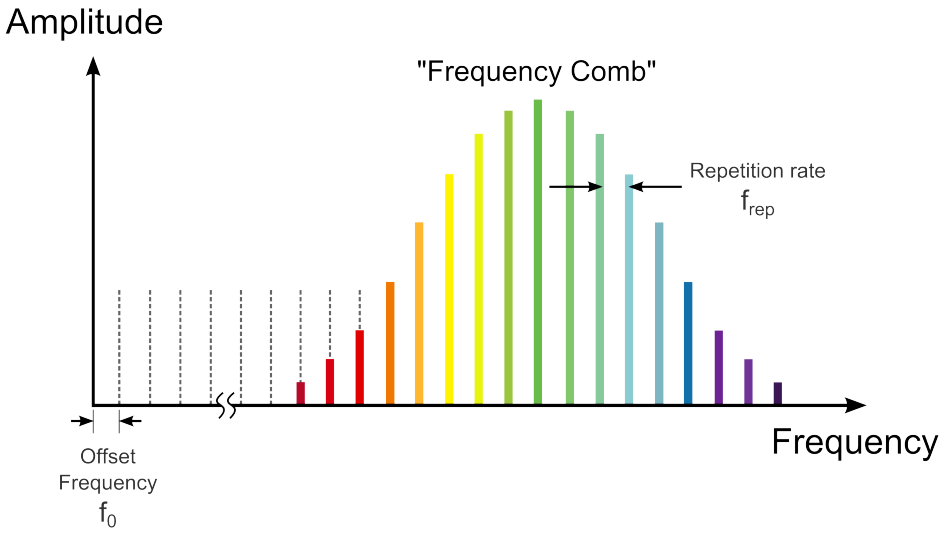

Figure 1.11: Illustration of a frequency comb, consisting of narrow lines seprated by the repetition rate of the laser f_{rep}, which is offset by the carrier envelope frequency f_0.

topic in biological sciences.

There are a number of ways of achieving such a frequency comb. A mode-locked laser that emits a train of ultrafast pulses (details in Chapter 2) typically emits a frequency comb. Other methods include using parametric systems such as DFG and OPOs, and also through nonlinear effects such as four wave mixing (Kerr comb generation). A thorough review on these processes has been provided by Schliesser [76]. Of the many sources the mode-locked fibre laser comb sources offer a stable and controllable environment, suitable for field-usable devices. Such a fibre laser comb source has been demonstrated to be stable even when subject to mechanical vibrations of up to 1.6 g [79]. This suggests that an ultrafast fibre laser operating in the mid-IR has potential to be a compact and robust frequency comb source.

However, before using the generated comb spectrum for measurements, it is necessary to *stablise* them. Typically combs generated in the above techniques have an n-th position given by $\nu_n = nf_{rep} - f_0$, where f_{rep} is the repetition rate of the laser cavity and f_0 is referred to as the carrier envelope off-set frequency. These are both needed to be accurately measured before performing comb spectroscopy. The repetition of the laser, f_{rep} can be easily measured and stabilized in a feedback loop using fast photodetectors. The off-set frequency shift caused by the mismatch between the group velocity and phase velocity in the cavity, causing a slippage of the electric field and the intensity envelope of the pulses. This can be measured using an f-to-2f interferometer [80], which requires an octave spanning spectrum, often achieved by generating a supercontinuum spectrum. Several materials are known to exhibit strong nonlinearity in the mid-IR, allowing the generation of octave spanning supercontinuum spectra [42, 81, 82]. Therefore an exciting route for mid-IR fibre lasers is to first produce ultrafast, high peak power, pulses to pump a nonlinear device, and then create a broad spectrum for frequency comb sensing. We touch on the details of this concept in Chapter 5.

1.4 Scope of this thesis

Research in fluoride fibre lasers has attracted significant interest, showing moderately high power operation near 3 μm, and some recent progress towards longer wavelengths. Motivated by the applications previously mentioned, there is also interest in making pulsed fluoride fibre lasers. This thesis investigates the primary methods for achieving ultrafast pulses from a fluoride fibre laser, and how far we can push these limits.

In the framework of this PhD I have demonstrated the ultrafast capability of fluoride fibre lasers near 3 μm. By using different pulse production mechanisms I have produced pulses from nanoseconds to picoseconds, and finally in the femtosecond regime. Although I have highlighted applications of the shorter pulses, each of these Chapters is equally important as they describe the design considerations of these pulsed fluoride fibre lasers across a range of pulse widths. Along with the generation of these pulses I have also developed mid-IR pulse measuring systems such as intensity autocorrelation and Frequency Resolved Optical Gating methods. The results indicate that fluoride fibres have the capability to operate in an ultrafast regime and hold a strong potential as a new source of mid-IR light.

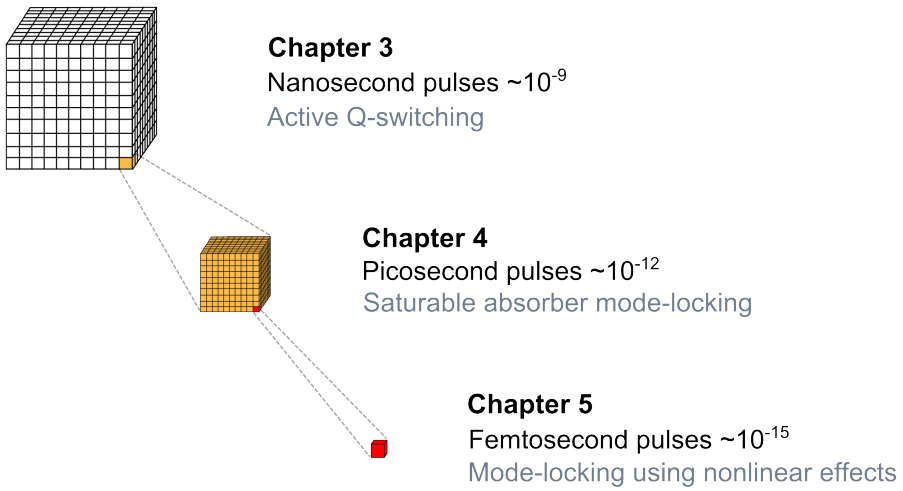

Figure 1.12: Working down to the ultrafast: Each Chapters 3, 4 and 5 will explore nanosecond, picosecond and femtosecond level pulses respectively. We describe the design considerations, methods and materials to achieve each case.

The remainder of this thesis is arranged as follows.

In Chapter 2, I describe the details of fibre lasers and ultrafast optics. We review fibre laser structures, design considerations, and basic physical principles of lasers. We then move to pulse production from lasers, focusing on mode-locking techniques. Detection methods of pulses in the mid-IR are also described here.

In the next three chapters I describe the results achieved in during my study. In Chapter 3 we look at the preliminary pulse production methods of Q-switching and understand how fluoride fibres perform with nanosecond-level pulses. In particular we study efficiency, power, and design of the fluoride fibre laser.

Chapter 4 marks the first step into the ultrafast regime by studying passive mode-locking via the use of saturable absorbers. We demonstrate picosecond pulses produced from a new fluoride fibre laser design showing the highest level of stability and self-starting mode-locking. The pulses were directly measured using an in-house built intensity autocorrelation technique.

Chapter 5 verifies the truly ultrafast capability of fluoride fibres, by pushing the mode-locked system to producing femtosecond-level pulses. Not only was this the shortest and highest peak power pulses produced from a fluoride fibre laser, we also conducted the first ambiguity-free pulse measurement using a Frequency Resolved Optical Gating method (also built in-house). This study revealed new parameters of fluoride fibres such as damage threshold, dispersion, and spectral phase characteristics, that are essential in the design of future mid-IR fibre laser systems.

Chapter 2

Pulses from a fibre laser: Theory, design and detection

This Chapter describes the details of optical fibre lasers and ultrafast optics. The terminology used in this thesis, common to those working in the laser field, will be defined here. We begin with an introduction to optical fibres, their geometries and application to lasers. I will then introduce the perspective of ultrafast optics in terms of pulse generation and measurement, which become crucial in Chapters 4 and 5.

2.1 Optical fibre waveguides

Conventional optical fibres use total internal reflection to guide light [83]. Typically the dielectric fibre consists of a core with refractive index n_{CO} and a surrounding cladding layer with index n_{CL}, with $n_{CO} > n_{CL}$ allowing the total internal reflection according to the ray optics approach.

For a step index fibre as shown in Fig 2.1, the difference in the core and cladding refractive indices defines an "acceptance cone" which are the set of ray angles that the core will guide via total internal reflection. The sine of the half-angle (θ) of this cone defines the numerical aperture (NA) as,

$$NA = \sin(\theta) = \sqrt{n_{CO}^2 - n_{CL}^2} \tag{2.1}$$

where a is the core radius. The radius of typical optical fibres are on the scale of 4-5 μm, which is on the scale of the wavelength of the light that is used (1.55 μm for telecommunication applications). A more rigorous approach is carried out by solving Maxwell's equations in a cylindrical geometry, which reveal numerous solutions of

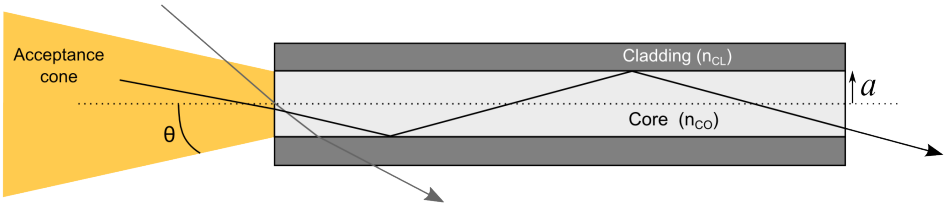

Figure 2.1: Cross section of a step index optical fibre. The acceptance cone describes the rays the core will guide via total internal reflection, defined by the numerical aperture of the fibre (NA).

light propagation along the fibre. These are known as 'modes' which have different spatial distribution of electric fields - some of which are displayed in Fig. 2.2. For most laser applications, including ultrafast lasers, often only the fundamental mode is desired due to its tightly confined Gaussian profile that propagates with the lowest loss.

To ensure that no higher order modes exist the V number of the fibre must be kept lower than a value of 2.405, defined as

$$V = \frac{2\pi}{\lambda} aNA \tag{2.2}$$

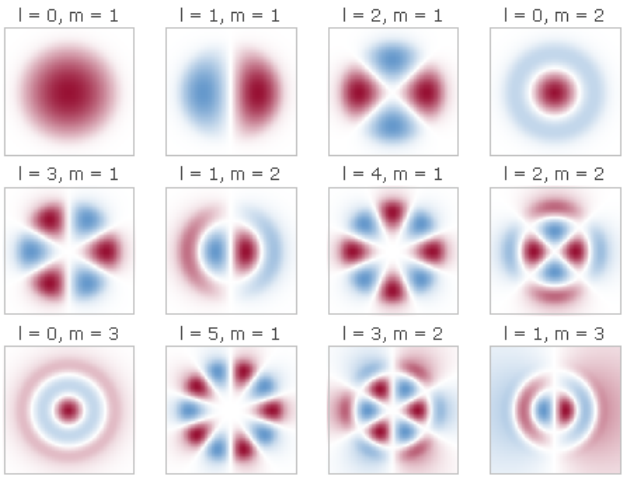

Figure 2.2: A selection of higher order spatial modes that can be excited inside an optical fibre. The fundamental mode (l=0, m=1) has a Gaussian distribution which is highly confined in the core of the fibre and is favoured in most cases. Image adapted from RP Photonics [84].

Therefore, given the wavelength of light, the radius and numerical aperture of the fibre must be chosen such that $V < 2.405$ to achieve single mode operation. For V numbers higher than this the number of modes able to exist in the fibre increases at a scale of $V^2/2$ [83].

2.1.1 Fibre lasers

The theory behind laser dynamics involves much detail, here I will provide a summarised explanation. Further details of laser systems can be found in Ref. [85].

A generic laser is shown in Fig. 2.3 with its essential components; a gain medium, a cavity formed by mirrors, and a pump source. Though there are countless configurations in which a laser can be made, Fig. 2.3 shows a simple case with a gain medium surrounded by two mirrors, with one mirror being partially reflecting to allow the output of the laser. Pumping is often done electrically or optically, to excite the gain medium to a higher energy state which emits light when spontaneously relaxing back to the ground state energy level. This light is then amplified by stimulated emission with the aid of the cavity, creating a coherent beam to be emitted as the output.

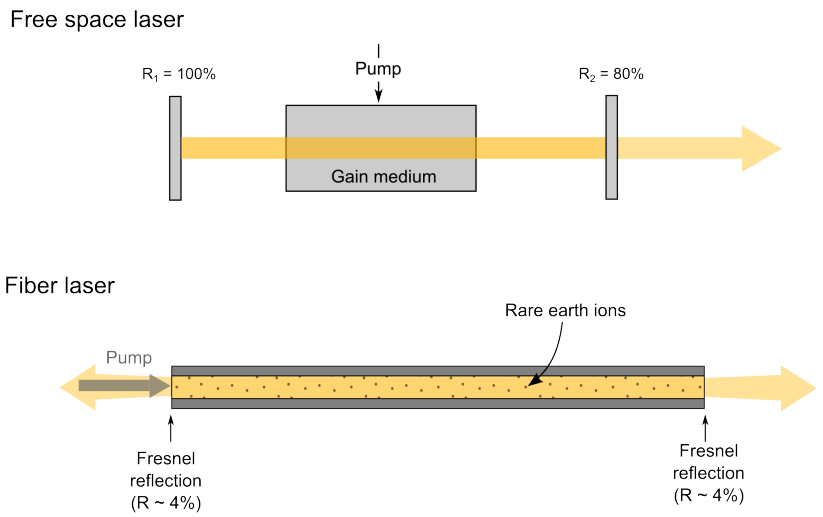

Figure 2.3: (Above) Generic components that make up a laser; a gain medium that is energetically pumped, and a cavity formed by mirrors to allow the build up of laser light. (Below) An equivalent laser system made from a rare earth ion doped optical fibre. In this example the dopants in the core act as the gain medium, and the Fresnel reflections at each side act as mirrors.

An optical fibre laser operates in a similar fashion, illustrated in Fig. 2.3(lower). Here, the fibre core is doped with elements to provide gain. Often the rare-earth elements (the lanthanides) are used as their atomic structure have electrons in f-orbitals which are electrically shielded by the configuration of other electrons. This makes them favourable to be doped into host materials (such as SiO_2 and ZBLAN glasses) as f-orbital electronic transitions remain relatively unaffected by the host and remain atomic-like. If the fibre ends are perpendicularly cleaved (i.e. creating flat ends) even the small Fresnel reflection from the tips ($\approx 4\%$ for SiO_2 glass) can create enough feedback for lasing, given that the gain is higher than the entire loss of the cavity. The ouput of the laser may emit in both directions as shown in Fig. 2.3, however the exact behaviour depends on the precise parameters of the laser. This is only the simplest form of a fibre laser and other forms exist which incorporate extending the output of one side to a mirror, or using Fibre Bragg Grating reflectors.

This type of laser, formed by two reflectors, is called a linear cavity and consists of many longitudinal modes (standing waves in the direction of the cavity), shown in Fig. 2.4. Typically thousands to millions of longitudinal modes exist in a laser which each are separated by $\Delta\nu = c/2L$, where L is the optical length of the cavity. Theoretically there are an infinite number of modes, but the finite spectral width of the gain medium will set a limit to the number of modes. The existence of these longitudinal modes becomes important in Section 2.3.1 where we look at mode-locking methods for pulse production. The inverse of this frequency spacing gives the *round trip time* of the cavity $\tau_{rp} = 1/\Delta\nu$, the time light takes to make one complete propagation cycle inside the cavity.

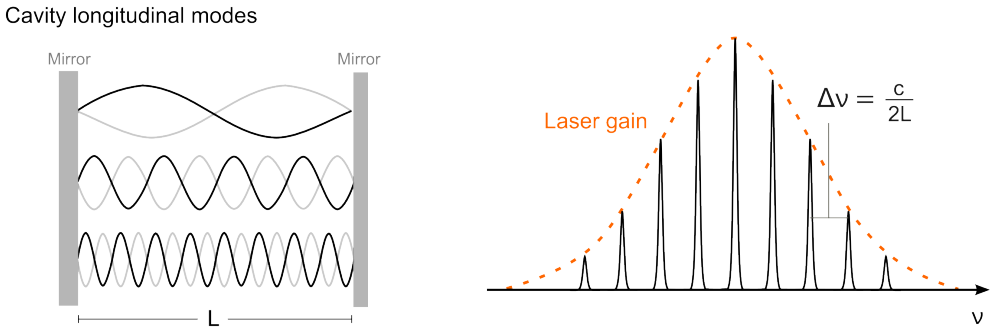

Figure 2.4: (Left) A linear cavity formed by two mirrors consist of an infinite number of longitudinal modes. (Right) These modes are equally spaced in frequency across the gain spectrum of a laser, which become important when considering the method of mode-locking.

An important parameter for a cavity is the Q-factor. This value is related to the ratio between the energy stored in the cavity to the energy lost per cycle, defined as

$$Q = 2\pi \frac{\text{stored energy}}{\text{energy loss per cycle}} \tag{2.3}$$

The Q is related to the amount of time a laser photon is contained inside the cavity (large values of Q refer to longer storage times). It can be shown [85] that for a resonant frequency ν_0 of spectral width $\Delta\nu$ (an optical frequency for lasers) the Q-factor is approximated to

$$Q \approx \frac{\nu_0}{\Delta\nu}\mathcal{F} \tag{2.4}$$

where $\mathcal{F}$ is the *finesse* of the cavity defined by

$$\mathcal{F} = \frac{\pi}{2\sin^{-1}\left(\frac{1-\sqrt{\rho}}{2\sqrt[4]{\rho}}\right)} \approx \frac{\pi}{1-\sqrt{\rho}} \approx \frac{2\pi}{1-\rho} \tag{2.5}$$

with ρ being the percentage of the ciruclating power left after one round-trip of the cavity (i.e. 1-ρ is the power lost per round-trip). The approximations hold for low round-trip losses (e.g. <10%, indicating high Finesse values). One can control the Q-factor of a laser by changing the conditions inside cavity (by either introducing losses or changing the pumping conditions). This technique was exploited in the early demonstrations of creating pulses from a fibre laser, which will become the subject of Chapter 3, Q-switched lasers.

2.1.2 Double clad optical fibres

Before moving onto the rare earth elements that allow emission of mid-IR light we will take a look at one final aspect of fibre geometry, the class of double-clad fibres.

One of the most significant advantages fibre lasers offer is their potential power-scalability. The large surface area to volume ratio makes fibre lasers excellent devices to release excess heat produced from high power pumping. Certain problems can occur however when directly pumping the core. At high power operation, despite the favourable geometry of the optical fibre, the thermal effects become significant. This makes alignment of optical devices at high powers overly critical, requiring a high quality pump beam. Also, in terms of the laser process, unwanted effects such as excited state absorption (multiple absorptions of pump photons from already

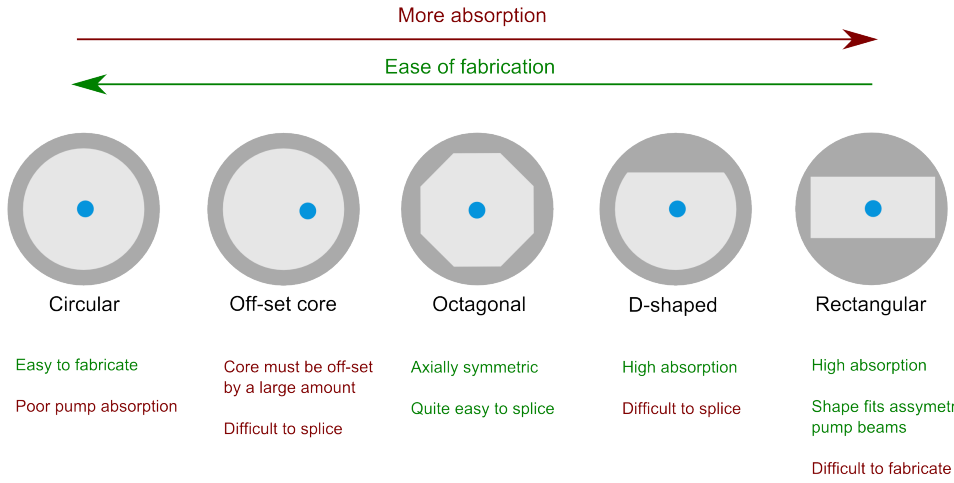

Figure 2.5: Double clad fibres have a specific second cladding to guide the pump light, so the core absorption can be done distributed over a long distance. A series of double-clad fibre geometries are shown, with some of their advantages and disadvantages listed.

excited states) may occur that terminate the lasing process. Therefore at higher powers it is often desirable to absorb the pump over a longer distance, and one way to achieve this is to use a double-clad fibre geometry.

As the name implies, a double clad fibre has two claddings. The core is doped with rare earth elements and often designed to be operating only at the fundamental mode. The core is then surrounded by a cladding which guides the pump light that, due to its larger diameter, is highly multi-moded. As the cladding guides the pump light, the guided modes intersect with the doped core. In this way, pumping of the rare earth ions is done distributively over a longer distance. Another benefit of this structure is that coupling light into the larger cladding is easier than the core, relaxing the conditions on the spatial beam quality of the pump light. This allows high power laser systems to be pumped by low-cost diode lasers. Finally the geometry (emission from a small core compared to the larger cladding) allows an enhancement in the brightness of the laser light if diode lasers are used as the pump.

Due to the larger cladding being highly multi-moded the spatial distribution of the pump light can be very complicated. For circular claddings there exist modes that do not have a high field overlap with the core and can lead to low absorption of the pump, making the laser inefficient. It has been reported that off setting the core in a circular double clad structure can produce better pump light absorption [86]. Alternatively, changing the shape of the cladding can also be effective. Fig. 2.5

shows some commonly used cladding structures. In these shapes the ray trajectories become chaotic, resulting from the relatively complex shapes, and interact with the core more efficiently. Numerical studies of these mode-overlaps have been performed on various cladding shapes [87, 88] . High absorption is an important parameter however more practical parameters exist such as difficulty of cleaving, splicing and fabrication. Fig. 2.5 highlights the advantages and disadvantages of various cladding shapes. By using these structures efficient absorption can be achieved along a distributed length of the fibre, avoiding the problems mentioned previously.

2.2 Rare earth ions for generating mid-infrared light

With the basic geometry and structure of fibre lasers established, we now consider which rare earth dopants are often used to generate mid-IR wavelengths.

As mentioned previously the rare earth ions are often used for doping into a host material to make a laser gain medium. In condensed matter the trivalent (3+) level of ionisation is most stable for the lanthanide ions [89], and these energy levels have been studied extensively [90,91]. Though there are numerous potential energy levels one may choose to excite to emit mid-IR radiation, the successfully demonstrated

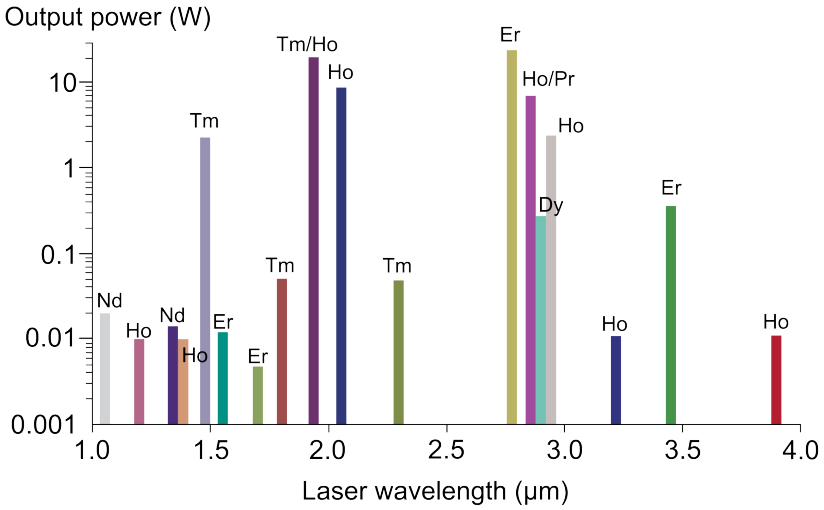

Figure 2.6: Rare earth ions that have been successfully doped into ZBLAN fibres to allow laser oscillation, and the average powers they have achieved.

transitions from doped ZBLAN fibres as of 2011 are highlighted in Ref. [92]. We show similar data in Fig. 2.6, with some updated results. With the development of new pump mechanisms and fibre dopant considerations more efficient systems are still emerging [93].

We focus on two particular elements, the holmium and erbium transitions which operate around the 2.7-3.0 μm wavelengths. In terms of near 3 μm fibre lasers, doping with holmium and erbium have shown high efficiencies of 28.5% [94] and 35.4% [68] respectively, where each laser was pumped using simple semiconductor diode lasers. As was mentioned in Chapter 1, these wavelengths are of importance in the medical laser surgery field, if operated in the ultrafast regime. Here we will take a close look at the energy levels of these elements.

2.2.1 Holmium based fibre lasers

Holmium atoms form a trivalent state when doped into ZBLAN glass (Ho^{3+}) and the energy levels arrange to that shown in Fig. 2.7. The ground state level is labelled $^5I_7$ in spectroscopic notation, with higher levels also shown. Emission wavelengths between the corresponding energy level transitions are labelled, however for our case the $^5I_6 \rightarrow {}^5I_7$ transition, corresponding to a wavelength of 2.85 μm is of interest. There is a problem that the lifetime of $^5I_6$ level (3.5 ms) is shorter than the lower level lifetime (12 ms), which prevents population inversion from taking place, making the transition self-terminating. To achieve stimulated emission from this transition the lower level must be sufficiently depopulated. Two ways to achieve this has been reported; by simultaneously allowing the lower transition ($^5I_7 \rightarrow {}^5I_8$) at 2.1 μm to also emit light, and by the addition of another dopant to depopulate the $^5I_7$ level through energy transfer processes.

For the former, sufficient population build up of the $^5I_7$ level can also make a laser at 2.1 μm, allowing subsequent inversion of the 2.85 μm transition. This system, called a cascaded laser, and has shown a combined power and efficiency of 3 W and 65% [95]. A theoretical analysis of the rate equations for this laser has been established [96], however experimental measurements reveal the system to be relatively complicated as it can behave midway between a 3 and 4 level system depending on the pump conditions [97]. Alternatively the $^5I_7$ level can be quenched by co-doping the ZBLAN host with praseodymium (Pr^{3+}). This $Ho^{3+}Pr^{3+}$ co-doped system has energy levels as shown in Fig. 2.8. Due to the $^3F_2$ level in Pr^{3+} that is energetically similar to the self-terminating $^5I_7$ level of Ho^{3+}, a resonant energy

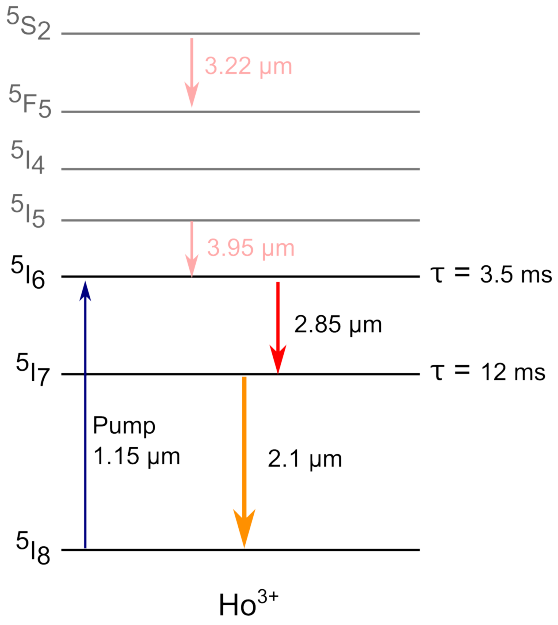

Figure 2.7: Energy level diagram of holmium ions in a trivalent configuration (Ho^{3+}). Pumping at 1.15 μm allows the emission of the 2.85 μm light, given the $^5I_7$ level is sufficiently depopulated. Other reported transitions at 3.22 μm and 3.95 μm are also shown.

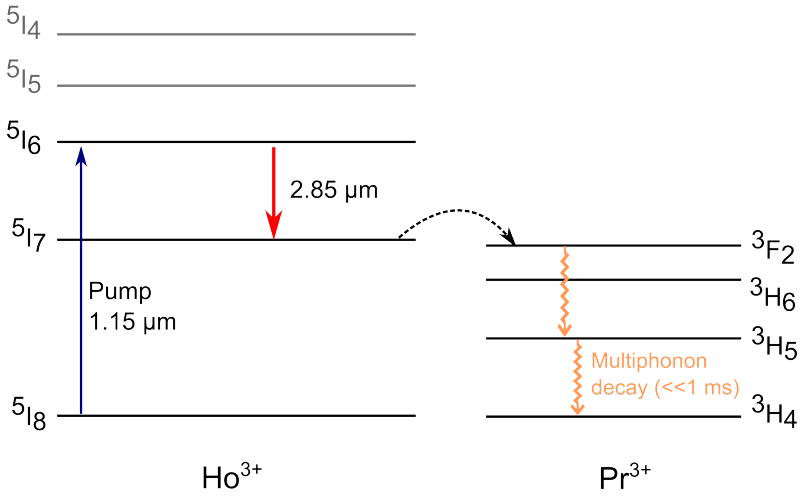

Figure 2.8: The addition of praseodymium (Pr^{3+}) to Ho^{3+} allows a resonant energy transfer process from the $^5I_7$ to the $^3F_2$ which then quickly decays via multiphonon decay. In this way the 2.85 μm emission from Ho^{3+} can be made very efficient.

transfer process (through dipole-dipole interaction) can take place, causing the Ho^{3+} ion to drop to the ground state. The excited Pr^{3+} ion is able to release this energy rapidly through multi-phonon decay to the lattice (taking place $\ll$ 1 ms). This system has produced up to 2.5 W of power emission at 2.94 μm with an efficiency up to 32% [98, 99]. The advantage of this system is the relatively simple transition to generate the near 3 μm light, which is closer to a 4-level laser. This dopant configuration was used for the work presented in Chapters 3 and 4.

2.2.2 Erbium based fibre lasers

The other rare earth ion allowing efficient generation of near 3 μm emission is the $^4I_{11/2} \rightarrow {}^4I_{13/2}$ of Er^{3+}, as shown in Fig. 2.9. Here, pumping with 980 nm light allows a transition centred at 2.75 μm. Similar to the Ho^{3+} levels, the upper laser level has a shorter lifetime than the lower, making this a self-terminating system as well. Here the bottom level can be depopulated through the process of energy transfer up-conversion (ETU). This occurs at high doping concentrations where nearby ions can exchange energies. In this case, an Er^{3+} ion in the $^4I_{13/2}$ state can transfer its energy to another ion in the same state causing it to be excited to the $^4I_{9/2}$ level, which then drops quickly via multiphonon decay to the $^4I_{11/2}$, aiding the population inversion of the 2.75 μm transition. The ion that gave up its energy drops to the ground state, and hence, the process quenches the $^4I_{13/2}$ level. It can be seen that an ion that has already emitted a 2.75 μm photon may, via the ETU process, be excited again to contribute the the lasing - referred to as energy recycling. This makes the Er^{3+} system extremely efficient, reports have already measured up to 35.4% with a theoretical maximum of 39.5% [68], the highest recorded efficiency from a near 3 μm fibre laser. More rigorously, there are other higher order energy transfer processes that can occur, of which the details are provided in Ref. [100].

The Er^{3+} system, despite the complexities introduced by high doping concentrations, has inherent advantages that the pump wavelength is at 980 nm for which low-cost and high power diodes lasers exist, due to its frequent use in the telecommunication industry. This has allowed the Er^{3+} lasers to achieve high output powers of >10 W [67, 68, 101]. We employed this Er^{3+} laser configuration in Chapter 5 where we present the shortest pulses produced from a ZBLAN fibre laser.

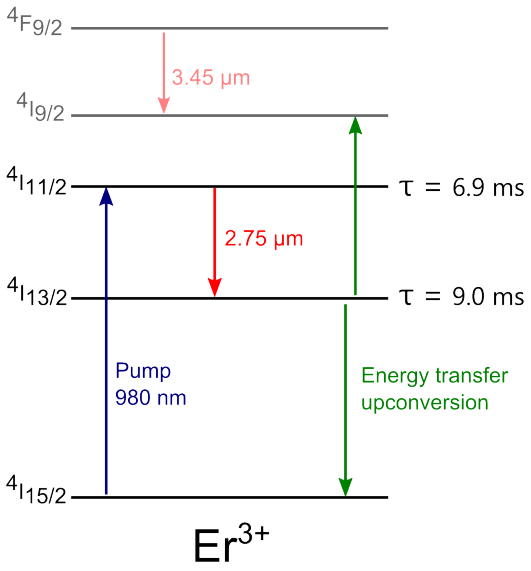

Figure 2.9: Energy level diagram of erbium ions (Er^{3+}). Pumping at 980 nm allows the 2.75 μm transition, which is again bottlenecked by the long life time of the $^4I_{13/2}$ level. However at high doping concentrations the energy transfer upconversion process depopulates this level and can create efficient emission from the 2.75 μm transition.

2.3 Ultrafast optics

Generating and measuring light at an ultrafast time scale, as challenging as it may be, has been well established and has enabled some of the most significant scientific discoveries. To understand these techniques we will first define the parameters that describe a light pulse.

An electric field of a light pulse can be written in terms of its intensity envelope (I) and its phase (ϕ) as a function of time (t) as,

$$E(t) \propto \mathbb{R}\{\sqrt{I(t)}\exp[i(\omega_0 t - \phi(t))]\} \tag{2.6}$$

The pulse shape is determined by I(t), and the phase ϕ is related to the instantaneous frequency of the pulse as

$$\omega(t) = \omega_0 - \frac{d\phi}{dt} \tag{2.7}$$

where ω_0 is the centre frequency of the light pulse. This electric field can also be written in the frequency domain

$$E(\omega) \propto \mathbb{R}\{\sqrt{S(\omega)}\exp[-i\phi(\omega)]\} \tag{2.8}$$

where S(ω) is the spectrum of the pulse and $\phi(\omega)$ is the spectral phase. Eq. 2.6 and 2.8 are related through a Fourier transform. From Fourier theory it is well known that shorter pulses in time require a wider spectrum. However this is not the entire picture as broadband light sources do not always emit ultrafast pulses, the phase (or spectral phase) characteristics are also crucial. More accurately, the phase of each spectral component must be equal at some point in time for a pulse to exist. Fig. 2.10 illustrates this fact where waves of varying frequencies are added in two cases; with equal phase and random phase. In the equal phase case the fields constructively interfere at one point, making a pulse, and destructively interfere elsewhere. If the phases are random, such as a "light bulb"-like source, there is no coherent addition of the waves in time and the result is a noisy output, often averaging out to a continuous wave characteristic. The process of oscillating frequency components in phase with each other is often achieved in a method called **mode-locking**.

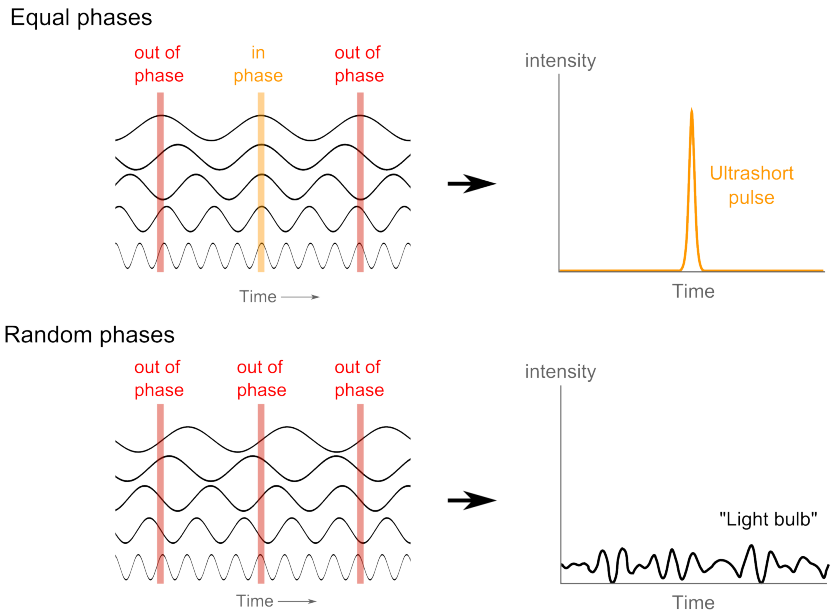

Figure 2.10: Producing an ultrafast pulse requires the coherent addition of many frequencies in phase (above). A broadband thermal source, e.g. a light bulb, has the potential to make ultrafast pulses but, because the phase distribution is so random, only a noisy temporal output is seen.

2.3.1 Mode-locked lasers

The temporal width of pulses from lasers initially had been limited to approximately the round-trip time of the cavity, the time scale of the laser dynamics, which is often on the order of nanoseconds. The first demonstration moving beyond this limit was demonstrated in 1964 which was later termed "mode-locking" [102]. Here, the loss inside the laser was modulated at exactly the round-trip time, which forced the longitudinal modes to oscillate in phase. It can be readily shown that a modulation of a frequency will lead to side-band generation which are in-phase with that of the original, and if this is done precisely at the cavity repetition rate, these side-bands will align with the longitudinal modes of the cavity allowing the build up of a pulse. This results in a series of spectral peaks that are in phase, Fig. 2.11, which combine to produce a train of pulses. This type of locking is called *active* mode-locking because direct modulation is required. At the time of this early demonstration the pulse width was not able to be measured as the detector speed used was limited to a rise time of $\approx$ 2.5 ns [102]. A pulse measurement technique called optical autocorrelation (described in Section 2.3.3) was developed soon after,

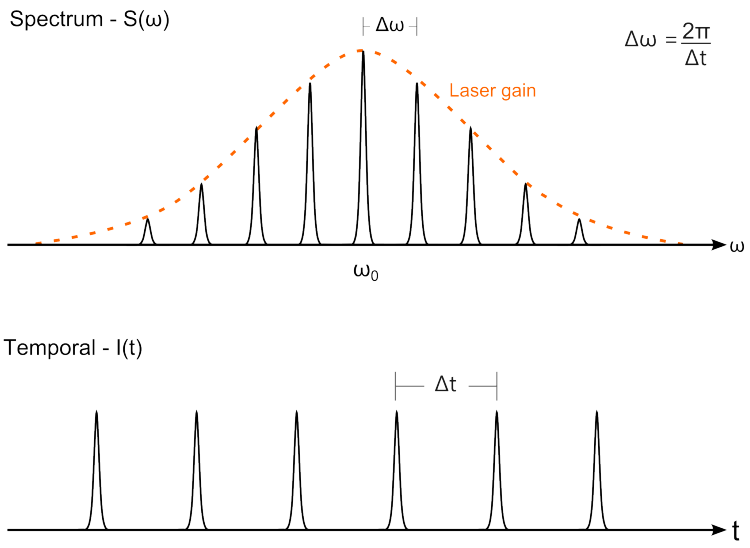

Figure 2.11: Concept of mode-locking a laser. (Above) The laser gain profile (orange, dotted) consists of a finite number of longitudinal modes set the by cavity size. If these modes oscillate in phase the temporal output (related by a Fourier transform) is a train of narrow pulses separated by Δt.

revealing that these mode-locked pulses had a full-width-half-maximum (FWHM) of 4 to 6 picoseconds [103].

Active mode-locking methods progressed with a thorough theoretical basis [104], however *passive* mode-locking methods were discovered which eventually led to shorter pulses. Passive methods achieve the same loss modulation induced pulse production, but use saturable absorbers to do this instead - materials with an intensity dependent absorption. Therefore the light field itself inside the cavity creates the loss per round-trip. Fig. 2.12 shows the typical absorption characteristic of such an absorber as a function of optical intensity. It was discovered that this absorption characteristic allowed the necessary amplitude modulation to force a laser into mode-locking [105]. Such a material will bias the laser to be pulsed (lower loss at higher peak powers), and if the cavity parameters are suitable, one single ultrafast pulse can traverse the cavity every round-trip. The first absorber used for mode-locking was cryptocyanine in methanol, since then dye lasers using Rhodamine 6G have produced 500 fs pulses [106], and more recently semiconductor materials are mostly used such as GaAs that have produced pulses less then 100 fs [107, 108]. More exotic materials that provide saturable absorption such as carbon nanotubes [109] and

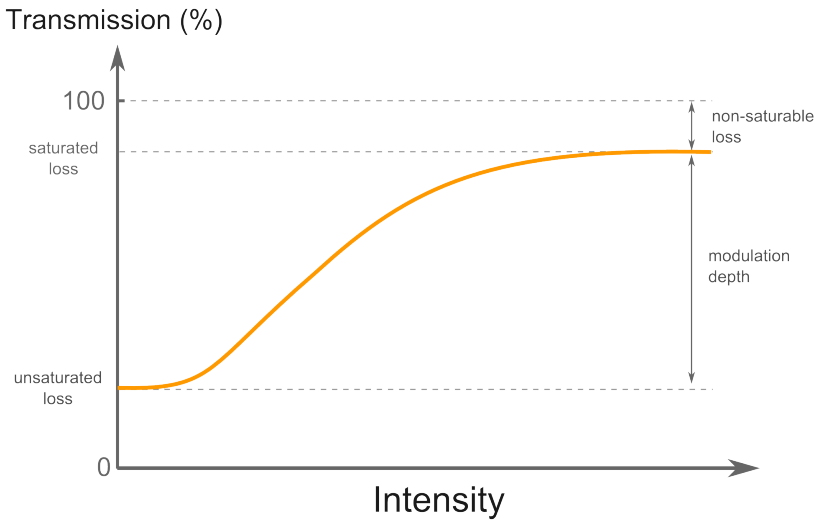

Figure 2.12: Transmission characteristic of a saturable absorber used for passive mode-locking. The transmission increases with optical intensity, with the difference between the two extremes defining the modulation depth of the absorber. This allows a bias towards higher peak power systems (pulsed), and can allow mode-locking to occur.

graphene [110] have also become heavily researched. Rather than using a physical absorber, some of the shortest pulses have been achieved using "effective saturable absorbers" using nonlinear optical effects such as nonlinear loop mirrors [111, 112], Kerr lens mode-locking [113], and nonlinear polarisation rotation [51]. These methods will be described in more detail in Chapter 5.

2.3.2 Cavity design for mode-locked lasers

Since the first demonstration of the mode-locked laser in 1964 [102] it has become evident that on top of the mode-locking mechanism, the specific design of the cavity is crucial to its performance. An intuitive understanding of the generation of short pulses was described in Section 2.3.1, however the precise dynamics of the process is complicated and involves effects of gain, dispersion, loss, nonlinearity and saturation effects. Group velocity dispersion (GVD), for example, is one crucial parameter to measure in the cavity which can ultimately determine the pulse width. In a previous study Ref. [113], a mode-locked Ti:Al_2O_3 laser system emitted 2 ps, but by reducing only the total cavity dispersion with the use of prism pairs, the pulses became as short as 60 fs. In fact, the overall sign of the GVD of the cavity determines the pulse dynamics.

In the case of anomalous second order dispersion ($\beta_2 < 0$) the dynamics typically follow soliton dynamics. Here the chirping effect induced by the anomalous dispersion is balanced by a nonlinear effect (self-phase modulation) to create a sech shaped pulse with a specific pulse width for a given energy. In practice as there are a number of other effects occurring, the pulse changes shape and power depending upon the position of the cavity. One method of modelling the effects of all these parameters is by using the cubic-quintic complex Ginzburg-Landau (CGL) equation which is generally written as:

$$i\frac{\partial A}{\partial z} + \frac{D}{2}\frac{\partial^2 A}{\partial T^2} + |A|^2 A + \nu|A|^4 A = i\delta A + i\epsilon|A|^2 A + i\beta\frac{\partial^2 A}{\partial T^2} + i\mu|A|^4 A \qquad (2.9)$$

Equation 2.9 describes the amplitude of the electric field (A) is it travels in the z direction based on a retarded time t. D represents second order dispersion, δ is the linear gain-loss coefficient, ν corresponds to the saturation of nonlinear refractive index, the term containing β (not to be confused with β_2) accounts for a finite parabolic spectral gain profile, ϵ represents nonlinear gain (related to saturable absorption), and μ is a measure of the saturation of nonlinear gain [114]. The CGL

equation describes a laser cavity in which all above effects are averaged out and take place simultaneously throughout the cavity, which is not the case in practice. Despite this, the equation accurately describes the on-set of complicated behaviours such as double pulsing and the on-set to chaotic dynamics [115]. Alternatively, mode-locked lasers are modelled using the generalised nonlinear Schrödinger equation (a subset of the CGL equation) where the effects of saturable absorption and nonlinear losses are applied abruptly at specific locations throughout the fibre [116]. In both approaches it is clear that the performance of the mode-locked laser is heavily dependant on various cavity parameters.

It is also worth mentioning that solitonic behaviour from anomalous dispersion is not necessary to generate ultrafast pulses. Several lasers have achieved ultrafast pulses from a cavity containing a net normal GVD. In the presence of nonlinearity, gain and normal dispersion pulses evolve in a self-similar fashion to a parabolic shape in time, known as a *similartion* [117]. A unique characteristic of these pulses is that even though they relatively broad pulses in time, they carry a linear frequency chirp, allowing for the pulse to be compressed with the use of dispersive optical elements. Pulses as short as 50 fs-level have been produced from a fibre laser system employing this effect [118]. The advantage in this work was that the pulse energy was up to two orders of magnitude higher than soliton based lasers. This is enabled due to the broadening of the pulse in time as it is amplified which avoids unwanted nonlinear effects, such as Raman scattering, which can lead to pulse break up [119]. An extension of these similariton lasers are known as the all-normal dispersion fibre lasers (ANDi lasers) which have a gain medium with normal dispersion and nonlinearity (giving rise to similariton dynamics) but also an extended cavity consisting of normal dispersion. These have shown fs-level pulse production with pulse energies reaching 200 times of what is available from soliton based lasers [120–122].

This shows that just considering second order dispersion alone, as one free parameter, gives rise to several regimes of ultrafast pulsed operation. Fig. 2.13 shows a map of various regimes described above depending on the sign of the group velocity dispersion (Image is an edited version from Ref. [123]). For fibre lasers operating at the near-infrared wavelengths, due to the availability of various optical fibres with both normal and anomalous dispersion, controlling the net group velocity dispersion in ultrafast lasers is relatively simple. It is more difficult to do this for the mid-infrared wavelengths as fibres and optical components operating at this wavelength regime is still in its infancy. As will be eluded to in Chapters 4 and 5, this remains a challenge for the performance of mid-infrared ultrafast fibre lasers, but certainly is a direction to be further explored in future.

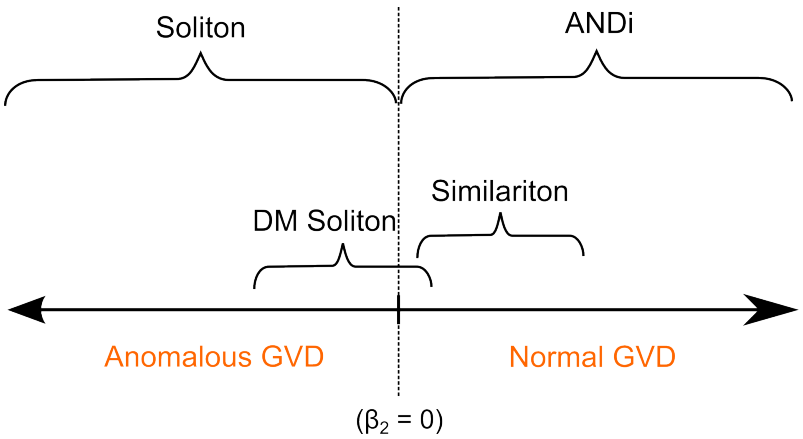

Figure 2.13: The net group velocity dispersion (GVD) of mode-locked laser cavity heavily determines the dynamics. For anomalous dispersion the dynaimcs follow soliton-like dynamics, whereas for normal dispersion pulses evolve in a self-similar (similariton) fashion. Both regimes are able to generate femtosecond scale pulses, however with different cavity parameters, which become important in the design of mode-locked lasers. Image is an edited version from Ref. [123].

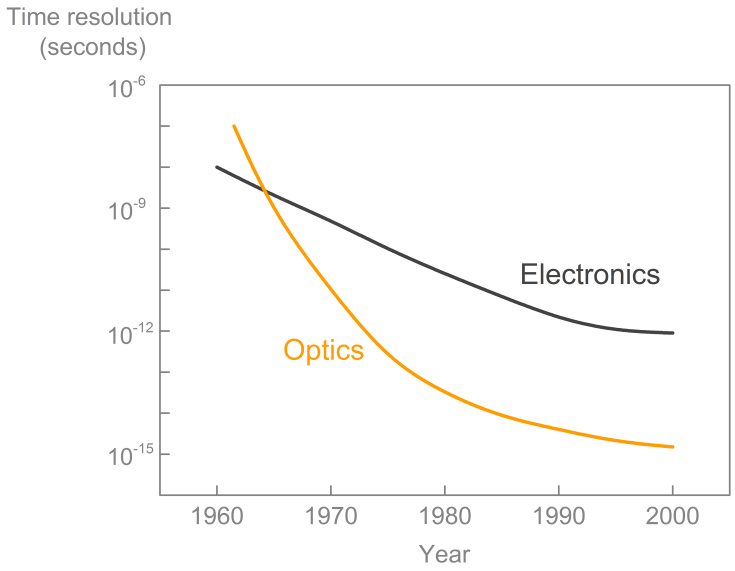

Figure 2.14: Characteristic time scales resolved by the two methods of electronics and optics between 1960 and 2000, figure courtesy of R. Trebino [124]. The speed of electronics remains at the picosecond level since 1990, whereas optics comfortably enters the femtosecond regime.

2.3.3 Measuring ultrafast pulses

The other major challenge after generating mode-locked pulses is measuring them, given that their pulse widths (typically picoseconds and shorter) cannot be resolved by currently available photodetectors. Fig. 2.14 shows the characteristic time resolution of electronic and optical devices that have been used. As can be seen, the speed of electronic devices begins to plateau at the picosecond level, whereas optical devices are reaching the femtosecond level. For example one of the fastest photodetectors today used in telecommunication systems has a bandwidth of 70 GHz, corresponding to a rise time of approximately 5 ps [125].

Intensity Autocorrelation

It was discovered that the pulse *itself* could be used to measure the pulse width, in a method known as optical autocorrelation [103]. In this method a pulse is split into two using a beam splitter, and then are superimposed temporally in a nonlinear medium. As a result, a new signal is produced from the overlap of the two pulses, which has a characteristic shape from which the pulse width can be estimated. It is

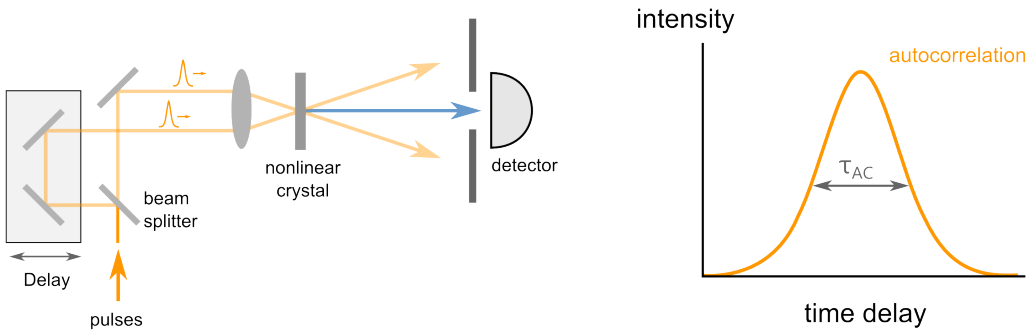

Figure 2.15: (Left) Schematic of an intensity autocorrelator. A pulse is split into two arms, where one is controllably delayed, and then recombined in a nonlinear crystal to generate an intensity-dependent signal. This signal is measured as a function of delay to produce an autocorrelation trace (right) to estimate the true pulse width.

important to point out that the nonlinearity does not serve as an ultrafast-response element, this resolution is achieved by using the ultrafast pulse itself to gate its own intensity. The resulting autocorrelation signal (as a function of the temporal overlap) is similar to that of a convolution of the two identical input pulses. Such an auotocorrelator is shown in Fig. 2.15, along with a typical measured signal. From the FWHM of this autocorrelation (τ_{AC}) the true pulse duration can be estimated. For example, in the case of a sech-shaped pulse, the pulse width is $\approx 0.65 \times \tau_{AC}$.

Autocorrelation methods have been adopted as a standard measurement of ultrafast pulses. Variations of the autocorrelation technique exist such as interferometric types which give some indication regarding the chirp of a pulse [126]. However, the autocorrelation fundamentally faces the following major disadvantages:

- The shape of the pulse has to be assumed prior to the measurement.
- The measurement is ambiguous.
- It does not reveal the pulse phase.
- The measurement can give rise to an artificial "coherent artefact".

Firstly, assuming the pulse shape before measurement already prevents autocorrelations from being a true pulse measurement. In some cases, such as when soliton dynamics are expected, a sech-shaped pulse is often assumed. However other shapes have different correction factors, e.g. for Gaussian pulses the duration is $\approx 0.71 \times$

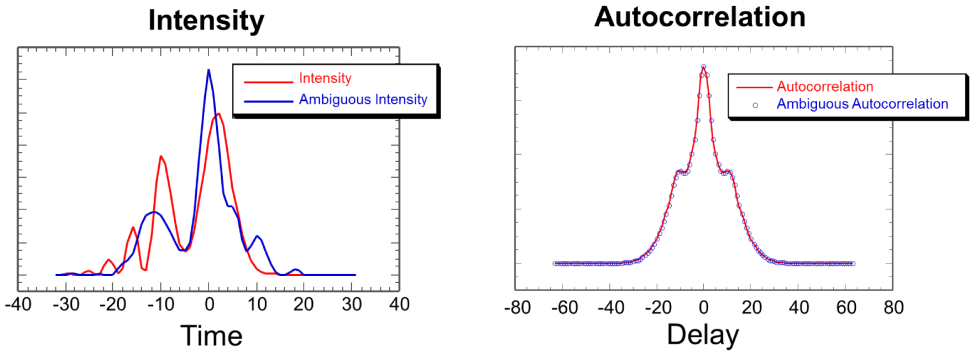

Figure 2.16: Autocorrelation traces can be ambiguous. Here two different pulse profiles give rise to a similar autocorrelation trace. Image adapted from Ref. [127].

τ_{AC}. In real systems it is rare that the pulse has such a well defined function, due to effects such as gain or loss in the cavity and high order dispersive effects.

The second problem with the autocorrelation is the measurement is not unique. Fig. 2.16 shows this directly with two different electric fields yielding the same autocorrelation signal. Moreover, as the autocorrelation is inherently symmetric it is not possible to determine whether the true pulse is asymmetric or not. Even when the autocorrelation trace looks clean, the true pulse can be substantially different. Fig. 2.17 shows two pulses with detailed structure giving a smooth autocorrelation, which could be confused from that of a Gaussian field profile. In short, the autocorrelation trace invites misinterpretation. The other obvious weakness of autocorrelations is that it does not measure the phase of the pulse.

On top of being an incomplete measurement, an autocorrelation can also give false information for complicated electric field distributions [128]. Fig. 2.18 shows the autocorrelations of a series of complicated pulses and it can be seen that the trace consists of a broad wing structure with a sharp "spike" at zero delay. Interpreting this spike as the pulse itself would give rise to a severe error in the true pulse shape and width. This is referred to as the "coherent artefact" and does not reveal any information about the pulse itself.

The problems associated with the optical autocorrelation is related to what are known as the "one dimensional phase retrieval problem" which states that it is impossible with this measurement to determine the electric fields uniquely. The challenge is to simultaneously measure the temporal intensity and phase, or spectral intensity and phase. Attempts to avoid doing this by combining information

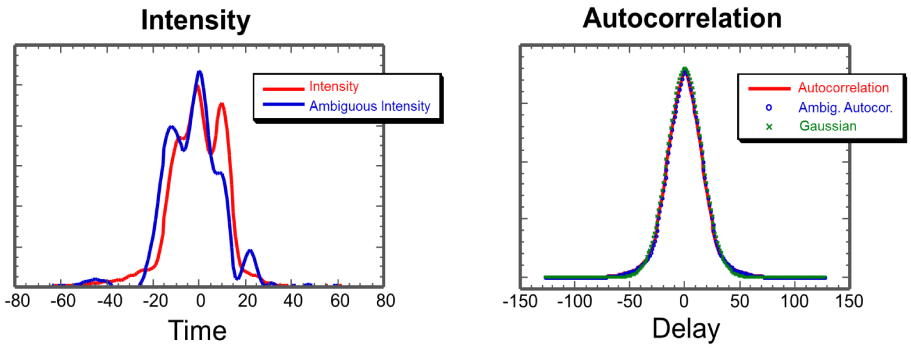

Figure 2.17: Autocorrelations traces can be misleading. Complicated pulses can give rise to a smooth looking autocorrelation that resembles that of a clean pulse. Image adapted from Ref. [127].

from the pulse spectrum and the intensity autocorrelation were suggested using an algorithmic approach [129], however this method was soon proven to still produce ambiguous results [130]. The only way to achieve a measurement of both inten-

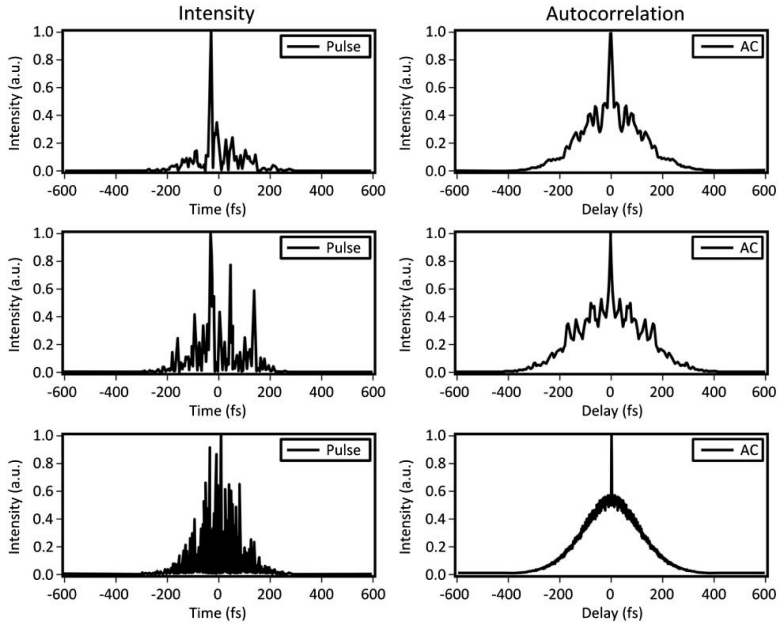

Figure 2.18: More complicated pulse profiles can give rise to a "coherent artefact" in the autocorrelation. This shows as a spike on top of a noise background which, if not careful, could be interpreted as an ultrafast pulse. Image adapted from Ref. [128].

sity and phase is to convert the problem into a "two dimensional phase retrieval problem", known to have unique solutions, using a technique known as Frequency Resolved Optical Gating.

Frequency Resolved Optical Gating

A method for uniquely determining the pulse information first appeared in 1993 in a technique known as Frequency Resolved Optical Gating (FROG) [131]. Surprisingly, the setup of such a measurement device is similar to that of intensity autocorrelations, Fig. 2.19, however the detector is replaced with a spectrometer (creating a spectrally-resolved-autocorrelation). The spectrum of the nonlinear signal is measured as a function of delay, producing a 2D map of intensities called a spectrogram. Although experimentally similar, the spectrogram contains profoundly different information compared to an autocorrelation.

Mathematically the spectrogram (I) is a function of frequency (ω) and time (t) is given by:

$$I(\omega, t) = \left| \int_{-\infty}^{\infty} E(t)\delta(t-\tau)\exp(-i\omega t)dt \right|^2 \tag{2.10}$$

$$= \left| \int_{-\infty}^{\infty} E(t)E(t-\tau)\exp(-i\omega t)dt \right|^2 \tag{2.11}$$

where $\delta(t-\tau)$ is the gating function, which in both the autocorrelation and the

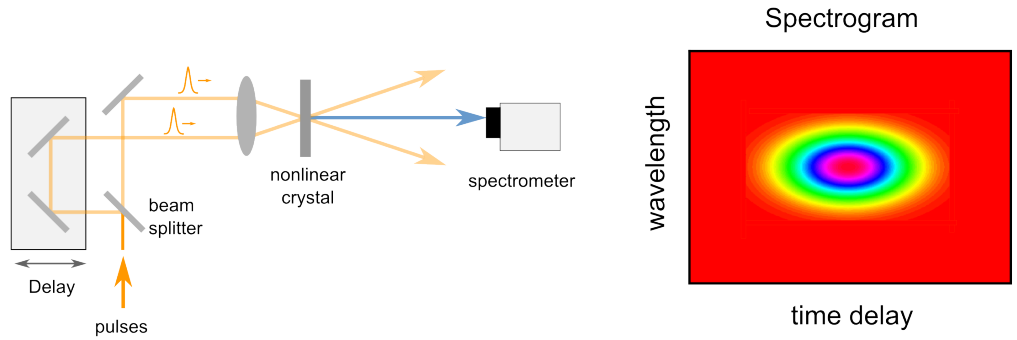

Figure 2.19: (Left) Schematic of Frequency Resolved Optical Gating (FROG) set up. The measurement is similar to an intensity autocorrelation, except the detector is replaced with a spectrometer. The resulting measurement, called a spectrogram (right), is a two dimensional function of wavelength and delay.

FROG is the pulse itself, E(t). When the gate function is known, the spectrogram can be inverted to retrieve the field function. However since in this case the gate function is also unknown, the problem becomes more difficult, but still possible. We first rewrite the above equation into form which is known to be solvable, by introducing a new field $E_{sig}(t,\tau) \propto E(t)|E(t-\tau)|^2$. If we can solve for this new signal it is easily shown that its Fourier transform, $\widehat{E}_{sig}(t,\Omega)$, is proportional to E(t) by setting $\Omega = 0$. Using this definition we can rewrite Eq. 2.11 as

$$I(\omega,\tau) = \left| \int_{-\infty}^{\infty} E_{sig}(t,\tau) \exp(-i\omega t) dt \right|^2 \tag{2.12}$$

$$= \left| \int_{-\infty}^{\infty} \int_{-\infty}^{\infty} \widehat{E}_{sig}(t,\Omega) \exp(-i\Omega t) d\Omega \exp(-i\omega t) dt \right|^2 \tag{2.13}$$

$$= \left| \int_{-\infty}^{\infty} \int_{-\infty}^{\infty} \widehat{E}_{sig}(t,\Omega) \exp(-i\omega t - i\Omega t) \ dt d\Omega \right|^2 \tag{2.14}$$

By introducing the E_{sig} term and representing it as its Fourier Transform the spectrogram is now written as a double integral. Given that $I(\omega,\tau)$ is a measured quantity, what remains is to perform a double-integral inversion algorithm to find $\widehat{E}_{sig}$, which will give us the field E(t). This specific problem is well known as the two dimensional phase retrieval problem and has been extensively studied in imaging sciences [133]. The problem has essentially unique solutions, meaning there are a few ambiguities but they are trivial (such as a solution with an infinite field distribution). From these studies the measured spectrogram can be inverted using known algorithms to reconstruct the field intensity and phase. An example of this is shown in Fig. 2.20 showing the measured spectrogram, from which the electric fields (both temporal and spectral) are fully retrieved. The accuracy of the process can be quantified in the FROG retrieval by comparing the difference between the measured and retrieved spectrograms.

FROG measurements have since proven to be the most accurate methods of carrying out pulse measurements [134, 135]. Not only does it reveal the phase, FROG measurements can also handle complicated pulses without producing a coherent noise spike. Fig. 2.21 shows a highly structured pulse in time (a) and its associated intensity and interferometric autocorrelations (c, d) - showing the unwanted coherent noise spike. However, the spectrogram (d) can be seen to also have detailed structure, accurately capturing the characteristics of the pulse. These measurements have proven to be so accurate that they can even resolve the temporal profile

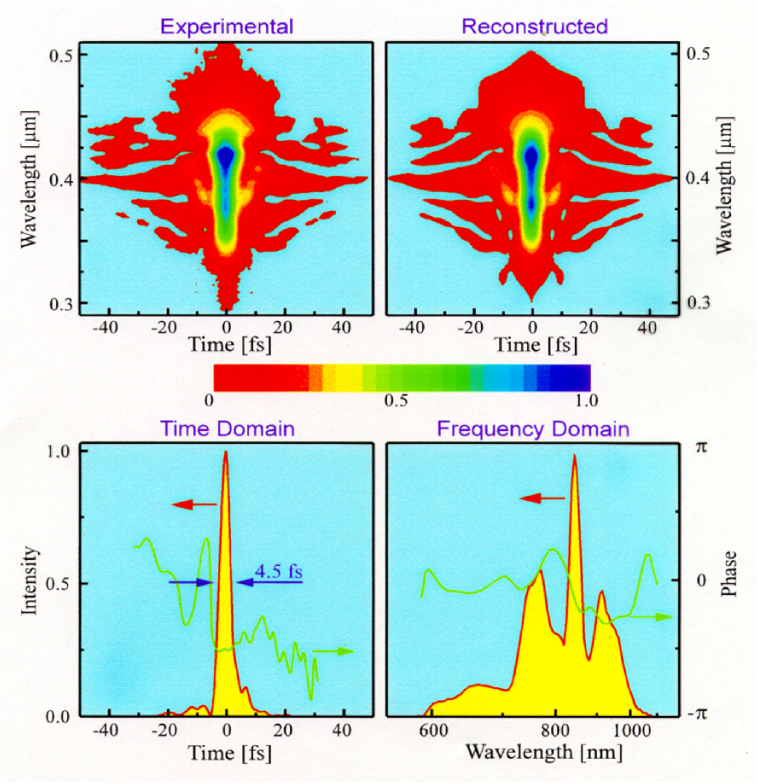

Figure 2.20: An example of a pulse field retrieval using FROG. The measured spectrogram is inverted using algorithms to retrieve the pulse in the time and spectral domain, along with the phase. The resulting retrieved spectrogram is compared to the measured in order to quantify the error in the measurement. Image adapted from Ref. [132].

of pulses generating a supercontinuum spectrum. These are pulses that have experienced highly nonlinear effects that broaden their spectrum over an octave. As a result their temporal profiles become highly distorted, nonetheless, successful pulse retrieval has been achieved [136].

It is undoubtable that a FROG measurement is the most accurate way to measure the pulse correctly. This method will become significant in Chapter 5 where I measure the complete field of the generated ultrafast pulses. In the remaining Chapters I will describe the approach taken towards the primary goal of this study, which was generating ultrafast pulses, and the use of the FROG technique to accurately measure the characteristics of these pulses.

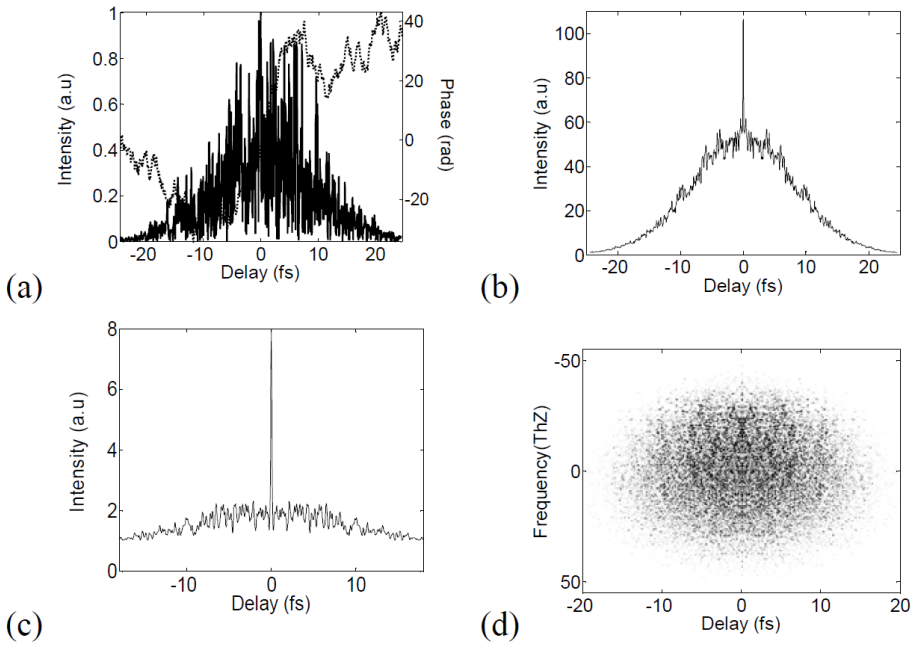

Figure 2.21: The FROG is able to resolve features of complicated pulse. A complicated pulse in time (a) gives rise to the coherent noise spike for intensity (b) and interferometric (c) autocorrelations, whereas the spectrogram (d) contains detailed structure of the initial pulse. Image adapted from Ref. [137].

Chapter 3

Q-switching Holmium Fibre Lasers

Pulses at the nanosecond regime

This Chapter refers to the work that was carried out in references [138, 139].

As discussed in Chapter 1, moderate power cw mid-IR fibre lasers have become well established. Of interest to my studies however was the ability to pulse these lasers, which remained a relatively unexplored area at the time. Pulsed lasers operating at visible to near-IR wavelengths, that emit the majority of their power in a short amount of time, have shown usages in many fields from biomedical imaging, industrial processing to nonlinear optics. In order to exploit the advantages of pulsed lasers in the mid-IR, I began by looking at the fundamental methods. The early studies , which were performed in 1962 were ruby lasers in specific arrangements which produced "giant optical pulses", several orders of magnitude larger than spontaneous pulses due to noise [140]. This physical process is known as *Q-switching*, and in this chapter I will discuss the work done in an effort to producing energetic pulses from a mid-IR fibre laser.

3.1 Principle of Q-switching

Instead of externally modulating a laser beam to make pulses, which merely result in "pulses" with a peak power equal to the cw power, by controlling the internal losses of a laser cavity one can produce extremely intense pulses. As the name suggests, Q-switching refers to directly modulating the cavity Q (defined in Chapter 2). A laser cavity containing a loss-modulator, which can be of many forms, is generically shown in Fig. 3.1. In order to Q-switch, this loss is increased above the gain per round trip, suppressing lasing, while the population inversion is maximised. This loss is then removed, rapidly providing strong feedback to the cavity, which results in the production of a giant pulse that sweeps through the cavity. Thus by doing this in a periodic manner a train of giant Q-switched pulses can be produced.

The loss modulation can be performed in a variety of different ways. The initial demonstration employed a Kerr-cell which rotated the polarisation of light in the cavity in order to make the gain crystal less efficient (and hence, introducing a relative loss). Other methods used mechanical shutters [141, 142], rotating mirrors [143], and electro-optic modulators [144] to achieve similar results. The methods mentioned so far are all known as *active* Q-switching but there are also *passive* Q-switching techniques which use saturable absorbers. This is discussed more in Chapter 4, but in this section we consider only active Q-switching which provided

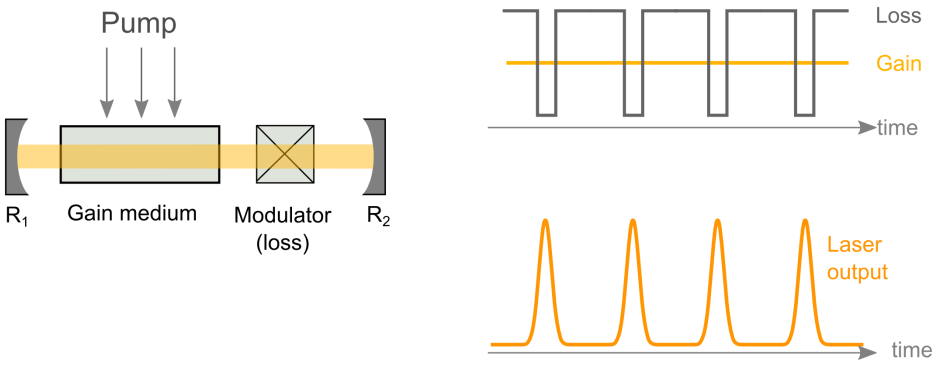

Figure 3.1: General layout of a Q-switched laser. (Left) A laser resonator containing a gain medium and an incavity loss modulator surrounded by two mirrors with reflectivities R_1 and R_2. (Right, upper) Time evolution of loss modulator which switches the loss above and beyond the available gain (Right, lower) Resulting output of laser producing Q-switched pulses soon after the loss is dropped below the available gain.

stable and shorter pulses.

In order to control the Q-switching dynamics, such as rate of loss modulation, one effective method is through the use of the acousto-optic effect. This allows for fast and tunable loss modulation and has low risk of optical damage through excessive absorption of light in the modulator.

3.2 Acousto-optic effect

3.2.1 Basic principle

Rather than inserting a loss modulator to absorb the light, which could be problematic at high power operation due to thermal effects, a preferred method is to *eject* the light from the cavity. The 'acousto-optic effect' allows this to be carried out in a controllable fashion without the need of moving mechanical components - by using sound waves inside a medium to diffract light in a certain direction. As sound waves are travelling compression waves, in certain materials this periodic density variation leads to variations in the refractive index of the material. This periodic change in the refractive index forms a Bragg grating, which is known to diffract light at certain angles. Fig. 3.2 shows this process with an input beam with power P_0 which is then diffracted by the acousto-optic device into the diffracted beam with power P_D. In practice, some residual light is transmitted through the device with power P_T as the process is not 100 % efficient. Thus by modulating the sound waves the device can act as an acousto-optic modulator, where the power can be switched between the transmitted and diffracted beams. By inserting this device into a laser cavity one can eject the beam from the cavity, inducing a high cavity loss, and can then create a Q-switched pulse by switching off the diffraction loss. For the diffraction to occur the Bragg condition must be met which is given by Eq. 3.1,

$$\sin\theta_B = \frac{\lambda}{2\Lambda} \tag{3.1}$$

Here λ is the wavelength of the light, and Λ is the wavelength of the sound waves inside the modulator. The efficiency of the acousto-optic deflector is defined as $\eta = P_D/P_T$, which ideally is 100%, but more typically around 80-90% for commercial products. The dependence of this efficiency to the input angle θ for a crystal of length L follows a sinc function of the form,

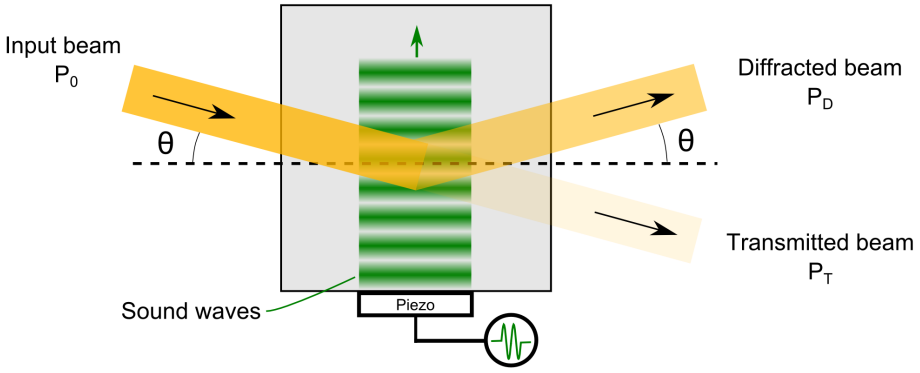

Figure 3.2: Principle of the acouto-optic effect. An input beam with power P_0 enters a material at an angle θ, which diffract off a compression wave of frequency ω, exiting at an angle θ. The efficiency of the process is defined by the ratio of the residual transmitted power to the diffracted beam power.

$$\eta = \eta_0 \ \text{sinc}\left[\frac{2L(\sin\theta - \sin\theta_B)}{\lambda}\right] \tag{3.2}$$

where η_0 is the peak efficiency of the AOM when the Bragg condition is met.

3.2.2 Characterising the TeO_2 acousto-optic crystal

In order to Q-switch the holmium-based fibre lasers we needed an acousto-optic material that was transparent for the mid-IR wavelengths. Tellurium dioxide (TeO_2) has a transparency out to 4.5 μm [145] and is used often as an acousto-optic device for lasers around 2 μm [146], but the performance at longer wavelengths was needed to be measured. At too low diffraction efficiencies the loss induced for Q-switching may not be high enough to prevent laser oscillation in the cavity. The crystal was approximately 2 cm long with a piezo-modulator attached to one side which oscillated at 41 MHz to create travelling compression waves through the crystal. This signal could be electronically controlled so that the AOM could be modulated at specific rates, later used for Q-switching. The first stage was to characterise the performance of this TeO_2 modulator at 2.86 μm using cw light generated from the holmium fibre laser.

The optical transmission of the TeO_2 crystal was measured as 85%, with the loss attributed to Fresnel reflections from the sides of the crystal. The crucial parameter

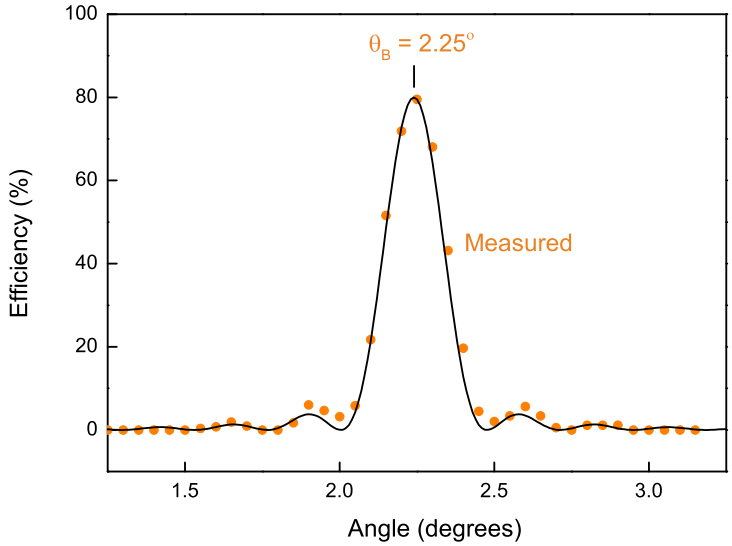

Figure 3.3: First order diffraction efficiency of the TeO_2 AOM at 2.86 μm as a function of beam input angle. A maximum efficiency of 80% was achieved at the Bragg angle of $\theta_B = 2.25°$

was the efficiency of the process, i.e the ability to shift power into the m = +1 order. As seen by Eq. 3.2 this is dependent on the input angle θ, so the AOM was rotated and the efficiency was measured. Fig. 3.3 shows the measured efficiency as a function of angle, fitted with the theoretical function from Eq. 3.2. As with most AOMs, efficient power diffraction occurs within only a small window of input angles from 2.0 - 2.5°. A maximum efficiency of 80% was achieved at the Bragg angle of 2.25°. This efficiency, although not ideal, was determined suitable for Q-switching as similar studies producing the shortest pulses was achieved with an AOM efficiency of approximately 50% [74].

3.3 Q-switching from the 0th order

As the efficiency and transmission was suitable for the AOM to be inserted into a laser cavity, a function generator was used to modulate the sound waves in a square wave pattern to allow the rapid periodic ejection of light from the cavity. The frequency of this will be referred to as the "switching rate" (Ω). For this work we used a $Ho^{3+}Pr^{3+}$-doped ZBLAN fibre, with a cross section as shown in Fig. 3.4.

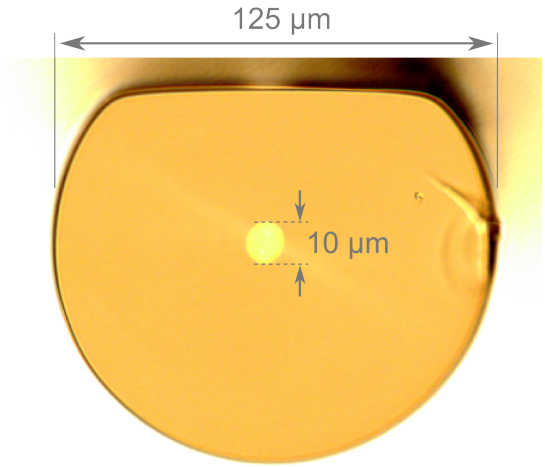

Figure 3.4: Cross sectional view of the ZBLAN fibre used for the work presented in this chapter. The doped core has a 10 μm diameter and a D-shaped cladding with diameter 125 μm.

This had a double-clad geometry where the core diameter was 10 μm, surrounded by a D-shaped cladding with a diameter of 125 μm. The dopant concentration of the Ho^{3+} and Pr^{3+} in the core was 30,000 ppm and 2500 ppm molar respectively.

This fibre was used as the gain medium for the Q-switched laser, in a set up shown in Fig. 3.5. The cavity consisted of a 4 meter long doped fibre (purchased from Fiberlabs Inc.), where the cavity reflectors are formed by the small Fresnel reflection from the front fibre tip, and a highly reflective gold mirror (R > 95%) the other side of the cavity, after passing through the TeO_2 AOM.

The cavity was pumped by two diode lasers at 1150 nm (Eagleyard Photonics) that provided up to 4 W of linearly polarised light each. The two diode outputs were multiplexed through a polarising beam splitter (PBS) and coupled into the fibre using a ZnSe lens (f = 6 mm). The highly reflective mirror was aligned to provide feedback from the 0th order of the AOM (the undeflected beam). The output was taken out using a dichroic mirror at the front end that was highly reflective for 2.9 μm at 45°, and highly transmitting at 1150 nm to preserve the pumping from the diodes. This specific arrangement where the cavity is formed by the Fresnel reflection ($\approx$ 4%) on onside and a high reflector (> 95%) was chosen for the work in this chapter as it has proven to be one with the highest efficiency [94], and directly comparable to the pioneering work done in this field [74].

A radio-frequency (rf) signal at 41 MHz drove the piezo-oscillator to create the

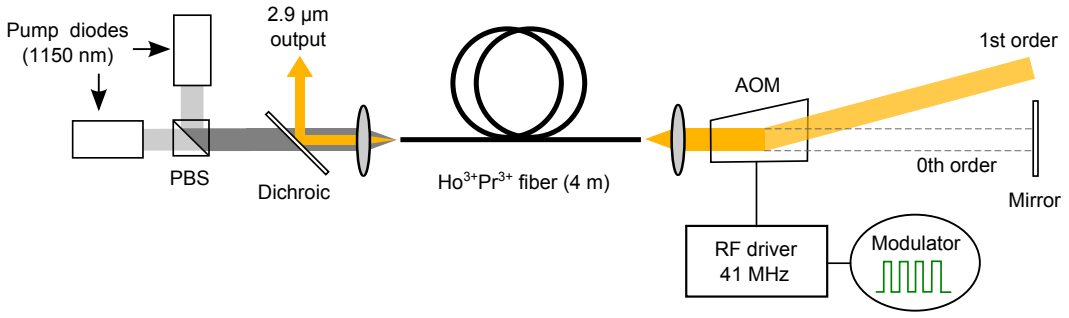

Figure 3.5: Schematic of the Q-switched 2.9 μm fibre laser. The laser is pumped by two diode lasers emitting at 1150 nm into 4 meters of $Ho^{3+}Pr^{3+}$ doped ZBLAN fibre. The cavity is extended to a high reflector and the AOM ejects the beam from the cavity in the first order to control the feedback from the mirror, allowing Q-switching dynamics.

compression waves in the AOM, and was modulated with a square wave pattern with a 50% duty cycle (on-off keying) using an electrical function generator over a range of 0-400 kHz. Therefore during the 'on' time the AOM held off the lasing in the cavity via first sorder diffraction, allowing the population inversion to maximise. As the AOM was switched 'off' the cavity suddenly was made to experience a strong feedback via the 0th order, creating a Q-switched pulse. It is worth mentioning this configuration faces a disadvantage as a small amount of feedback always exists from the 0th order path since the AOM was only 80% efficient. This is addressed in Section 3.4, however for direct comparison to the most recent results of 3 μm class Q-switched fibre lasers at the time [74], this set up was initially tested.

While the AOM was switched off, the laser operated in a continuous wave mode. Measuring the output power in this state yielded a maximum output power of 720 mW, giving an efficiency with respect to the launched pump power of 20%. This under performs the previous similar investigations which achieved an efficiency of 28.5% [94], a result most likely due to the transmission losses from the AOM inside the cavity. Once the AOM was modulated the laser was operated in a Q-switched mode and the pulses were measured using an InAs photodetetctor with a bandwidth of 10 MHz. The measured pulse repetition rate from the laser matched that of the AOM switching rate, as expected for active modulation. A typical temporal output is shown in Fig. 3.6, at a rate of 88 kHz. A series of sharp pulses can be seen, with the inset single pulse width of 83 ns (FWHM). The shortest possible pulse was 78 ns achieved at a repetition rate of 120 kHz, having a calculated peak power of 77 W.

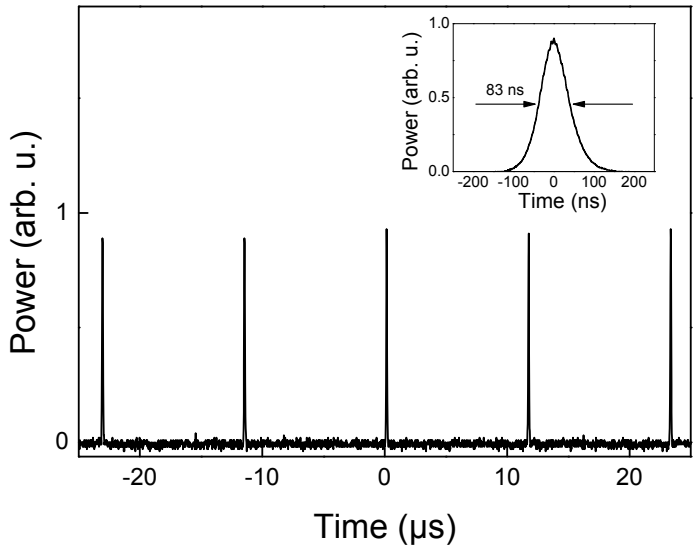

Figure 3.6: Typical temporal output of the Q-switched fibre laser. Pulses are produced here at a repetition rate of 88 kHz, inset shows a single pulse with a width of 83 ns.

As the AOM switching rate was increased from 0 to 400 kHz it was found that there were certain windows where stable Q-switched pulses would be produced, which also depended on the amount of pump power provided. For example, with a fixed pump power of 0.38 W, stable Q-switched pulses were produced for switching rates of 35 - 70 kHz. However at an increased pump power of 3.63 W the stable switching rates were from 120 - 300 kHz. This change in the switching rate and power effected the pulse widths also, and typically the shortest pulses were produced at the lowest switching rates and higher powers. The relation between these parameters are displayed in Fig. 3.7, showing the points of stable of repetition rates and their corresponding pulse widths, for certain pump powers.

All levels of pump powers showed a linear increase in the pulse width for increasing repetition rates, a typical feature of Q-switched lasers. Beyond the stable window, multiple pulses formed outside the switching times of the AOM resulting in an unstable pulse train. This behaviour can be understood by considering two characteristic times of; the AOM switching (τ_{switch}), and the pulse buildup time ($\tau_{buildup}$). For lower frequencies, τ_{switch} was long enough for the small feedback from the 0th order (from the residual light in the 0th order caused by the imperfect AOM efficiency) to build and cause parasitic lasing. At too high switching rates $\tau_{switch} << \tau_{buildup}$, the feedback was switched off before the gain medium could be

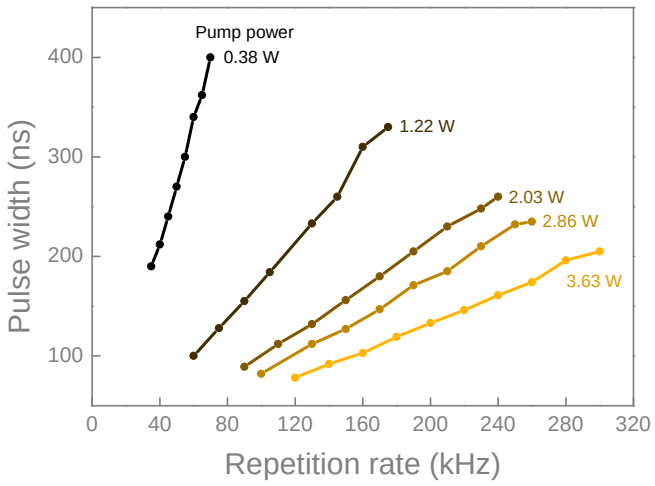

Figure 3.7: For a given pump power, Q-switching is only stable for a window of repetition rates. Too high switching rates does not give the cavity enough time to build up light, too low switching rates resulted in multiple pulse build up. This window shifts to higher frequencies as the pump power is increased.

maximally pumped, and resulted in pulses of different profiles - unstable output. As seen from Fig. 3.7 the stable range of pulses shifts towards higher repetition rates with pump power. This is also consistent with the description provided since the $\tau_{buildup}$ becomes shorter for higher pump powers. The lower limit increases as extra power causes the onset of parasitic lasing to occur earlier, and higher repetition rates are available due to the build-up time being shorter.

The optical spectrum of the pulses was measured using a scanning monochromator and is shown in Fig. 3.8(left). A spectral peak at 2867 nm was measured and corresponds to the $^5I_7 \rightarrow {}^5I_8$ transition of Ho^{3+}, with a width of 9 nm. Although the spectrum is quite wide compared to the pulse width, due to the slow scanning speed of the monochromator, it is likely the spectrum may have been unstable and that this measurement was an ensemble of various spectra. With the current configuration the maximum average power able to be produced was 720 mW which was limited by the output of the pump diodes. This corresponded to a launched power efficiency of 20%, as shown in Fig. 3.8(right).

In this demonstration active Q-switching of the 2.86 μm $Ho^{3+}Pr^{3+}$ transition was shown for the first time [138]. Although the highest reported peak power at these wavelengths was 0.9 kW from a multimode fibre [74], this current system

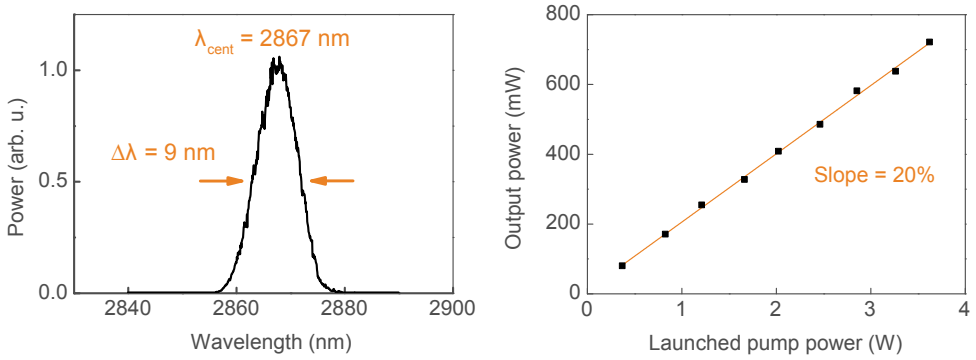

Figure 3.8: (Left) Spectrum of Q-switched laser output, centered at 2867 nm and having a bandwidth of 9 nm. (Right) Output average power as a function of launched pump power, yielding a slope efficiency of 20 %.

demonstrated the higher efficiency from a single mode fibre, producing the shorter pulses at 78 ns. This marks the first step towards the generation and detection of pulses near the 3 μm wavelengths. There were two limiting factors in the design of this Q-switched laser. Firstly, as mentioned before, the residual light in the 0th order provided a small, yet significant, amount of feedback. Second, the perpendicularly cleaved fibre end inside the cavity was also likely contributing to some unwanted feedback causing a cw background. Although this background is not evident from the temporal traces in Fig. 3.6, it may have effected the peak power calculations, given that it contributes to the average power used to determine the peak power. As mentioned earlier this specific geometry was chosen for direct comparison of the holmium Q-switched fibre laser to similar published erbium studies [74].

3.4 Q-switching from the 1st order - background free

After the demonstration of the 0th order Q-switching in the $Ho^{3+}Pr^{3+}$ laser we moved to creating an optimized design. In order to do this we changed the cavity feedback to come from the first order diffraction of the AOM instead. This ensured that while the lasing is held off, there was absolutely no feedback. We also used a shorter length of fibre so the Q-switched pulse can develop faster to ensure there was no limitation set by the cavity round-trip time (which relates to the pulse build up time). In addition to above changes we also angle cleaved the fibre facet inside

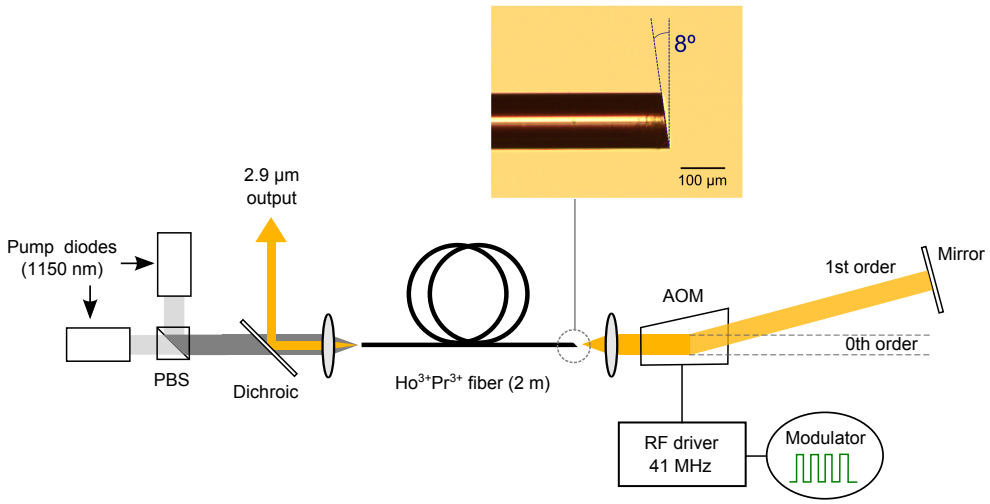

Figure 3.9: Schematic of Q-switched fibre laser used in 1st order diffraction mode to achieve higher performance. The in-cavity fibre tip was angle cleaved at 8°to prevent parasitic lasing, and the high reflector was placed at the 1st order diffraction of the AOM.

the cavity to prevent any Fresnel reflection coupling back into the fibre that may have created a cw background. Although the technique of angled cleaving has been long known as a method to prevent back reflections in optical fibres, a consistent method for cleaving ZBLAN fibres was needed to be developed, and was crucial for the majority of the work done in this thesis. Given the NA of the fibre was 0.25, an angle cleave of at least 7.5°was required to suppress back reflection to feedback into the core. As ZBLAN is a soft-glass the cleaving technique is relatively difficult however could be performed using a standard York FK-12 angled cleaver (tension levels of 40 g and an angle setting of 12 °gave the desired result).

The above modifications were made to the Q-switched laser cavity as illustrated in Fig. 3.9. It was similar to the previous setup however the feedback was now provided from the first order diffracted beam. Though there is a loss in power due to the imperfect efficiency (80%) of the first order, while the AOM is off 100% of the light is in the zeroth order which does not feedback to the cavity. An inset shows an image of the fibre tip with an angled cleave of 8°. The fibre had the same geometry and dopant concentration to the previous laser, however the length was reduced to 2 m. Finally due to the expected shorter pulse widths, the previous detector was replaced with an InAs detector of bandwidth quoted to be 64 MHz (rise time of 5.5 ns).

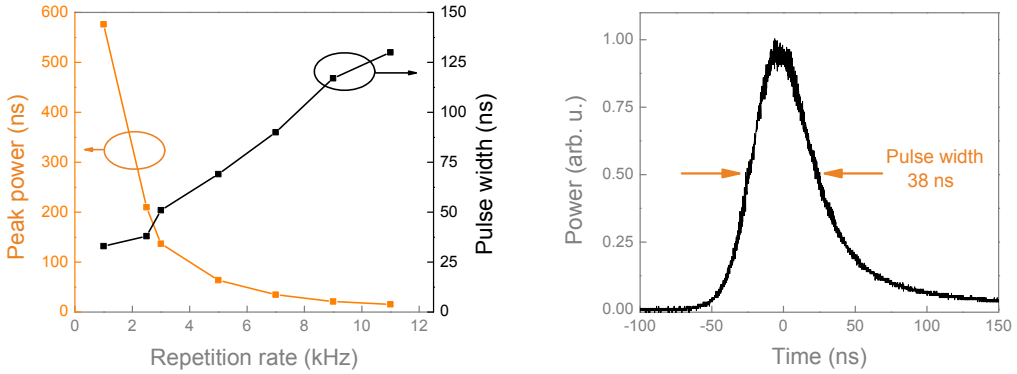

Figure 3.10: Output characteristics of the Q-switched laser used in first order diffraction (Left) Highest peak powers and shortest pulses were achieved at the lowest switching rates (Right) Single pulse trace showing a 38 ns FWHM.

Due to the new geometry Q-switching was achieved with an improved performance. First, while the AOM was switched off no laser light was produced due to the lack of feedback to the cavity, and only amplified spontaneous emission was measured at the output. Once the modulation was provided, stable Q-switched pulses were produced similar to the previous demonstration. With the unwanted feedback now removed, the Q-switching was stable at much lower repetition rates compared to the work in Ref. [138]. At a pump power of 0.34 W, Q-switched pulses were produced at 1 - 11 kHz and the corresponding pulse widths and peak powers are shown in Fig. 3.10(left). As expected from the previous work the pulse width increased with repetition rate, whilst the average power remained constant. The shortest pulse was produced at 1 kHz with a width of 33 ns, and a corresponding peak power of 576 W. A single pulse profile is shown in Fig. 3.10(right) with a width 38 ns. The asymmetric shape can now be seen which is typical of Q-switched pulses [85].

The pulse width of 33 ns is the shortest Q-switched pulse produced from a 3 μm class fibre laser [139]. Our results are now comparable with the highest peak power of 900 W which was produced from a multimode Er^{3+}-doped ZBLAN fibre laser. The two improvements of angle cleaving and use first order feedback were studied separately. Preventing the feedback from the fibre tip eliminated any background cw light to exist between the pulses. Changing the AOM arrangement ensured there was no prelasing from the cavity mirror, allowed lower repetition rates, and hence higher peak powers. A significant advantage of our laser system compared to Ref. [74] is the single-moded nature of output, which allows efficient coupling into

fibres and planar waveguides.

3.5 Summary

The primary goal of this project was to create and measure ultrafast pulses from a mid-IR fibre laser. In this chapter we have demonstrated the method of Q-switching to produce pulses on the scale of 10's of ns. This is marks the first steps towards achieving ultrafast pulses, where eventually we would like to move to picosecond pulses and shorter. The foundations were laid using active Q-switching using an AOM, and optimisation lead to a maximum pulse peak power of 575 W from a 33 ns pulse. The two key results of this Chapter, shown in Table 3.1, are in agreement with the underlying theory of Q-switched lasers referred to in Section 3.3. By optimising the cavity design we allow stable oscillation of the cavity at lower repetition rates, which allows maximising the gain, which results in a shorter pulse. If prelasing effects are removed completely the pulse width limitation using Q-switching is limited a scale of round trip time of the cavity - which would be 9.3 ns in this work. In the context of nonlinear optical effects as an application for this laser, we are now reaching the required peak power. However typically kW's of peak power is desired to see significant effects. This is due to the inherent coupling and transmission losses when entering a nonlinear medium (such as waveguides or fibres). Moving to other methods, such as mode-locking, not only allows for shorter pulses with higher powers, but also open applications in metrology via the use of frequency combs, as was mentioned in Chapter 1 - Section 1.3. Therefore although these are the shortest, most efficiently, generated Q-switched pulses near 3 μm there is more space to explore - towards even shorter pulses.

Method	Repetition rates	Pulse width	Peak Power	Ref.
Zeroth order	40-320 kHz	78 ns	77 W	[138]
First order	1-11 kHz	33 ns	575 W	[139]

Table 3.1: Summary of pulse parameters achieved from active Q-switching the $Ho^{3+}Pr^{3+}$ doped fibre lasers. These mark the first results towards achieving ultrafast pulses from a mid-IR fibre laser.

Chapter 4

Saturable absorber mode-locking

Picosecond pulse generation

This Chapter refers to the work that was carried out in reference [147].

In the previous chapter, we presented experiments and results on the generation of nanosecond level pulses using Q-switching techniques. However as described in Chapter 2, in order to produce ultrafast laser pulses, the method of mode-locking is needed to be investigated. Here we establish the primary method of mode-locking a fluoride fibre laser in terms of cavity design and measurements to confirm the stability. Prior to this investigation, passive mode-locking near 3 μm fibre lasers had been reported in two cases; using $Ho^{3+}Pr^{3+}$ [148] and the Er^{3+} [149] doped ZBLAN fibre lasers. However in both cases it was questionable if stable mode-locking had been achieved, and further investigation was required.

4.1 The issue with linear cavities

In the first case, Ref. [148], partial mode-locking was only claimed because the resulting pulses were unstable. In this study a linear cavity containing an InAs semiconductor saturable absorbing mirror (SESAM) was used to mode-lock the laser. By focusing the in-cavity light onto the SESAM, as shown in Fig. 4.1 (above), the intensity dependent reflection created a bias towards pulsed operation and resulted in train of pulses at the repetition rate of the cavity. However the measurements did not satisfy a crucial parameter for mode locked lasers - a strong mode-locked beat signal. This is measured by the radio frequency signal-to-noise ratio (rf SNR) of the pulse repetition rate. Here this value was 50 dB, whereas typical stable mode-locked systems have $>$ 60 dB. As a result only partial mode-locking was claimed by the authors. Nonetheless, an intensity autocorrelation measurement was made revealing a pulse width of 24 ps. In the latter demonstration, Ref. [149], a similar cavity was employed with an Er^{3+}-doped ZBLAN fibre laser Fig. 4.1 (lower), using a Fe:ZnSe crystal for the saturable absorber, also resulting in the produc-

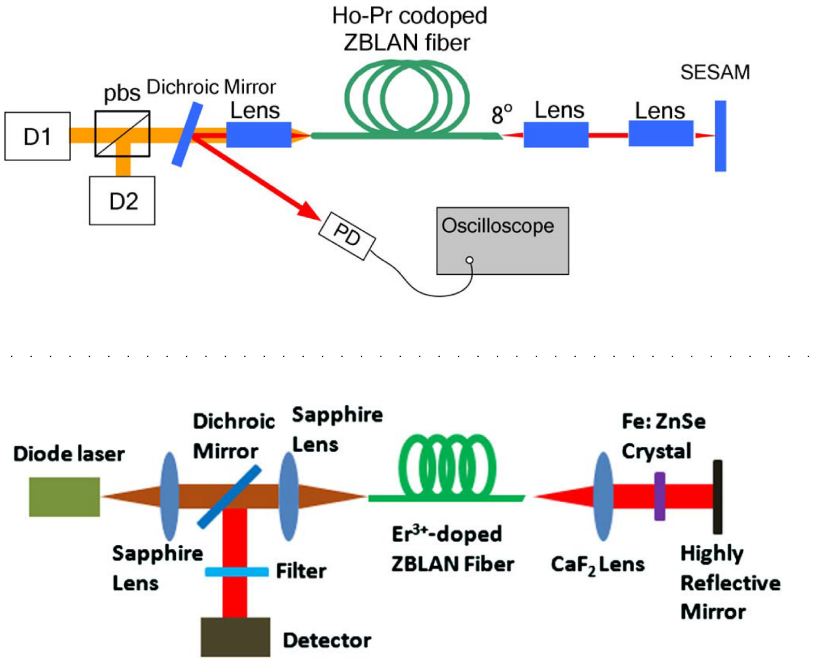

Figure 4.1: Experimental layout of two previously reported passively mode-locked 3 μm fibre lasers. (Above) A $Ho^{3+}Pr^{3+}$ fibre laser operating at 2.86 μm passively switched using an InAs SESAM. Here the pulse repetition rate was deemed unstable and only partial mode-locking was achieved. (Below) An Er^{3+} doped fibre laser operating at 2.7 μm was mode-locked using an Fe:ZnSe crystal. Detailed measurements were not performed here, making it unclear whether stable mode-locking was achieved.

tion of pulses. In this case, however, no measurement of the rf SNR was mentioned and no autocorrelation had been made. Based on the spectrum of the output, and assuming transform limited pulses, the pulse width was estimated to be 19 ps. Later another similar Er^{3+} system was claimed to be mode-locked [150], which contained thorough rf measurements, however no direct pulse measurement was made. The pulse width was estimated again assuming a transform limited pulse from spectrum to be 60 ps.

Despite the numerous claims in the literature, no single demonstration of a near 3 μm mode-locked fibre laser had shown satisfactory evidence for *stable* mode-locking. In fact, it is well known that claiming mode-locked systems requires strong evidence and careful characterisation. For instance, measuring a pulse train from a laser with a strong rf beat can even occur from a cw laser [151]. It is also stated that conclusions should not be drawn simply from the optical spectrum (such as the inferred pulse widths in Ref. [149, 150]).

According to Ref. [151], the traditional measurements for characterising a stable mode-

locked system are:

- The steady production of a pulses at the repetition rate of the cavity
- An optical spectrum
- A stable mode-locked beat signal (rf SNR > 60 dB)
- A direct pulse measurement (e.g. optical autocorrelation)

Assessing the above points are well known in visible to near-IR mode-locked systems, however careful analysis was not taken in the recent demonstrations for the mid-IR. It is indeed difficult to achieve the same level of analysis at these wavelengths, due to the relative lack of optical components, though the criteria must not be relaxed. As a result, it remains unclear whether these systems were stably mode-locked. It is essential to perform the correct characterisations to progress the field so that improved systems can be designed. In this chapter we demonstrate the above points simultaneously from a single mode-locked system. The primary methods of achieving this were explored using the $Ho^{3+}Pr^{3+}$ system, as it operates on a simpler transition compared to the Er^{3+} system.

4.1.1 Ring cavity geometry for achieving stability

In most of the previous studies there had been no direct pulse measurements, and in one case an autocorrelation was made, but it was obvious the pulse train was not stable. One critical reason for this may have been that all of the cavities employed were *linear* cavities. As the light propagates in both directions, unwanted back reflections from in-cavity optics can experience gain in the opposite direction, as shown in Fig. 4.2(left). This can create multiple pulses in the cavity that compete for gain, and eventually lead to an unstable output. Although carefully designed linear cavities with appropriate anti-reflection coated optics can achieve mode-locking [152], more often mode-locked lasers are built in a *ring* geometry operating unidirectionally (with the use of an optical isolator). In this case the back reflections are removed by the optical isolator given, with the isolator was positioned correctly in the cavity, unable to experience gain - see Fig. 4.2(right). Here we aimed to overcome the problems of unstable output performances by changing to a ring cavity.

4.1.2 Continuous wave $Ho^{3+}Pr^{3+}$ ring laser

The fibre used for this study was a double-clad $Ho^{3+}Pr^{3+}$-doped ZBLAN fibre with concentrations of 30,000 and 2,500 ppm respectively (same concentrations as the fibre used in Chapter 3). The cladding was octagonally shaped which performed similar to the D-

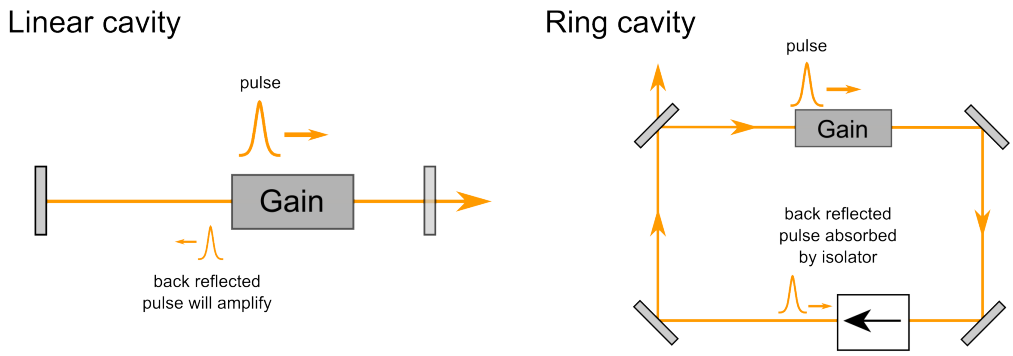

Figure 4.2: Layout of linear and ring optical cavities. In the case of linear cavities (left) back reflections from optics can build up and experience gain, eventually destabilising the output. In the case of a unidirectional ring cavity (right) the optical isolator will prevent any counter-propagating reflections and prevent them from being amplified.

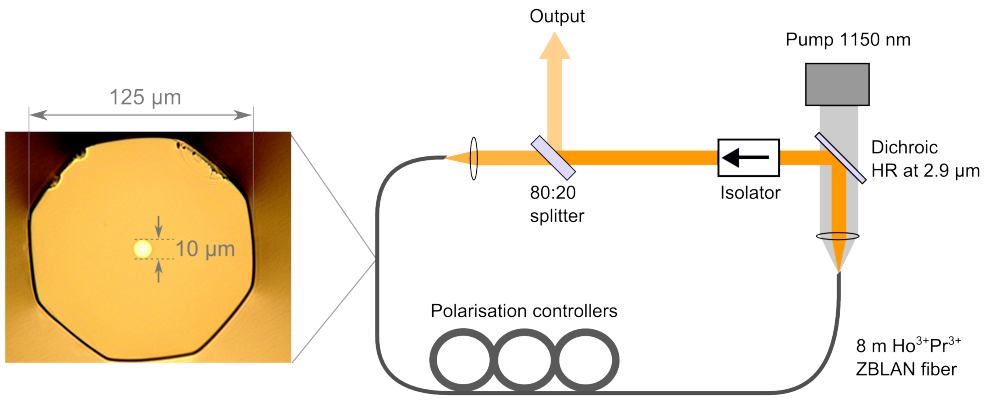

Figure 4.3: Experimental setup of a cw ring laser. Cavity consists of an 8 m long $Ho^{3+}Pr^{3+}$-doped double clad fibre arranged in a ring geometry using an optical isolator. A dielectric mirror extracted 20% of the light for the output.

clad fibres but with easier cleaving and handling properties. The core/cladding sizes were 10/125 μm, Fig. 4.3.

The core had a quoted NA of 0.2, setting the single mode cutoff wavelength at 2.61 μm. A ring laser was set up as shown in Fig. 4.3 containing an 8 m long fibre, where unidirectional operation was forced by a Faraday rotation based optical isolator (the Faraday material was bismuth iron-garnate). The isolator had an 80% transmission at a wavelength of 2.9 μm and provided 29 dB isolation in the opposite direction. The output of

the laser was taken from a CaF_2 dielectric mirror that out coupled 20% of the light, and the remaining light was coupled back into the fibre. A crucial component for the ring laser was the inclusion of polarisation controllers, consisting of three paddles in a 2-4-2 loop configuration (65 mm diameter each). These controllers allowed the compensation of the birefringence in the fibre that changed the polarisation state of the light after one round trip, causing unwanted loss at the polarisation based isolator. This improvement is shown in Fig. 4.4 which compares the slope efficiencies for two cavities with and without polarisation control. The launched power efficiency of the laser was improved by 60% with the inclusion of these controllers, from 11% to 17%.

This output power fluctuation was monitored over 20 minutes and was observed to be <1.4% (limited by the power meter resolution). The optical spectrum was centred at 2895.5 nm measured using a Horiba iHR 550 spectrometer. The linewidth was 0.2 nm, corresponding to a bandwidth of 7.3 GHz, much narrower than the Q-switched lasers in Chapter 2. This is attributed to the cw nature of the output and the ring geometry which suffers from no spatial hole burning effects that would otherwise broaden the spectrum.

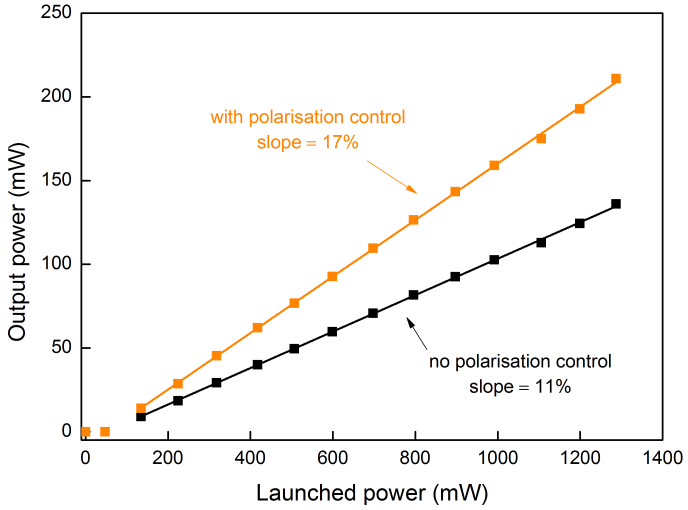

Figure 4.4: The launched power efficiency of a cw $Ho^{3+}Pr^{3+}$ ring fibre laser increases from 11% (black) to 17% (orange) with the inclusion of polarisation controllers inside the cavity.

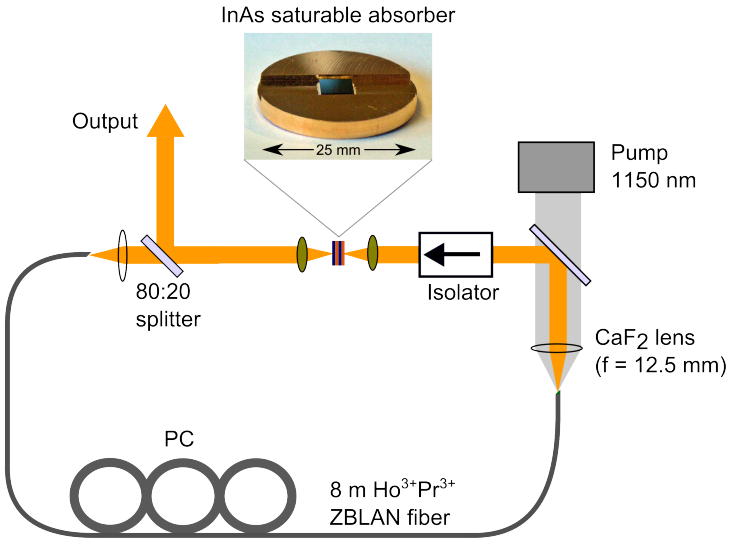

Figure 4.5: An InAs saturable absorber was inserted into the previous ring cavity to achieve mode-locking. The absorber is placed in a confocal arrangement to increase the optical intensity so that saturation could be reached.

4.2 Passively mode-locked $Ho^{3+}Pr^{3+}$ fibre laser

4.2.1 Experimental Setup

Using the ring geometry, a setup designed for passive mode-locking was constructed by inserting a transmission based saturable absorber into the cavity, Fig. 4.5, purchased from Batop Optoelectronics GmbH. This was contained in a 2 mm thick piece of semiconductor material containing a 625 μm layer of InAs that provided the saturable absorption. The quoted parameters of the saturable absorber are listed below:

Property	**Value (at 2.8 μm)**
Transmittance	90%
Absorptance	10%
Modulation Depth	4 %
Non-saturable loss	4 %
Saturation fluence	300 μJ/cm^2
Relaxation time constant	$\approx$ 10 ps

The absorber was placed in a confocal arrangement surrounded by two ZnSe lenses, with a focal length of 6 mm each, to create a high-intensity focus at the centre. The output of the laser was monitored using a mercury-cadmium-telluride (MCT) photodetector with a rise time of < 1 ns (Boston Electronics), which was then electronically amplified (400 MHz) before being viewed on an oscilloscope.

4.2.2 Results

Similar to the previous reports the temporal output of the laser varied depending on the amount of pump power provided. At launched pump powers below 1.25 W, the output was a typical Q-switched mode-locked profile, shown in Fig. 4.6(left). Here a large envelope approximately 1 μs long is produced, with sharp features at a 24.8 MHz repetition rate that matched the inverse of the round trip time of the cavity. This regime is known to occur in passively mode-locked systems when the absorber has not yet completely saturated. Upon increasing the power beyond 1.25 W, the output changed to a "cw mode-locked" state where the Q-switching envelope disappeared and only a train of pulses at 24.8 MHz was seen with a constant amplitude, Fig. 4.6(right). The width of the individual pulses ($\approx$ 2 ns) was limited by the detector and amplifier bandwidth. The output average power reached 70 mW, providing a launched power efficiency of 5%. The relatively low efficiency in this cavity is caused by the losses in the free space optics (the isolator transmission being 80%, each ZnSe lens having a transmission of 85%), and the loss in the saturable absorber. Due to the increased amount of optical elements in the free-space section, we also suspected this effected the beam quality and its coupling efficiency back into the core of the fibre.

The optical spectrum was measured and shown in Fig. 4.7, which compares the spectrum when mode-locked to the spectrum under cw operation. It can be seen that the width increased vastly from 0.2 nm to 5 nm, broadening by a factor of 25. This is a characteristic effect seen in mode-locked lasers that shorter pulses require more Fourier spectral components, and therefore requiring a wider spectrum.

The rf spectrum of the pulses were also measured and is showed in Fig. 4.8. The peak was centred at 24.8 MHz and the SNR was 73 dB, and measured to be stable from amplitude variation and jitter over several hours. Compared to the previous closest report of this class of laser which gave a SNR of 50 dB [148], this system was remarkably more stable in terms of the mode-locking beat signal.

4.2.3 Autocorrelation using two-photon absorption

An intensity autocorrelator was built to measure the width of the mode-locked pulses. A Mach-Zehnder interferometer, illustrated in Fig. 4.9, was used as the geometry ensured no

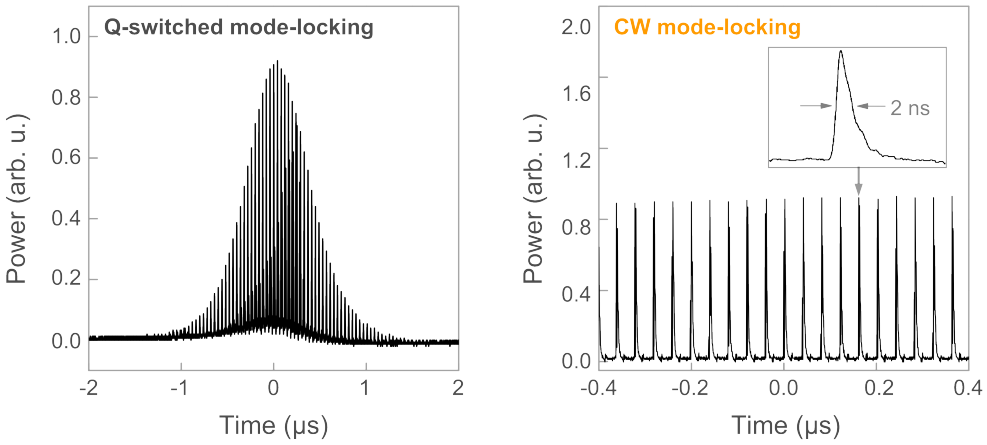

Figure 4.6: Temporal output characteristics of the laser in two regimes. (Left) Below a launched pump power of 1.25 W a Q-switch mode-locked output was seen, consisting of a large ≈ 1 μs Q-switched envelope, modulated at the cavity repetition rate. (Right) At higher pump powers the output changed to cw-mode-locking where a train of pulses with constant amplitude was produced. The inset shows the waveform of a single pulse, 2 ns wide, which was limited by the detector bandwidth.

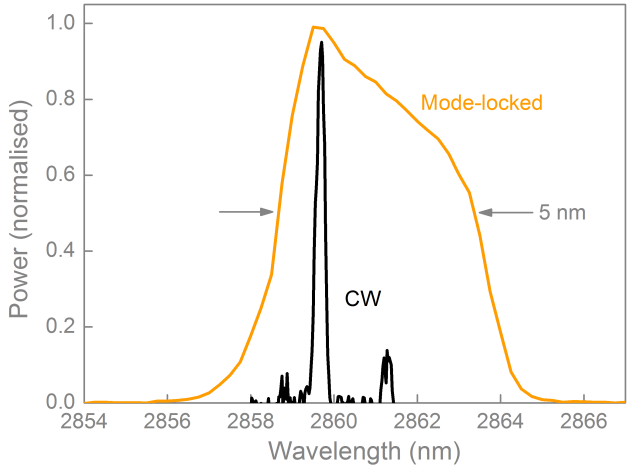

Figure 4.7: Optical spectrum of the cw mode-locked pulses (orange) compared to that of the ring laser from Section 4.1.2 (black). Due to shorter pulses being produced the bandwidth increased from 0.2 to 5 nm, as expected from mode-locked lasers.

back reflections to couple back into the laser cavity (which would occur for a Michaelson-type interferometer). Here, the pulse is split into two, delayed with respect to each other,

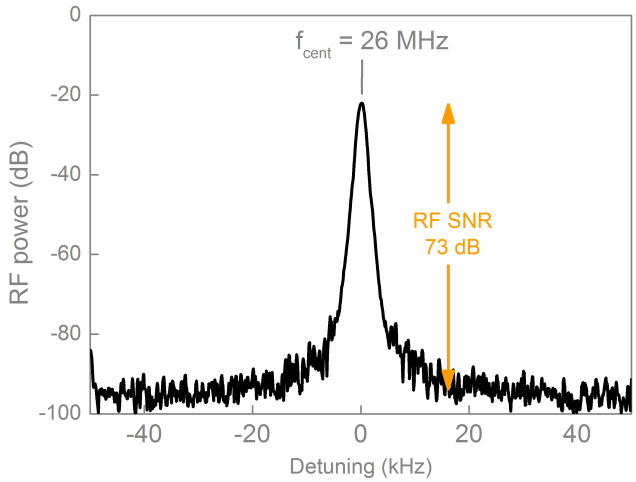

Figure 4.8: The rf beat spectrum of the mode-locked pulses was centered at 24.8 MHz, spanning 100 kHZ. The SNR measured was 73 dB (resolution bandwidth of 1 kHz), typical of stable mode-locked lasers.

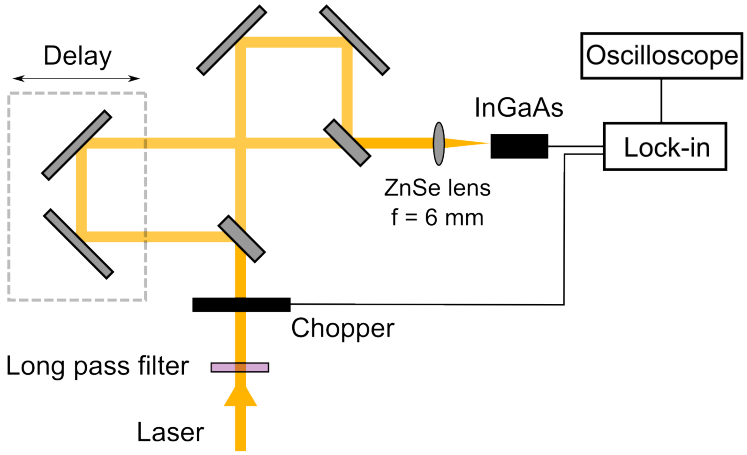

Figure 4.9: Design of intensity autocorrelator to measure the mode-locked pulses at 2.86 μm. The pulses are split and delayed inside an Mach-Zehnder interferometer and recombined on an InGaAs photodiode. The weak two photon absorption signal was measured by using a lock-in amplifier.

and then recombined on an InGaAs photodiode. The laser photon at 2.86 μm (0.43 eV) is not enough to bridge bandgap of InGaAs (0.69 eV), however the two photon absorption

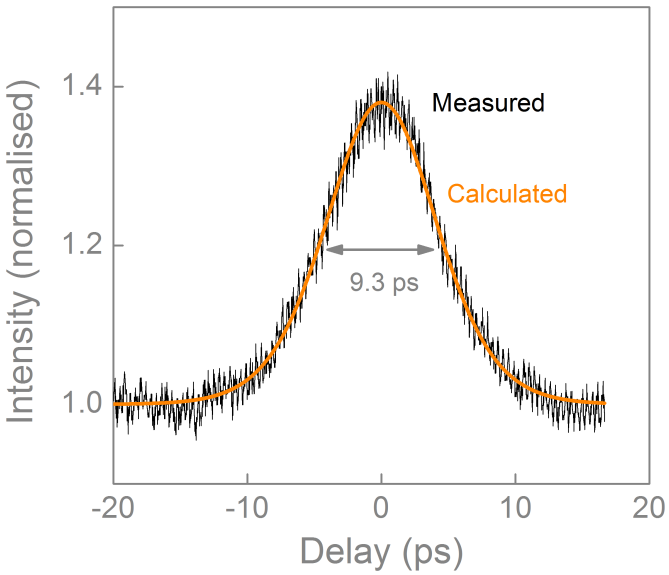

Figure 4.10: Measured intensity autocorrelation trace (black) from the mode-locked pulses. This trace is fitted using Eq. 4.1 (orange), revealing a FWHM of 9.3 ps, and a pulse width of 6 ps assuming a sech-shaped pulse.

signal can be measured for the autocorrelation. In this case the detector itself acts as the intensity dependent nonlinear medium. The pulses were first passed through a long pass filter (transmitting > 2.4 μm) to remove any unabsorbed pump light from the laser output, and then sent through the autocorrelation device. The weak two photon signal was maximised by tightly focusing the beams onto the detector, and using a lock-in amplifier. In this set up the envelope of the autocorrelation signal as a function of delay is known to have a form [153]:

$$I_2(\tau) \propto 1 + a\left(6\frac{b\tau\cosh(b\tau) - \sinh(b\tau)}{\sinh^3(b\tau)}\right) \tag{4.1}$$

where b $= 2.72/\tau_{ac}$, with τ_{ac} being the FWHM of the autocorrelation trace. The true pulse width is $\tau_p = \tau_{ac}/k$, where k is the deconvolution factor. For sech-shaped pulses k is 1.543. Lastly, a is a constant that accounts for the unequal splitting of the beam (ideally 50/50) inside the autocorrelator.

The measured autocorrelation is shown in Fig. 4.10 along with the calculated trace from Eq. 4.1. The FWHM of the trace was 9.3 ps and the calculated trace was best fitted assuming a sech shaped pulse. Ideally the contrast ratio between the background and the signal peak for this measurement is should be 1:4, however in this measurement we only

acheived 1:1.4. This is highly suspected to be caused by the non-optimal performance of our beam splitter (being 40:60 rather than 50:50) and perhaps a beam overlap problem due to the autocorrelator being built in house. Nonetheless the pulse length that we measure is expected given the properties of the cavity, discussed later in this section. The dispersion of ZBLAN fibre at these wavelengths is expected to be anomalous [154], indicating soliton dynamics inside the cavity, which would indicate a sech-shaped pulse. From this assumption we deduced the pulse width to be 6 ps (using k = 1.543). Over a delay of 200 ps there were no subsequent peaks in the autocorrelation, which suggests that there were no multiple pulses within a round trip time of the laser. The associated time-bandwidth product of the pulses was 1.1, which indicated that our pulses were not transform limited (which would provide a 2.4 ps). The pulse lengthening was most likely due to group velocity dispersion in the fibre, causing broadening in the temporal domain and inducing a chirp, since no dispersion management was considered in the design of the cavity. Once the laser was in a cw mode-locked state the power and temporal output did not show any unstable performance over a course of 12 hours. Given the launched pump power was greater than 1.25 W, cw mode-locking was self-starting. With a measured average power of 69.2 mW, this results in a calculated peak power of 497 W.

4.2.4 Transition dynamics to CW mode-locking

The transition from Q-switched to CW mode-locking was investigated in detail to confirm that mode-locking mechanism was indeed caused by the saturable absorber. As mentioned earlier, at lower pump powers the output of the laser was in a Q-switched mode-locked state. The repetition rate of the Q-switching steadily increased from 50 to 150 kHz as the pump power was increased, Fig. 4.11. At a pump power of 1.25 W, the Q-switching stopped, and CW mode-locking took over. Q-switch mode-locking is known to occur when the in-cavity pulse energy is not enough to completely saturate the absorber [155]. It is stated that this threshold pulse energy E_{th} is given by

$$E_{th}^2 = E_{sat,g} E_{sat,a} \Delta R \tag{4.2}$$

where $E_{sat,g}$ is the saturation energy of the gain medium, $E_{sat,a}$ is the saturation energy of the absorber, and ΔR is the modulation depth (4%). $E_{sat,g}$ can be calculated using the cross section of the emission line from the gain medium and, in the case of the holmium transition, this value is 90 μJ (values taken from [96]). $E_{sat,a}$ is calculated using the saturation fluence of the absorber (quoted as 300 μJ/cm^2) multiplied by the area of the focused light, which was calculated using the lens equation, and gave a value of 49 pJ. From Eq. 4.2 the threshold in-cavity pulse energy is 13.3 nJ. We calculate that this occurs at an output average power of 40 mW, which corresponded to a pump power of 1.25 W.

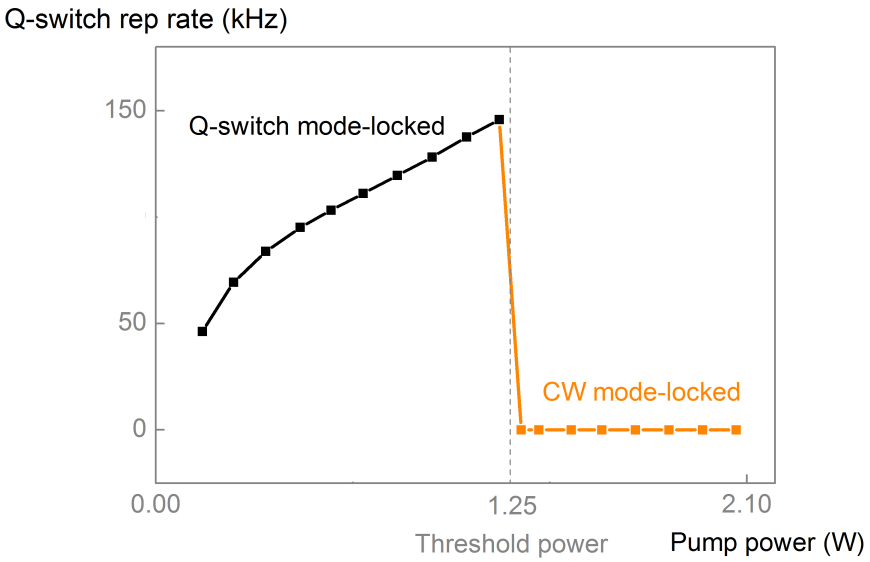

Figure 4.11: Analysis of the transition between Q-switch mode-locking and cw mode-locking as the pump power increased. The Q-switch envelope repetition rate increases from 50 to 150 kHz, until at a 1.25 W pump power it drops to zero as cw mode-locking takes over. This transisiton pulse energy corresponds precisely to what is calculated (vertical dotted line) according to Eq. 4.2.

From Fig. 4.11 this precisely corresponds to where we observe a change in the output dynamics. This result, along with the temporal and spectral measurements, confirm that the InAs saturable absorber was providing stable and self-starting mode-locking of the $Ho^{3+}Pr^{3+}$ doped fibre laser.

4.3 Summary

In this chapter we presented a mode-locked fluoride fibre laser that operated at 2.86 μm, producing 6 ps pulses with a peak power of 497 W. In the general scope of long wavelength fibre lasers these results still stand quite undeveloped compared to the thulium silica fibre lasers at 2 μm, which have produced femtosecond level pulses [156, 157]. However in terms of wavelengths beyond those available from silica fibres only a few studies have been performed. The earliest work at 2.7 μm involved a vibrating mirror technique [158] however no stable train of pulses were produced. More recently the linear cavity designs using an InAs SESAM was employed but the output was deemed unstable. A pulse train output

had been observed from two other systems [149, 150] however in both cases no extensive study on the stability was made, nor was any direct pulse measurement performed. The current $Ho^{3+}Pr^{3+}$ ring fibre laser, however, has shown stable self-starting mode-locking. We satisfy all four criteria for stable mode-locking by achieving; the measurement of a stable train of pulses, an optical spectrum, an rf SNR greater than 60 dB, and a direct intensity autocorrelation measurement. This performance marks the first mid-IR fibre laser that is beginning to access the peak powers and pulse widths previously offered only by optical parametric oscillators and amplifier systems. Although fs-level, kW-peak power systems are more appealing, for example in mid-IR nonlinear optics, this result opens the pathway for fibre lasers to be a key technology for this field.

It is important to mention that mapping of the net group velocity dispersion in the cavity was not considered in this study. As was mentioned in Section 2.3.2 the net GVD is a crucial parameter for the performance of the mode-locked laser. Unlike the near-infrared wavelengths which is much easier to insert sections of normally dispersive silica fibre, it is not so the case at these wavelengths. Chalcogenide fibre is known to be normally dispersive at these wavelengths (compared to fluoride fibre) and may be a potential candidate to balance dispersion in the cavity. However its relatively higher loss and compatibility with fluoride in terms of splicing and index mismatch remains a challenge. A free-space dispersion compensating section using prisms or grating pairs may be more suitable on the short term as has been done previously in silica fibre systems [159], and is certainly a direction to be explored in future.

I conclude this chapter with a road map of the achievements in terms of pulsed fluoride fibre lasers operating near 3 μm, and the progression towards ultrafast high peak power systems. This is illustrated in Fig. 4.12, which shows the pulse widths and peak powers accessed by different methods. Early works began with pulsing using passive Q-switching techniques resulting in μs pulses [160]. A significant step was made by moving to gain switching [73] and active Q-switching techniques [74, 138], entering the nanosecond pulse regime, with the shortest being 33 ns [139]. Partial mode-locking and nominally mode-locked systems claimed pulse production from 60 ps down to 19 ps [148–150]. Then finally with the confirmed demonstration of a stable mode-locked system, presented in this chapter, we confirm the demonstration at the picosecond level (6 ps). There are, however, shorter regimes to be exploited at the femtosecond level. It is well known that the Ho^{3+} and Er^{3+} transitions have enough spectral bandwidth to support these pulses [161]. Reaching this regime will truly reveal the potential that fluoride fibre lasers have as a competitive source of ultrafast mid-IR laser pulses. This will be the topic of study in Chapter 5.

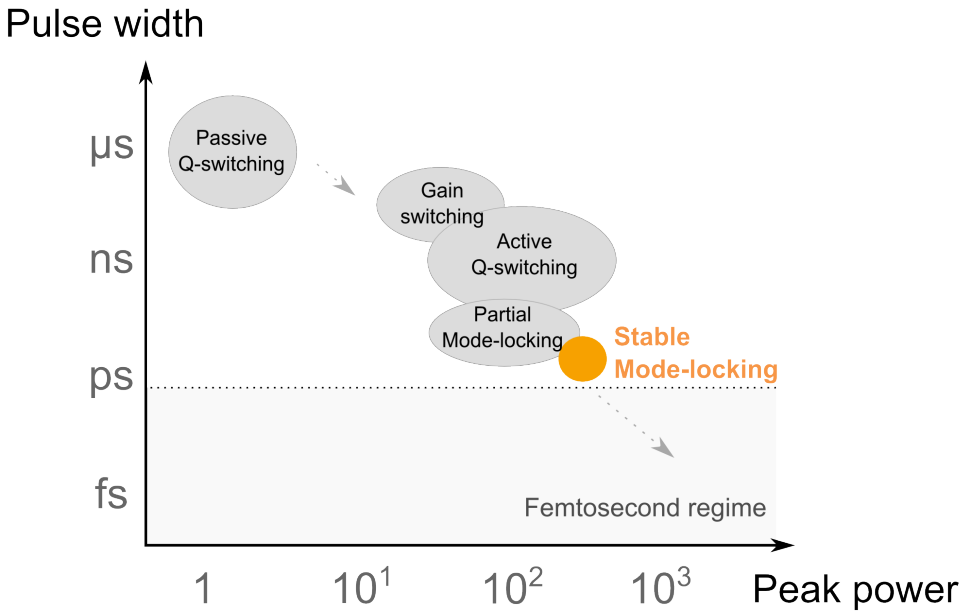

Figure 4.12: Performance of pulsed near 3 μm fibre lasers towards ultrafast, high peak power systems. Initial results began with μs-level passive Q-switching, to gain switching and active Q-switching at the nanosecond level, then most recently to mode-locking methods that provided picosecond pulses. Entering the femtosecond regime will enable the kW peak powers required in areas such as nonlinear optics and frequency comb generation.

Chapter 5

Mode-locking with nonlinear effects

This Chapter refers to the work that was carried out in reference [162].

Diving into the femtosecond regime

In this chapter we present results on the first sub-picosecond pulses produced from a mid-IR fibre laser. Building on the knowledge in creating stable mode-locked systems from Chapter 4, here we achieved mode-locking via nonlinear optical effects to produce femtosecond-level pulses. We also show, for the first time, a complete pulse characterisation using frequency resolved optical gating (FROG) methods. This demonstrates the potential that mid-IR fibre lasers have in producing ultrafast, high peak power, pulses of light.

5.1 Physical limits of saturable absorbers

The use of saturable absorbers inside laser cavities enables self-starting and stable mode-locked systems. As described in Section 2.3.2 the design of the cavity, in particular the net GVD, is important to achieve shorter pulses. However due to the infancy and unavailability of optical components in this wavelength range, mapping the net GVD is a substantial task. Future systems may incorporate methods to control the dispersion however in this chapter we explore the effects of another parameter - the relaxation time of the absorber. The InAs saturable absorber used in the experiments from previous chapter had a relaxation time of 10 ps. Although this value is not the ultimate pulse width limit the pulses are generally limited to the order of the relaxation time. To push the near 3 μm fibre lasers to even shorter pulses, other saturable absorbers or mode-locking mechanisms could be considered.

Graphene is an exciting saturable absorber that has a faster relaxation time of 1.67

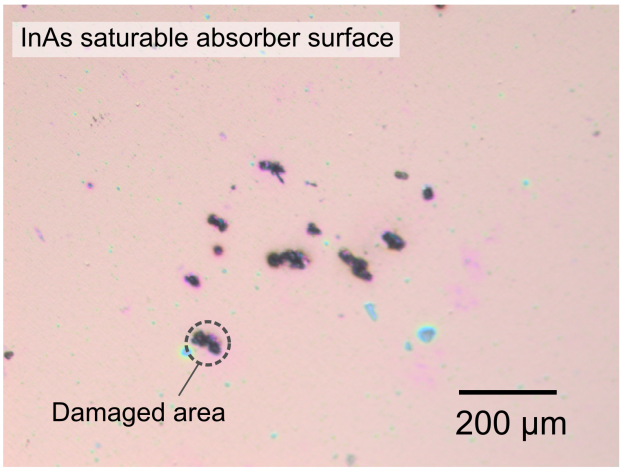

Figure 5.1: Microscope image of the InAs saturable absorber after multiple attempts at high power operation. Several damaged areas can be seen, which are due to the relatively low threshold of 2 mJ/cm^2.

ps. A near-IR graphene mode-locked fibre laser has reported the generation of 756 fs pulses [110]. These have also been explored for the near 3 μm fibre lasers [163], however mode-locking has not yet been demonstrated. It has been suggested that the uniformity of the graphene samples are crucial for high performance [164]. That being said, there is an exciting opportunity here to exploit the wavelength independent saturable absorption of graphene to mode-lock a mid-IR fibre laser.

There is, however, another issue associated with saturable absorbers is they eventually face an optical damage threshold limit. For example the InAs saturable absorber used in Chapter 4 had a peak energy fluence limit of 2 mJ/cm^2. For a typical focus spot size we achieve ($\approx$ 10 μm) damage occurs at a pulse energy of 6.3 nJ. Although we estimated slightly higher pulse energies from the previous laser cavity (10-15 nJ) this indicated we were close to damaging the saturable absorber. This was confirmed when damage was seen on the InAs absorber when attempting higher cavity energies, Fig. 5.1. This prevented achieving shorter, more energetic, pulses using this material.

Instead, the shortest pulses (sub-100 fs) have been produced using nonlinear optical processes to act as saturable absorbers. The relaxation time of these "effective saturable absorbers" are limited by the speed of the Kerr nonlinearity, which is on the order of femtoseconds [165]. Since there is no physical absorber there are also no issues with damage. These effective saturable absorbers are used to mode-lock lasers in various configurations such as Kerr lens mode-locking [113], nonlinear polarisation rotation [51] or nonlinear loop mirrors [111, 112]. The titanium-sapphire lasers often employ the Kerr lens mode-locking

which have produced pulses as short as 4.3 fs [32], and nonlinear polarisation rotation in a near-IR all fibre laser has produced 33 fs pulses [51]. In this Chapter we utilize nonlinear polarisation rotation due to its relative simplicity and ability to be performed inside an optical fibre.

5.1.1 Nonlinear Polarisation Rotation

Nonlinear polarisation rotation (NPR) is a process that can be implemented along with polarising optics to make an effective saturable absorber inside a laser cavity. The effect is an intensity dependent rotation of elliptically polarised light due to the Kerr nonlinearity. Elliptically polarised light can be described as a sum of left-hand and right-hand circularly polarised components of different intensities. Each of these components accumulate a nonlinear phase shift (that depends on intensity), and as a result the elliptical state rotates whilst maintaining ellipticity and handedness [166, 167]. With the combination of this effect and a linear polariser, an effective saturable absorber can be made.

This effect can be better described with the aid of Fig. 5.2 which describes pulse shortening using NPR. Here an input pulse is shown which has an elliptical polarisation across the entire intensity envelope, which then passes through an optical fibre. Due to the NPR process, an intensity dependent rotation of the polarisation occurs. The peak of the pulse experiences the greatest amount of rotation whereas the wings of the pulse do not rotate as much. By passing this pulse through a linear polariser that is aligned

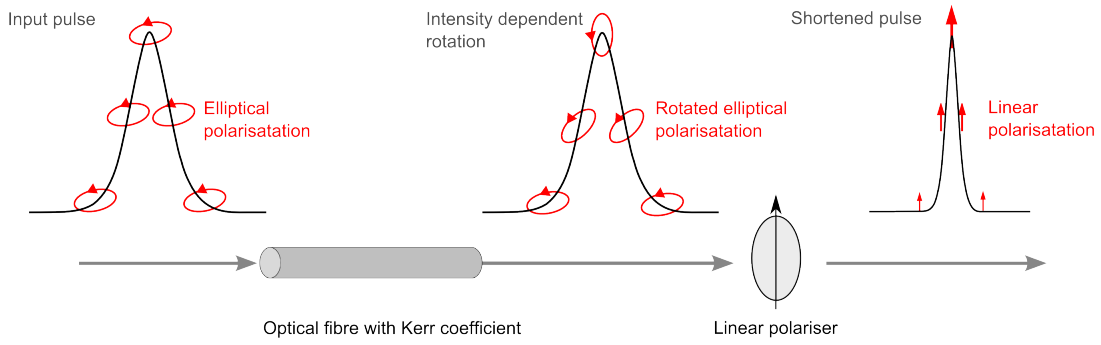

Figure 5.2: Concept of nonlinear polarisation rotation used to shorten pulses. An elliptically polarised pulse enters a Kerr medium which causes an intensity dependent rotation of the polarisation. By aligning a linear polariser at the correct orientation, the peak of the pulse can be maximally transmitted whereas the wings of the pulse experience more loss, and result in a "trimmed" pulse. Employing this inside a laser cavity can create an effective saturable absorber to allow mode-locking.

closer to the polarisation at the peak of the pulse, the wings experience a higher loss and are essentially "trimmed", leaving a shorter transmitted pulse. By repeating this process inside a laser cavity an effective saturable absorber is created, where there is an intensity dependant absorption, which can bias pulsed operation. As the final pulse is now linearly polarised, if the process were to be repeated a combination of waveplates are needed to produce the necessary elliptical polarised state - which will be shown in Section 5.2.

5.1.2 Er^{3+}-doped ZBLAN fibre laser

After demonstrating that mode-locking was possible with the $Ho^{3+}Pr^{3+}$ system in Chapter 4, we decided to explore the Er^{3+}-doped fibre lasers for this study. This was based on two reasons; having better fibre quality and higher available pump powers. The Er^{3+}-doped fluoride fibre (purchased from Le Verre Fluoré) was quoted to have the lowest background loss, and had identical parameters to the study conducted in Ref. [68] which is to date the most efficient 3 μm class fibre laser. The second point is that the Er^{3+} system is pumped at 980 nm, where higher power laser diodes are available. In this work a single diode laser (InGaAs) able to produce 10 W of power was used (compared to 4 W of power for the Ho^{3+}-system). Therefore this Er^{3+}-doped configuration was thought to most likely achieve NPR mode-locking.

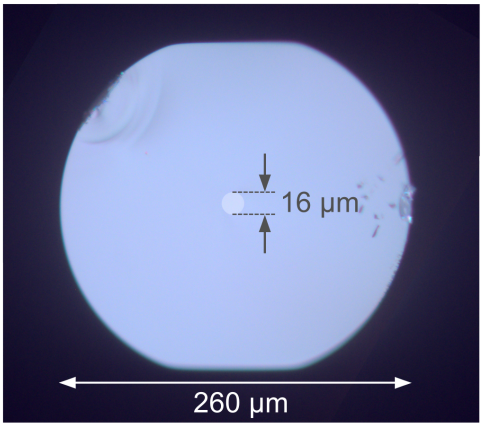

Figure 5.3: Cross sectional view of the Er^{3+} doped ZBLAN fibre purchased from Le Verre Fluoré. The doped core had a diameter of 16 μm surrounded by a cladding approximately 260 μm wide. It was truncated on two edges to promote high order modes that intersect with the core efficiently.

The fibre consisted of a double-clad structure as shown in Fig. 5.3. The core diameter was 16 μm with an NA of 0.12 doped at 7 mol.%. The cladding had a circular shape of

diameter 260 μm, but truncated at the top and bottom with two parallel edges. By angle cleaving this fibre on two ends a cw ring laser was made and showed high efficiency of 30%.

5.2 NPR mode-locking using fluoride fibre

Using the fibre in Fig. 5.3 we designed a mode-locked ring laser based on NPR. The experimental setup is shown in Fig. 5.4. The cavity consisted of 3 m of the Er^{3+}-doped ZBLAN fibre, with a free space section containing a combination of waveplates, an optical isolator and a polarising beam splitter to out-couple the light. The polarising beam splitter acted as the linear polariser to shorten the pulse through the NPR process, where the rejected beam was used as the output. The $\lambda/4$ and $\lambda/2$ plates before the PBS set the required output coupling ratio and ellipticity for the NPR process. The linearly polarised light that remained in the cavity then passed an isolator and a $\lambda/4$ plate to create an elliptical polarisation again to allow the NPR to occur in the next round trip.

At a launched pump power of approximately 4 W, and by orienting the waveplates correctly, NPR based mode-locking was achieved. In practice, at a fixed pump power the waveplates were adjusted such that mode-locking was achieved. During this process Q-swithced pulses and Q-switched mode-locked pulses were seen also, however the cw mode locked state was of most interest here. A pulse train at a repetition rate of 56.7 MHz

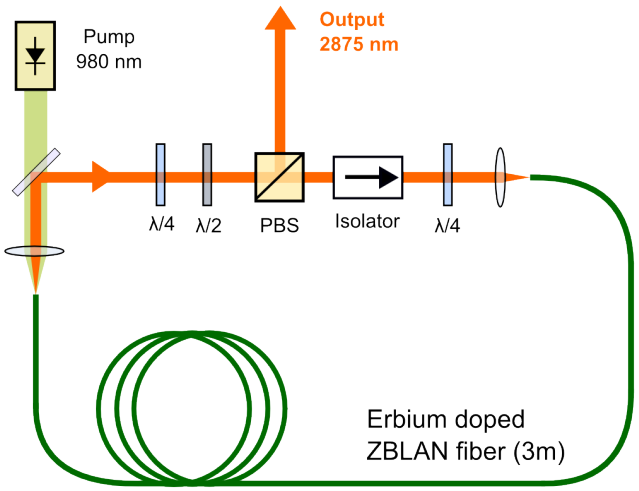

Figure 5.4: Experimental layout of the Er^{3+} doped fibre laser mode-locked via NPR. The ring cavity consisted of a free space section with waveplates to create the conditions for NPR, where the polarising beam splitter simultaneously outcoupled the beam and shortened the pulses in the NPR process.

was seen, and its rf spectrum was also measured - Fig. 5.5. The width of each measured temporal pulse, once again, was limited by the detector bandwidth. The rf spectrum was measured up to 500 MHz, showing the fundamental beat strength of the mode-locked pulses (with a SNR of 73 dB), but also the higher harmonics. The signal strength of the harmonics can be observed to drop steadily with frequency, which is due to the detector bandwidth roll off. The significance here is that all higher harmonics are evenly spaced and their amplitudes rolled off smoothly - which indicates no multiple pulse beating effects.

The optical spectrum, shown in Fig. 5.6, had an rms FWHM of 20.1 nm centred at 2793 nm. On each side of the main spectral peak there are smaller peaks which are known as Kelly sidebands, characteristics well-known in soliton-based mode-locked lasers [168]. We also show the mode-locked spectrum (at high resolution) in Fig. 5.7 compared to the amplified spontaneous emission (ASE) from the laser. The ASE spectrum (orange, vertically shifted for clarity) spans approximately 2700 to 2800 nm, and consists of sharp absorption lines, some of which are also imprinted on the mode-locked spectrum (inset). These originate from the OH molecular absorption lines from water vapour. Despite the small interaction length with the air, at these mid-IR wavelengths, these effects are obvious and may be the limiting factor for the available spectral bandwidth of the laser. For future systems it would be desirable to remove these absorption lines (for example, nitrogen purging the environment) and explore if the entire ASE bandwidth can be accessed, which would theoretically support 70 fs pulses [161].

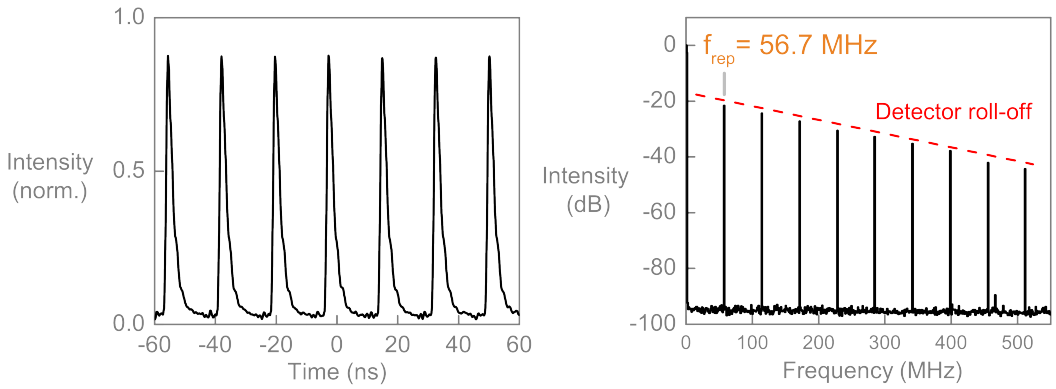

Figure 5.5: (Left) Temporal output of the fibre laser, emitting pulses at a repetition rate of 56.7 MHz. (Right) rf spectrum of the measured pulses over a 500 MHz bandwidth (detector bandwidth and amplifier quoted to be 400 MHz). The rf SNR was 73 dB at the fundamental beat, and higher order peaks show a smooth roll off with the detector bandwidth, indicating no multiple pulse beating effects.

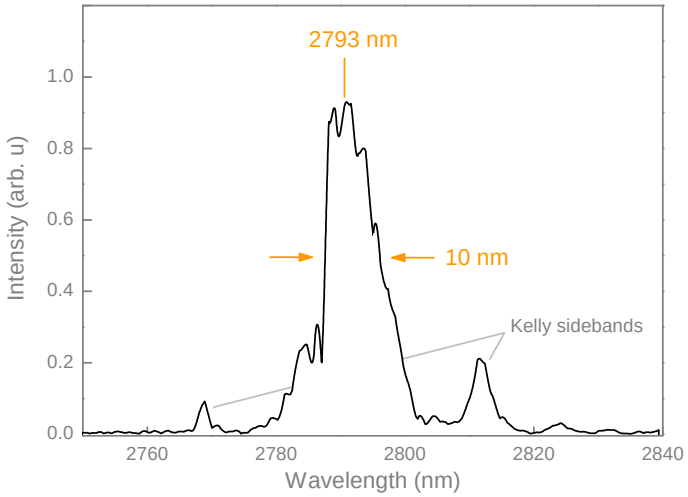

Figure 5.6: Optical spectrum of the laser output measured on an FTIR (Fourier transform infrared spectroscopy). The centre wavelength was 2793 nm with a bandwidth of 10 nm. Kelly sidebands deriving form soliton dynamics can be seen on each side of the spectrum.

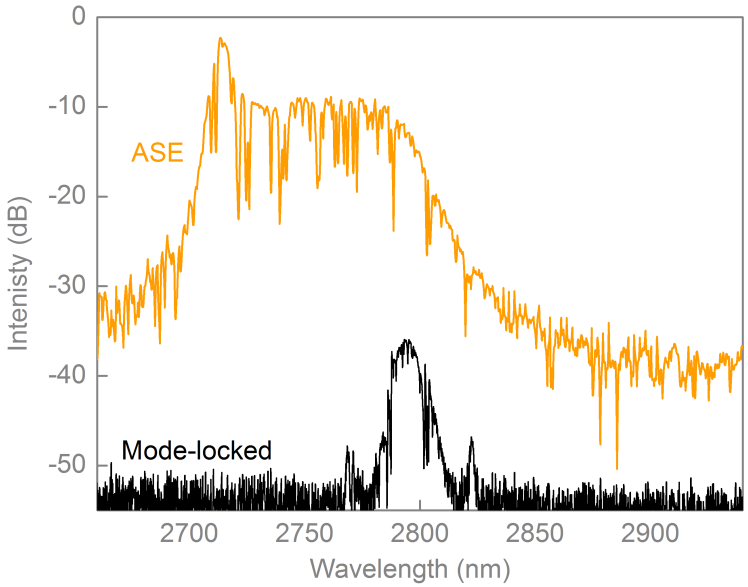

Figure 5.7: High resolution scan of the mode-locked laser spectrum (black, lower) compared to that of the ASE spectrum (orange, upper). The sharp dips in both spectra derive from OH absorptions in the air, may also be limiting the available spectral bandwidth.

5.3 Complete pulse retrieval using Frequency Resolved Optical Gating

Up until this point, the only reported direct measurement of pulses from a mid-IR mode-locked fibre laser was using an intensity autocorrelation [147] which, as explained in Chapter 2 - Section 2.3.3, is known to be ambiguous and fails to provide phase information. To overcome this problem we constructed a mid-IR compatible FROG measurement system.

5.3.1 Design of the mid-infrared FROG

A FROG measurement requires a spectrally resolved autocorrelation signal. The autocorrelation configuration used in Chapter 4, using two photon absorption, does not allow this as the nonlinear medium was the detector itself, preventing spectral resolution of the signal. Here we design a setup using a $AgGaS_2$ crystal to produce the second harmonic light which was to be spectrally resolved. This crystal is transparent across 0.53 to 12 μm and has been used as a nonlinear crystal for optical parametric oscillators in the mid-IR [44]. The overall architecture of the FROG system is shown in Fig. 5.8. Similar to an autocorrelation the laser pulse is split into two, delayed with respect to each other, and then overlapped at the location where the nonlinear process occurs.

Second harmonic generation (SHG) is a well known phenomena which utilizes a nonlinear crystal and its $\chi^{(2)}$ response. In order to achieve sufficient conversion of 2.8 μm

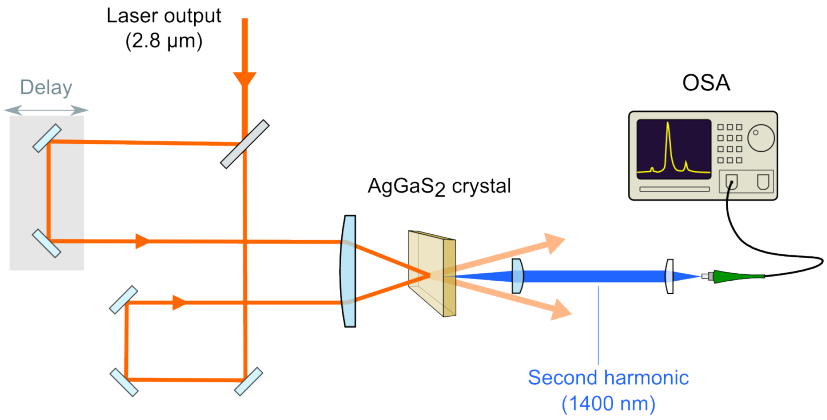

Figure 5.8: Schematic of the SHG FROG measurement system. The laser pulse is split, delayed, and recombined on the $AgGaS_2$ crystal to generate a signal at 1400 nm. This signal is then collected in a smf-28 fibre and spectrally analysed on an OSA as a function of delay, to construct a spectrogram.

light into 1.4 μm (frequency doubling) phase matching of the crystal is required. We designed the SHG process to be achieved through Type 1 phase matching using a 2 mm long $AgGaS_2$ crystal cut with an optic axis of $\phi = 38.5$ °. This optic axis results in a phase matched angle (θ) of 2.2 °which corresponds to what is practically achievable using the optics in the experiment. The relatively large thickness was chosen so that sufficient SHG conversion could be achieved. However with increased thickness there is a risk of loss in temporal resolution of the FROG measurement as the group velocity mismatch (GVM) causes a temporal walk-off between the fundamental and second harmonic pulses, diminishing the conversion efficiency. This is given by;

$$GVM = \frac{1}{v_g(\lambda_0/2)} - \frac{1}{v_g(\lambda_0)} \tag{5.1}$$

$$= \frac{\lambda_0}{c_0}\left[n'(\lambda_0) - \frac{1}{2}n'(\lambda_0/2)\right] \tag{5.2}$$

where λ_0 and $\lambda_0/2$ refers to the fundamental and second harmonic wavelengths. $n'(\lambda)$ refers to the chromatic dispersion at a wavelength λ. For $AgGaS_2$, these have been measured at wavelengths of 2.8 μm and 1.4 μm as -7.43 nm^{-1} and -38.6 nm^{-1} respectively [169]. Inserting these values into the above we find the GVM is 112 ps/m, and for a 2 mm long crystal, the corresponding time resolution is 224 fs. Therefore given the length of the crystal, pulses sufficiently longer this value can be resolved.

5.3.2 FROG measurement

With the Er^{3+} fibre laser in a NPR mode-locked state the second harmonic beam at approximately 1400 nm was generated using the setup in Fig. 5.8. This was then coupled into a single-mode silica fibre (smf-28) and then spectrally resolved on an optical spectrum analyser as a function of temporal delay. This results in a spectrogram of the pulses, shown in Fig. 5.9 (a). This spectrogram was then analysed using commercial software (Swamp Optics) to perform an integral inversion algorithm to retrieve the fields (intensity and phase) in both the temporal and spectral domains, Fig. 5.9 (c) and (d) respectively. The retrieved spectrogram is also displayed in Fig. 5.9 (b) which is in good agreement with the measured. The advantage of the FROG measurement is that it can also monitor the accuracy of the retrieval, which typically requires the algorithm error to be less than 5×10^{-3}. In our case the error was 2×10^{-4}, which quantitatively provides evidence for a successful pulse measurement. The retrieved temporal pulse revealed a pulse width of 497 fs, the first sub-picosecond pulse from a mid-IR fibre laser. With an average output power of 206 mW at 56.7 MHz, this gives a peak power calculation of 6.4 kW. This is the first time multiple kW peak powers have been achieved at these wavelengths from a fluoride fibre laser. The FROG measurement also reveals the spectral phase which can be used to

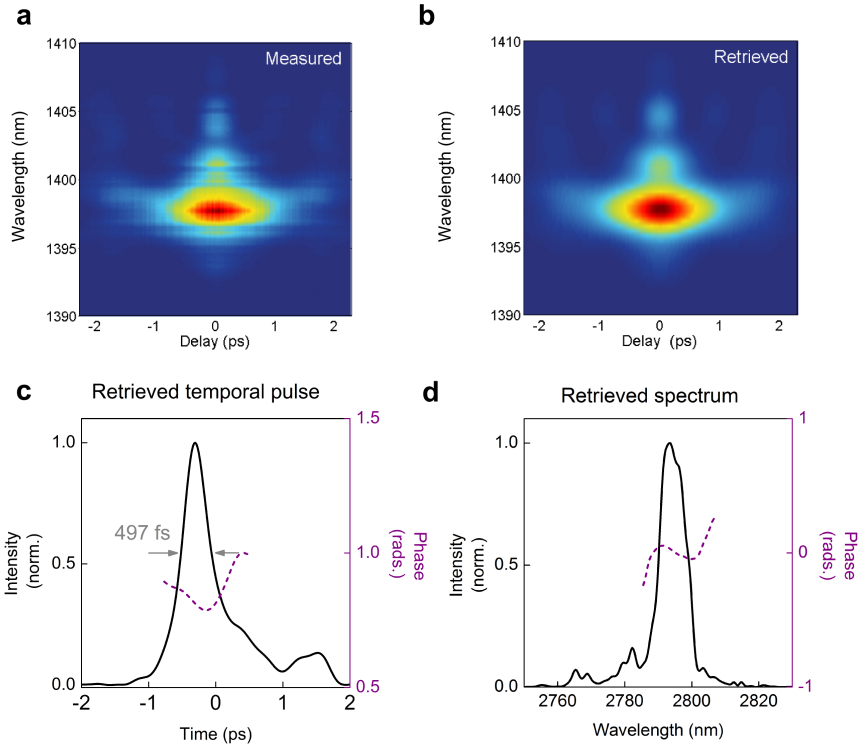

Figure 5.9: Results of the FROG measurement system. (a) Experimentally measured spectrogram, revealing the pulse in temporal (c) and spectral (d) domains. The retrieved pulse width was 497 fs. From the retrieved field, the retrieved spectrogram (b) is calculated and is in good agreement with the measured.

understand the chirp on the pulses. By fitting a polynomial to the spectral phase curve we calculate a relatively low second order chirp of 5.8×10^{-2} ps^2, and a third order chirp of 6.7×10^{-2} ps^3. These values indicate little effects from the anomalous dispersion (as expected for soliton dynamics) whereas the third order chirp is more substantial. This results in the existence of a trailing satellite pulse in Fig. 5.9 (c). We note that the rms spectral bandwidth of the laser was calculated to be 20.1 nm, and this gives a time bandwidth product of 0.4, consistent with the existence of second order dispersion induced chirp from the FROG measurement.

We now compare the retrieved pulse width to what is expected from well-established mode-locked laser theory. The corresponding energy of the pulses based on the average power and the pulse width is 3.62 nJ. As we expect the pulses to be soliton-like (based on the anomalous group velocity dispersion of the fibre) the pulses are expected to follow the soliton area theorem. This states that the energy (E_p) of a pulse with width τ, for a given amount of second order dispersion (β_2 and nonlinearity (γ) is given by,

$$E_p = \frac{2|\beta_2|}{\gamma\tau}$$

The group velocity dispersion of ZBLAN glass from bulk measurements is well known [154], which then can be used to calculate the second order dispersion at 2.9 μm to be a value of 22.9 ps/nm.km [161], which translates to a β_2 of -8.1 $\times$ 10^{-25} s^2/m. Based on the fibre core geometry the mode area is calculated to be 284 μm^2, which gives an value for $\gamma = 1.67 \times 10^{-24}$ Wm^{-1}. Using these values the soliton pulse energy is calcualted to be 3.44 nJ, with a peak power of 6.13 kW, which is in close agreement with the previously calculated values.

5.3.3 Damage threshold of ZBLAN at 2.8 μm

The common belief about fluoride fibres is that they have a low damage threshold that prevents them from operating at high powers. Although this may be true at high average power operation [170], our demonstration shows that high peak power induced damage is not of immediate concern. The peak intensity on the fluoride fibre facet here was at least 3.2 GW/cm^2 (based on the out-coupled power, we expect the in-cavity power to be higher). This is the highest reported peak intensity a fluoride fibre has been exposed to at these wavelengths without suffering damage. The ultrafast multiple kW power performance previous to this study was unclear, with the highest being only 25 MW/cm^2 using 10 ms pulses [101]. Thus fluoride fibres, contrary to problems associated with achieving high average power, have now shown the capability of operating in the ultrafast high peak power regime.

These newly derived parameters in ZBLAN glass at mid-IR wavelengths will allow better designs for improved performance. In particular a greater portion of the erbium bandwidth could be accessed by removing absorptions in the air, which could theoretically support sub-100 fs pulses [161].

5.4 Epilogue - Towards mid-infrared frequency combs

Here we have demonstrated the first femtosecond-level pulses produced from a mid-IR fibre laser. We anticipate that these results will have a strong impact in the future for the generation of frequency combs. As was mentioned in Chapter 1, the output of a mode-locked laser consists of a comb structured spectrum. In order to utilize these combs the two parameters of f_{rep} and f_0 must be stabilised. The repetition rate, f_{rep} (on the order of 100 MHz), can be measured using MCT detectors, which have a bandwidth of several GHz, and allow for constructing a feedback loop for stabilisation. It is more difficult to

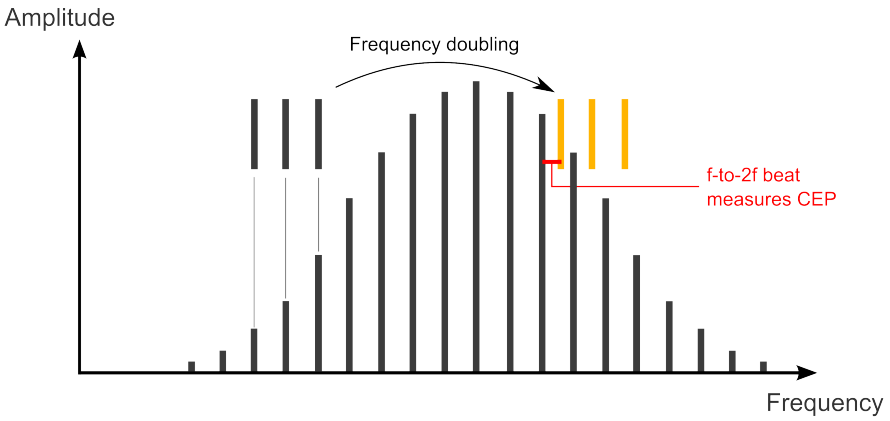

Figure 5.10: Illustration of the f-to-2f measurement to determine the carrier envelope phase. The frequency comb is first broaden more than an octave via a nonlinear process. Once achieving this, the lower frequencies are frequency doubled to match the higher frequency side of the spectrum. The beat note generated between these two can be used to derive the carrier envelope phase, which can later be used as a feedback mechanism to stabilse the comb.

stablise the CEP offset frequency f_0, which can only be measured using interferometric methods from a coherent octave spanning spectrum. The process of how this can be measured is shown in Fig. 5.10. Firstly the comb spectrum needs to be broadened to at least an octave via a nonlinear process, e.g. supercontinuum generation. Following this, the lower end frequencies are then doubled (via SHG), so that it can be interfered with the higher frequencies to measure a beat signal. This beat is related to f_0 which can then be stabilised using feedback mechanisms [80].

Therefore we investigate the feasibility of using the output of the NPR mode-locked laser to generate an octave spanning supercontinuum in a nonlinear medium. There are many highly nonlinear platforms that can allow this. The chalcogenide waveguides have shown immense nonlinearity and transparency in the mid-IR resulting in 1.8 μm to >7.5 μm [42]. Similar results have been achieved using silicon waveguides, revealing a continuum spanning 1.9-4.9 μm [81]. Alternatively, studies using high-NA chalcogenide fibres have reported broad continuum generation as long as 1.4 μm to 13.3 μm [82,171]. Fibre based platforms are appealing as they offer compatibility with our fibre based sources, which potentially could be made into an all-fibre system.

The performance from chalcogenide fibres can be enhanced by tapering, which allows for dispersion engineering and a reduced mode area (and hence larger nonlinearity). This allows low-threshold octave-spanning spectra with short propagation lengths [172]. Using the pulses retrieved from the FROG measurement we simulate the generation of an octave spanning spectrum in a chalcogenide taper.

The geometry of the modelled taper is shown in Fig. 5.11, where the chalcogenide fibre composition was As_2S_3. The tapered region of the fibre is 50 mm long, with a diameter of 2.5 μm (consistent with the standard taper construction methods [173]). From R-SOFT simulations we calculate a dispersion value of +155 ps/(nm.km) and a nonlinear parameter of 0.8 Wm^{-1}. The supercontiunuum is modelled using an adaptive split step Fourier method [174]. In order to calculate the coherence properties of the spectrum, we adopted the definition from Ref. [175] as:

$$|g_{12}^{(1)}(\lambda, t_1 - t_2)| = \left| \frac{\langle E_1^*(\lambda, t_1) E_2(\lambda, t_2) \rangle}{[\langle |E_1(\lambda, t_1)|^2 \rangle \langle |E_2(\lambda, t_2)|^2 \rangle]^{1/2}} \right| \tag{5.3}$$

which provides the first order coherence function as a function of wavelength. The angle brackets signify an ensemble average over separately generated super continuum pairs E_i and E_j. The coherence function was calculated by performing 200 sets of super contiunuum simulations with a 1% amplitude fluctuation. The resulting supercontinuum and its coherence is shown in Fig. 5.11. For our ≈500 fs pulses, the width between the -20 dB points spanned from 1.4 μm to 4.2 μm (1.6 octaves). The coherence of this spectrum is also shown. While the coherence would benefit from shorter pulses, high power, high coherence octave points are already visible (for example, at 1.44 μm and 2.88 μm) with the current performance. In contrast, by moving to a 100 fs pulse, which is able to be supported by gain bandwidth of this transition, the coherence greatly increases. In this way it is possible to envisage a f-to-2f interferometer using the generated supercontinuum, in order to measure the carrier envelope offset frequency.

In this Chapter we have demonstrated 497 fs pulses generated at a wavelength of 2.79 μm, with a peak power of 6.4 kW. This work represents the first near 3 μm fibre laser operating in the femtosecond-level, one of the primary goals of this thesis. On top of this, the pulses were characterised using a FROG measurement, making this the most accurately measured mid-IR pulse generated from a fibre laser. The peak power now compares well with other ultrafast mid-IR sources, such as OPOs and DFGs. Although the fibre lasers do not offer broad tunability like these other sources, their inherent advantages make them a significant pulsed mid-IR source. However the NPR mode-locking method used in this Chapter is but one of a number of methods to achieve ultrafast pulses. Specifically NPR is sensitive to environmental changes (temperature or any strain induced on the fibre) and may not be the best solution for future mode-locked mid-IR fibre lasers. A dispersion controlled cavity using a suitable saturable absorber may be more sufficient, or other techniques such as using nonlinear optical loop mirrors allow and all-fibre format cavity that is free from OH absorption in the air. As I will describe in the conclusion, the next challenge for the near 3 μm fibre lasers is the availability of basic components, such as dispersion compensating fibres, and the ability to splice these components into an all-fibre format. This will open the field of ultrafast mid-IR fibre lasers to the many different types

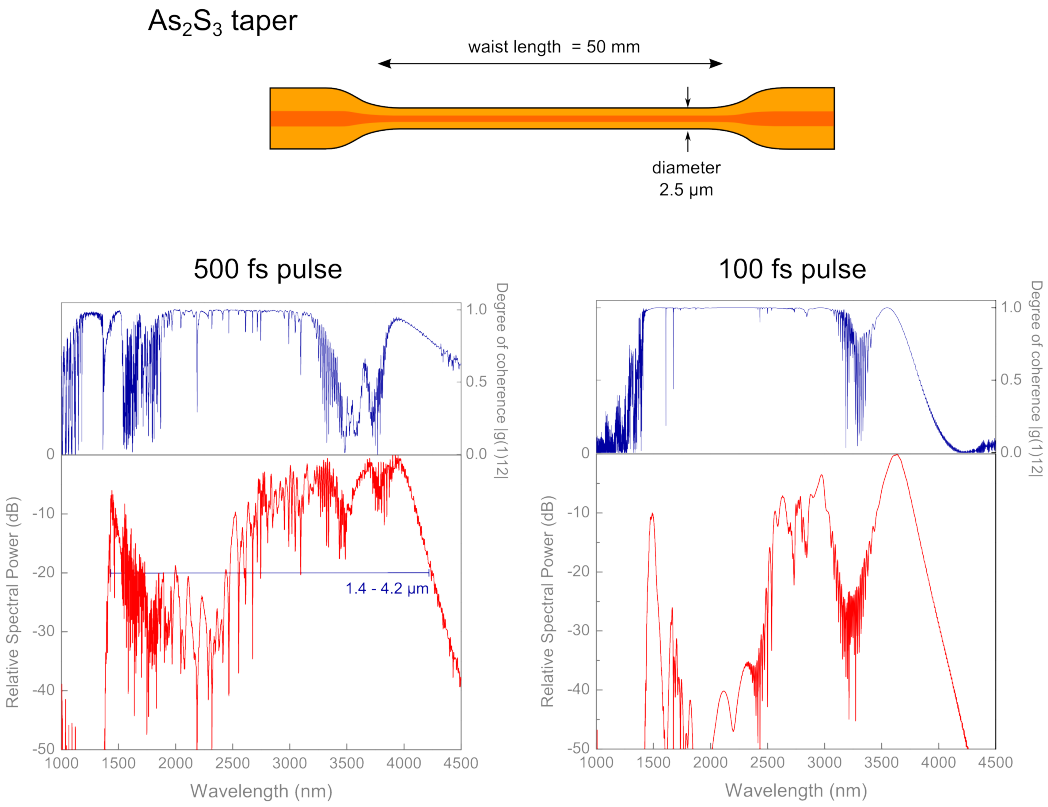

Figure 5.11: Simulated supercontinuum spectra and coherence generated within an As_2S_3 taper using the pulses generated from the mode-locked Er^{3+} laser. For 500 fs pulses a continuuim across 1.4 - 4.2 μm is simulated with relatively high coherence points. Moving to 100 fs siginciantly improves the coherence properties, making it more feasible to perform CEP stabilisation.

that was described in Section 2.3.2 from soliton lasers to all-normal dispersion fibre lasers.

We finally conclude with a completed road map of the progress of pulsed near 3 μm fibre lasers in Fig. 5.12. Many challenges lie ahead in order to achieve applications, such as the generation of a stable frequency comb, but the performances demonstrated in this thesis now put us in the position to begin some serious attempts.

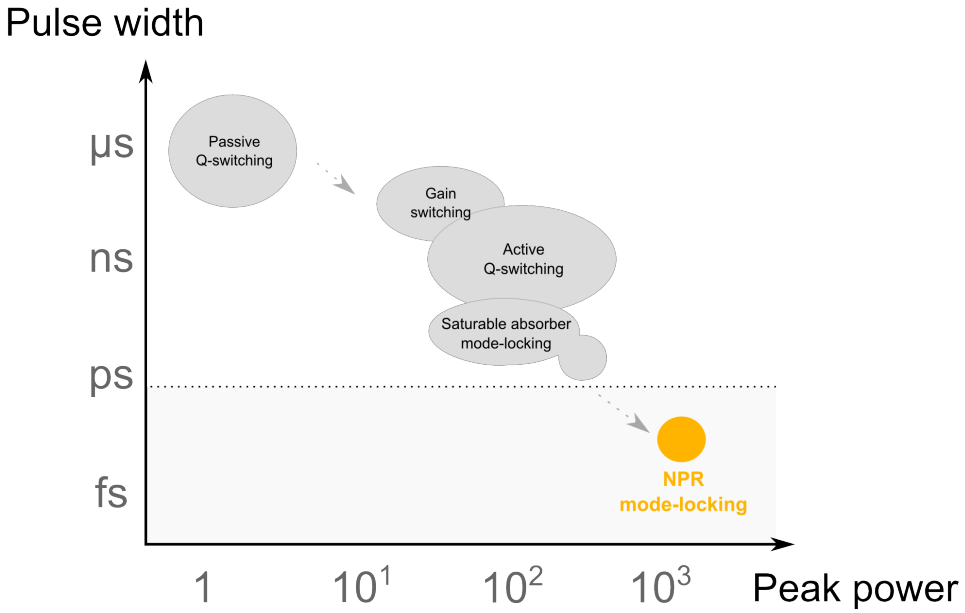

Figure 5.12: Performance progress of near 3 μm fluoride fibre lasers, showing the results of this chapter that broke into the femtosecond regime. The kW-scale peak powers now open applications in nonlinear optics and frequency comb generation for the first time.

Chapter 6

Comments and Outlook

We now arrive at the concluding chapter of this thesis. I will only provide a brief summary of the work presented in this thesis, I shall not repeat myself, but will instead concentrate on where I see this field moving to in the future.

Mid-infrared photonics is a great field which promises many applications spanning from fundamental molecular sciences to the next generation tools of laser surgery. In every technology, a substantial amount of time and research is needed to be invested before it can deliver applications. I see the mid-infrared technologies to be at the end of this many years of basic research, and their applications are just around the corner. For example, detectors in the infrared were at first expensive and required cryogenic cooling. The InSb camera for thermal imaging was at first a military grade technology, but is today commercially available as a hand-held attachment to a mobile phone (for the iPhone 5, costing around $350 AUD). In terms of laser sources, the quantum cascade lasers began as fundamental semiconductor engineering research, and are now deployed on auto-mobiles and satellites for sensing research, such as monitoring greenhouse gases. These applications had been long known, but it was not until 50 years or so of persistent and accurate scientific research in the methods and materials that has brought us here today.

Therefore it would actually be modest to say that the mid-infrared technologies are around the corner, in fact, we are experiencing the surge of their applications today.

As these mid-infrared technologies are deployed the fundamental light sources, and their field-usability, will be important. As mentioned earlier the quantum cascade lasers are a leading technology, however other methods such as parametric devices and solid state lasers will also be a key player. The fibre lasers, that become a globally disruptive technology at the near-infrared wavelengths, were an uncertain technology for the mid-IR as standard fibres did not allow transmission at these wavelengths. With the work

conducted in this thesis it is evident that fluoride (e.g. ZBLAN) fibres have remarkable potential to operate as an ultrafast mid-IR fibre laser. We have explored from Q-switching (nanosecond pulses), to saturable absorber mode-locking (picosecond pulses), and finally to mode-locking based on nonlinear effects (femtosecond pulses) to verify this. In terms of progressing to even shorter pulses the ultimate limit is set by the bandwidth of our gain medium. For the holmium and erbium transitions these are approximately 100 nm wide, which can theoretically support $\approx$ 70 fs pulses. By improving the laser cavity design, as mentioned in Chapter 5, reaching these pulse widths may well be possible.

This being said the next challenge for the fluoride fibre lasers will be engineering these systems. The true benefits of a fibre laser being environmentally stable and alignment free are only accessed when they become *all-fibre* formats. The systems explored in this thesis have encompassed a free space section due to fluoride fibre components not being available. Components such as fibre-based optical couplers/splitters, wavelength division multiplexers, and fibre coupled pump lasers are needed to realise all-fibre systems. The exciting challenge is to build these components using fluoride fibres, borrowing from the knowledge of the well-developed near-infared silica based products. In this way, turn-key mid-infared fibre lasers (continuous wave or pulsed) can be developed not only near 3 μm, but also at longer wavelengths which are still emerging. At the research level, the mode-locked lasers are also expected to spur interest in the field of mid-infrared frequency combs. These lasers have the potential to the be gateway to accessing precision frequency measurements which have profound scientific implications in the formation of chiral molecules, including the origin of biological molecules.

To finish, I would like to step back and see how this fits in the more general scope of physics. Most people forget that the greatest scientific discoveries are the result of being able to generate and measure light more accurately. Microscopes and telescopes have revealed dimensions of the universe we never would have previously imagined. If it were not for accurate spectrometers that revealed discrete atomic spectra, quantum mechanics would not have been developed. If it were not for the Michelson interferometer measuring the speed of light so accurately, Einstein's theory of relativity would not have been confirmed. In terms of light generation, obviously most of the discoveries have been enabled by lasers. These are countless, from the most accurate optical clocks, the modern telecommunication network, to LED displays/lighting and data storage. The work in this thesis is just but one small advance of these lasers in one particular direction, which may one day give rise to more discoveries.

As I first began... *much of our world is enabled by lasers*

...and this will continue to be the case.

well...

...that we all knew.

Oh!

... maybe if ...

hmm... no... forget it.

- End of Thesis -

Bibliography

[1] J. P. Gordon, H. J. Zeiger, and C. H. Townes, "The Maser - New Type of Microwave Amplifier, Frequency Standard, and Spectrometer," *Phys. Rev. Lett.*, vol. 99, no. 4, pp. 1264–1274, 1955.

[2] T. H. Maiman, "Stimulated optical radiation in ruby," *Nature*, vol. 187, pp. 493–494, 1960.

[3] "Daylight Solutions - Quantum Cascade Lasers Technology - http://www.daylightsolutions.com/technology/qcl_technology.htm," 2015.

[4] G. N. Rao and A. Karpf, "Extremely sensitive detection of NO2 employing off-axis integrated cavity output spectroscopy coupled with multiple-line integrated absorption spectroscopy," *Appl. Opt.*, vol. 50, pp. 1915–24, May 2011.

[5] I. Galli, S. Bartalini, S. Borri, P. Cancio, D. Mazzotti, P. De Natale, and G. Giusfredi, "Molecular Gas Sensing Below Parts Per Trillion: Radiocarbon-Dioxide Optical Detection," *Phys. Rev. Lett.*, vol. 107, p. 270802, Dec. 2011.

[6] E. Bergles, "BaySpec White Paper: Telecom's 'Boom and Bust' -Enables Dispersive Raman Instrumentation in the Longer Near-Infrared, 1064 nm and Beyond," tech. rep., 2008.

[7] J. Manne, O. Sukhorukov, W. Jäger, and J. Tulip, "Pulsed quantum cascade laser-based cavity ring-down spectroscopy for ammonia detection in breath," *Appl. Opt.*, vol. 45, no. 36, p. 9230, 2006.

[8] A. B. Seddon, "Mid-infrared (IR) - A hot topic: The potential for using mid-IR light for non-invasive early detection of skin cancer in vivo," *Phys. Status Solidi*, vol. 250, pp. 1020–1027, May 2013.

[9] C. W. Robertson and D. Williams, "Lambert Absorption Coefficients of Water in the Infrared," *J. Opt. Soc. Am.*, vol. 61, p. 1316, Oct. 1971.

[10] D. M. Wieliczka, S. Weng, and M. R. Querry, "Wedge shaped cell for highly absorbent liquids: infrared optical constants of water.," *Appl. Opt.*, vol. 28, pp. 1714–9, May 1989.

[11] R. C. Smith and K. S. Baker, "Optical properties of the clearest natural waters (200-800 nm).," *Appl. Opt.*, vol. 20, pp. 177–84, Jan. 1981.

[12] J.-L. Boulnois, "Photophysical processes in recent medical laser developments: A review," *Lasers Med. Sci.*, vol. 1, pp. 47–66, Jan. 1986.

[13] J. Bertie and Z. Lan, "Infrared Intensities of Liquids XX : The Intensity of the OH Stretching Band of Liquid Water Revisited , and the Best Current Values of the Optical Constants of H20(I) at 25 C between 15 ,000 and 1 cm-1," *Appl. Spectrosc.*, vol. 20, no. 8, pp. 1047–1057, 1996.

[14] S. Ashihara, N. Huse, A. Espagne, E. T. J. Nibbering, and T. Elsaesser, "Ultrafast structural dynamics of water induced by dissipation of vibrational energy.," *J. Phys. Chem. A*, vol. 111, pp. 743–6, Feb. 2007.

[15] M. E. Stokes, X. Ye, M. Shah, K. Mercaldi, M. W. Reynolds, M. F. T. Rupnow, and J. Hammond, "Impact of bleeding-related complications and/or blood product transfusions on hospital costs in inpatient surgical patients.," *BMC Health Serv. Res.*, vol. 11, p. 135, Jan. 2011.

[16] S. Amini-Nik, D. Kraemer, M. L. Cowan, K. Gunaratne, P. Nadesan, B. a. Alman, and R. J. D. Miller, "Ultrafast mid-IR laser scalpel: protein signals of the fundamental limits to minimally invasive surgery.," *PLoS One*, vol. 5, pp. 1–6, Jan. 2010.

[17] G. Motta, E. Esposito, S. Motta, G. Tartaro, and D. Testa, "CO(2) laser surgery in the treatment of glottic cancer.," *Head Neck*, vol. 27, pp. 566–73; discussion 573–4, July 2005.

[18] A. M. Chapas, L. Brightman, S. Sukal, E. Hale, D. Daniel, L. J. Bernstein, and R. G. Geronemus, "Successful treatment of acneiform scarring with CO2 ablative fractional resurfacing.," *Lasers Surg. Med.*, vol. 40, pp. 381–6, Aug. 2008.

[19] A. Böttcher, S. Kucher, R. Knecht, N. Jowett, P. Krötz, R. Reimer, U. Schumacher, S. Anders, A. Münscher, C. V. Dalchow, and R. J. D. Miller, "Reduction of thermocoagulative injury via use of a picosecond infrared laser (PIRL) in laryngeal tissues.," *Eur. Arch. Oto-Rhino-Laryngology*, pp. 1–8, Jan. 2015.

[20] A. H. Zewail, "Femtochemistry: Atomic-Scale Dynamics of the Chemical Bond," *J. Phys. Chem. A*, vol. 104, pp. 5660–5694, June 2000.

[21] C. W. Rudy, "Mid-IR Lasers: Power and pulse capability ramp up for mid-IR lasers - http://www.laserfocusworld.com/articles/print/volume-50/issue-05/features/mid-ir-lasers-power-and-pulse-capability-ramp-up-for-mid-ir-lasers.html," 2014.

[22] I. Vurgaftman, C. L. Canedy, C. S. Kim, M. Kim, W. W. Bewley, J. R. Lindle, J. Abell, and J. R. Meyer, "Mid-infrared interband cascade lasers operating at ambient temperatures," *New J. Phys.*, vol. 11, p. 125015, Dec. 2009.

[23] J. Faist, F. Capasso, D. L. Sivco, C. Sirtori, A. L. Hutchinson, and A. Y. Cho, "Quantum cascade laser," *Science (80-.).*, vol. 264, pp. 553–6, Apr. 1994.

[24] J. Devenson, R. Teissier, O. Cathabard, and a. N. Baranov, "InAsAlSb quantum cascade lasers emitting below 3μm," *Appl. Phys. Lett.*, vol. 90, no. 11, p. 111118, 2007.

[25] O. Cathabard, R. Teissier, J. Devenson, J. C. Moreno, and a. N. Baranov, "Quantum cascade lasers emitting near 2.6μm," *Appl. Phys. Lett.*, vol. 96, no. 14, p. 141110, 2010.

[26] J. Devenson, O. Cathabard, R. Teissier, and a. N. Baranov, "InAsAlSb quantum cascade lasers emitting at 2.75 - 2.97 μm," *Appl. Phys. Lett.*, vol. 91, no. 25, p. 251102, 2007.

[27] S. Kumar, B. S. Williams, Q. Hu, and J. L. Reno, "1.9THz quantum-cascade lasers with one-well injector," *Appl. Phys. Lett.*, vol. 88, no. 12, p. 121123, 2006.

[28] P. Q. Liu, A. J. Hoffman, M. D. Escarra, K. J. Franz, J. B. Khurgin, Y. Dikmelik, X. Wang, J.-Y. Fan, and C. F. Gmachl, "Highly power-efficient quantum cascade lasers," *Nat. Photonics*, vol. 4, pp. 95–98, Jan. 2010.

[29] J. Hu and C. Gmachl, "QCL-based sensors target health and environmental applications," *Laser Focus World*, no. February, pp. 39–43, 2012.

[30] A. Hugi, G. Villares, S. Blaser, H. C. Liu, and J. Faist, "Mid-infrared frequency comb based on a quantum cascade laser.," *Nature*, vol. 492, pp. 229–33, Dec. 2012.

[31] C. Y. Wang, L. Kuznetsova, V. M. Gkortsas, L. Diehl, F. X. Kärtner, M. a. Belkin, a. Belyanin, X. Li, D. Ham, H. Schneider, P. Grant, C. Y. Song, S. Haffouz, Z. R. Wasilewski, H. Liu, and F. Capasso, "Mode-locked pulses from mid-infrared Quantum Cascade Lasers," *Opt. Express*, vol. 17, p. 12929, July 2009.

[32] U. Morgner, F. X. Kärtner, S. H. Cho, Y. Chen, H. a. Haus, J. G. Fujimoto, E. P. Ippen, V. Scheuer, G. Angelow, and T. Tschudi, "Sub-two-cycle pulses from a Kerr-lens mode-locked Ti:sapphire laser," *Opt. Lett.*, vol. 24, p. 411, Mar. 1999.

[33] C. Crosse, "Mid-IR Pulse Generation Using Cr2+:ZnSe - http://www.slideshare.net/ChelseyCrosse/midir-pulse-generation-using-cr2znse," 2013.

[34] G. J. Wagner, T. J. Carrig, R. H. Page, K. I. Schaffers, J.-O. Ndap, X. Ma, and A. Burger, "Continuous-wave broadly tunable Cr2+:ZnSe laser," *Opt. Lett.*, vol. 24, p. 19, Jan. 1999.

[35] E. Sorokin, "Ultrabroad continuous-wave tuning of ceramic Cr:ZnSe and Cr:ZnS lasers," in *Adv. Solid-State Photonics*, p. AMC2, 2010.

[36] M. N. Cizmeciyan, H. Cankaya, A. Kurt, and A. Sennaroglu, "Kerr-lens mode-locked femtosecond Cr(2+):ZnSe laser at 2420 nm.," *Opt. Lett.*, vol. 34, pp. 3056–8, Oct. 2009.

[37] V. Fedorov, S. Mirov, A. Gallian, D. Badikov, M. Frolov, Y. Korostelin, V. Kozlovsky, A. Landman, Y. Podmar'kov, V. Akimov, and A. Voronov, "3.77-5.05 μm tunable solid-state lasers based on Fe2+-doped ZnSe crystals operating at low and room temperatures," *IEEE J. Quantum Electron.*, vol. 42, pp. 907–917, Sept. 2006.

[38] V. Fedorov, D. V. Martyshkin, M. Mirov, I. Moskalev, S. Vasyliev, and S. B. Mirov, "High Energy 4.1-4.6 μm Fe:ZnSe laser," *Conf. Lasers Electro-Optics*, p. CM3D.3, 2012.

[39] J. R. Macdonald, S. J. Beecher, P. a. Berry, K. L. Schepler, and a. K. Kar, "Compact mid-infrared Cr:ZnSe channel waveguide laser," *Appl. Phys. Lett.*, vol. 102, no. 16, p. 161110, 2013.

[40] N. Leindecker, A. Marandi, R. L. Byer, K. L. Vodopyanov, J. Jiang, I. Hartl, M. Fermann, and P. G. Schunemann, "Octave-spanning ultrafast OPO with 2.6-6.1 μm instantaneous bandwidth pumped by femtosecond Tm-fiber laser.," *Opt. Express*, vol. 20, pp. 7046–53, Mar. 2012.

[41] S. Marzenell, R. Beigang, and R. Wallenstein, "Synchronously pumped femtosecond optical parametric oscillator based on AgGaSe2 tunable from 2 μm to 8 μm," *Appl. Phys. B*, vol. 69, pp. 423–428, Apr. 2014.

[42] Y. Yu, X. Gai, P. Ma, D.-Y. Choi, Z. Yang, R. Wang, S. Debbarma, S. J. Madden, and B. Luther-Davies, "A broadband, quasi-continuous, mid-infrared supercontinuum generated in a chalcogenide glass waveguide," *Laser Photon. Rev.*, vol. 8, pp. 792–798, Sept. 2014.

[43] M. Giguère, "Difference frequency generation makes tunable mid-IR lasers possible," *SPIE Newsrooms*, pp. 10–12, Oct. 2013.

[44] K. L. Vodopyanov, J. P. Maffetone, I. Zwieback, and W. Ruderman, "AgGaS2 optical parametric oscillator continuously tunable from 3.9 to 11.3 μm," *Appl. Phys. Lett.*, vol. 75, no. 9, p. 1204, 1999.

[45] S. Chandra, T. H. Allik, G. Catella, R. Utano, and J. A. Hutchinson, "Continuously tunable, 6 - 14 μm silver-gallium selenide optical parametric oscillator pumped at 1.57 μm," *Appl. Phys. Lett.*, vol. 71, no. 5, p. 584, 1997.

[46] K. L. Vodopyanov, O. Levi, P. S. Kuo, T. J. Pinguet, J. S. Harris, M. M. Fejer, B. Gerard, L. Becouarn, and E. Lallier, "Optical parametric oscillation in quasi-phase-matched GaAs," *Opt. Lett.*, vol. 29, no. 16, p. 1912, 2004.

[47] "Fiberoptic Components - http://www.lightguides.com/applications/laser."

[48] "CALMAR Laser - Mendocino - Fiber Based Femtosecond Laser (FPL) http://www.calmarlaser.com/products/fiber_laser/mendocino.php," 2014.

[49] "Corning SMF-28: Optical Fiber Technology Product Information www.corning.com/docs/opticalfiber/pi1463.pdf," 2006.

[50] Y. Jeong, J. K. Sahu, D. N. Payne, and J. Nilsson, "Ytterbium-doped large-core fiber laser with 1.36 kW continuous-wave output power," *Opt. Express*, vol. 12, no. 25, p. 6088, 2004.

[51] D. Ma, Y. Cai, C. Zhou, W. Zong, L. Chen, and Z. Zhang, "37.4 fs pulse generation in an Er:fiber laser at a 225 MHz repetition rate.," *Opt. Lett.*, vol. 35, pp. 2858–60, Sept. 2010.

[52] S. O. Antipov, V. A. Kamynin, O. I. Medvedkov, A. V. Marakulin, L. A. Minashina, A. S. Kurkov, and A. V. Baranikov, "Holmium fibre laser emitting at 2.21 μm," *Quantum Electron.*, vol. 43, pp. 603–604, July 2013.

[53] E. Slobodtchikov, P. F. Moulton, and G. Frith, "Efficient, High-Power, Tm-Doped Silica Fiber Laser," *Adv. Solid-State Photonics*, p. MF2, 2007.

[54] M. Meleshkevich, N. Platonov, D. Gapontsev, A. Drozhzhin, V. Sergeev, and V. Gapontsev, "415W Single-Mode CW Thulium Fiber Laser in all-fiber format," in *2007 Eur. Conf. Lasers Electro-Optics Int. Quantum Electron. Conf.*, pp. 1–1, IEEE, June 2007.

[55] T. Ehrenreich, R. Leveille, I. Majid, K. Tankala, G. Rines, and P. F. Moutlon, "1-kW , All-Glass Tm : fiber Laser," *SPIE Photonics West 2010 LASE, Fiber Lasers VII Technol. Syst. Appl.*, vol. Session 16, no. Late-Breaking News, 2010.

[56] J. S. Sanghera, L. B. Shaw, and L. E. Busse, "Development and Infrared Applications of Chalcogenide Glass Optical Fibers," *Fiber Integr. Opt.*, vol. 19, pp. 251–274, July 2000.

[57] S. Sakuragi, M. Saito, Y. Kubo, K. Imagawa, H. Kotani, T. Morikawa, and J. Shimada, "KRS-5 optical fibers capable of transmitting high-power CO2 laser beam," *Opt. Lett.*, vol. 6, p. 629, Dec. 1981.

[58] I. Paiss, F. Moser, and A. Katzir, "Core-clad silver halide fibres for CO2 laser power transmission," *Opt. Fibers Med.*, vol. 1420, pp. 141–148, July 1991.

[59] A. Hongo, K. Morosawa, K. Matsumoto, T. Shiota, and T. Hashimoto, "Transmission of kilowatt-class CO(2) laser light through dielectric-coated metallic hollow waveguides for material processing.," *Appl. Opt.*, vol. 31, pp. 5114–20, Aug. 1992.

[60] J. Kriesel, N. Gat, B. Bernacki, T. Myers, C. Bledt, and J. Harrington, "Fiber delivery of mid-IR lasers," *SPIE Newsroom*, pp. 10–12, Aug. 2011.

[61] T. Schweizer, B. Samson, R. Moore, D. Hewak, and D. Payne, "Rare-earth doped chalcogenide glass fibre laser," *Electron. Lett.*, vol. 33, no. 5, p. 414, 1997.

[62] A. B. Seddon, Z. Tang, D. Furniss, S. Sujecki, and T. M. Benson, "Progress in rare-earth-doped mid-infrared fiber lasers.," *Opt. Express*, vol. 18, pp. 26704–19, Dec. 2010.

[63] L. Sójka, Z. Tang, H. Zhu, E. Bereś-Pawlik, D. Furniss, A. B. Seddon, T. M. Benson, and S. Sujecki, "Study of mid-infrared laser action in chalcogenide rare earth doped glass with Dy3+, Pr3+and Tb3+," *Opt. Mater. Express*, vol. 2, p. 1632, Oct. 2012.

[64] "Fiberlabs Inc. - http://www.fiberlabs-inc.com/."

[65] D. Szebesta, S. Davey, J. Williams, and M. Moore, "OH absorption in the low loss window of ZBLAN(P) glass fibre," *J. Non. Cryst. Solids*, vol. 161, pp. 18–22, Aug. 1993.

[66] X. Zhu and N. Peyghambarian, "High-Power ZBLAN Glass Fiber Lasers: Review and Prospect," *Adv. Optoelectron.*, vol. 2010, pp. 1–23, 2010.

[67] S. Tokita, M. Murakami, S. Shimizu, M. Hashida, and S. Sakabe, "Liquid-cooled 24 W mid-infrared Er:ZBLAN fiber laser.," *Opt. Lett.*, vol. 34, pp. 3062–4, Oct. 2009.

[68] D. Faucher, M. Bernier, G. Androz, N. Caron, and R. Vallée, "20 W passively cooled single-mode all-fiber laser at 2.8 μm.," *Opt. Lett.*, vol. 36, pp. 1104–6, Apr. 2011.

[69] C. Carbonnier, H. Tobben, and U. Unrau, "Room temperature CW fibre laser at 3.22 μm," *Electron. Lett.*, vol. 34, no. 9, p. 893, 1998.

[70] H. Tobben, "Room temperature cw fibre laser at 3.5 μm in Er3+-doped ZBLAN glass," *Electron. Lett.*, vol. 28, no. 14, p. 1361, 1992.

[71] J. Schneider, C. Carbonnier, and U. B. Unrau, "Characterization of a Ho3+-doped fluoride fiber laser with a 3.9-μm emission wavelength," *Appl. Opt.*, vol. 36, p. 8595, Nov. 1997.

[72] S. D. Jackson, "Towards high-power mid-infrared emission from a fibre laser," *Nat. Photonics*, vol. 6, pp. 423–431, June 2012.

[73] M. Gorjan, R. Petkovšek, M. Marinček, and M. Čopič, "High-power pulsed diode-pumped Er:ZBLAN fiber laser.," *Opt. Lett.*, vol. 36, pp. 1923–5, May 2011.

[74] S. Tokita, M. Murakami, S. Shimizu, M. Hashida, and S. Sakabe, "12 W Q-switched Er:ZBLAN fiber laser at 2.8 μm.," *Opt. Lett.*, vol. 36, pp. 2812–4, Aug. 2011.

[75] C. W. Chou, D. B. Hume, J. C. J. Koelemeij, D. J. Wineland, and T. Rosenband, "Frequency Comparison of Two High-Accuracy Al+ Optical Clocks," *Phys. Rev. Lett.*, vol. 104, p. 070802, Feb. 2010.

[76] A. Schliesser, N. Picqué, and T. W. Hänsch, "Mid-infrared frequency combs," *Nat. Photonics*, vol. 6, pp. 440–449, June 2012.

[77] G. Villares, A. Hugi, S. Blaser, and J. Faist, "Dual-comb spectroscopy based on quantum-cascade-laser frequency combs.," *Nat. Commun.*, vol. 5, p. 5192, Jan. 2014.

[78] C. Stoeffler, A. Shelkovnikov, C. Daussy, A. Amy-klein, and U. M. R. Universite, "Review Article Progress Toward the First Observation of Parity Violation in Chiral Molecules by High-Resolution Laser Spectroscopy," *Chirality*, vol. 220, no. September, pp. 870–884, 2010.

[79] E. Baumann, F. R. Giorgetta, J. W. Nicholson, W. C. Swann, I. Coddington, and N. R. Newbury, "High-performance, vibration-immune, fiber-laser frequency comb," *Opt. Lett.*, vol. 34, p. 638, Feb. 2009.

[80] S. Diddams, D. Jones, J. Ye, S. Cundiff, J. Hall, J. Ranka, R. Windeler, R. Holzwarth, T. Udem, and T. Hänsch, "Direct Link between Microwave and Optical Frequencies with a 300 THz Femtosecond Laser Comb," *Phys. Rev. Lett.*, vol. 84, pp. 5102–5105, May 2000.

[81] D. D. Hudson, N. Singh, Y. Yu, C. Grillet, S. D. Jackson, A. Casas-Bedoya, A. Read, P. Atanackovic, S. G. Duval, S. Palombo, D. J. Moss, B. Luther-Davies, S. J. Madden, and B. J. Eggleton, "Octave spanning mid-IR supercontinuum generation in a silicon-on-sapphire waveguide," *Adv. Photonics*, vol. 1, p. JTu6A.6, 2014.

[82] C. R. Petersen, U. Mø ller, I. Kubat, B. Zhou, S. Dupont, J. Ramsay, T. Benson, S. Sujecki, N. Abdel-Moneim, Z. Tang, D. Furniss, A. Seddon, and O. Bang, "Mid-infrared supercontinuum covering the 1.4 - 13.3 μm molecular fingerprint region using ultra-high NA chalcogenide step-index fibre," *Nat. Photonics*, vol. 8, pp. 830–834, Sept. 2014.

[83] A. W. Snyder and J. D. Love, *Optical waveguide theory.* Chapman & Hall, London, 1996.

[84] R. Paschotta, "RP Photonics - Properties of LP modes http://www.rp-photonics.com/lp_modes.html," 2008.

[85] B. E. A. Saleh and M. C. Teich, *Fundamentals of Photonics.* John Wiley & Sons, Inc., Hoboken, New Jersey, 2 ed., 2007.

[86] K. Ueda, "The absorption characteristics of circular, offset, and rectangular double-clad fibers," *Opt. Commun.*, vol. 132, pp. 511–518, Dec. 1996.

[87] D. Kouznetsov, J. V. Moloney, and E. M. Wright, "Efficiency of pump absorption in double-clad fiber amplifiers. I. Fiber with circular symmetry," *J. Opt. Soc. Am. B*, vol. 18, no. 6, p. 743, 2001.

[88] D. Kouznetsov and J. V. Moloney, "Efficiency of pump absorption in double-clad fiber amplifiers. II. Broken circular symmetry," *J. Opt. Soc. Am. B*, vol. 19, p. 1259, June 2002.

[89] M. J. F. Digonnet, *Rare-Earth-Doped Fiber Lasers and Amplifiers, Revied and Expanded.* CRC Press, 2001, 2001.

[90] G. H. Dieke and H. M. Crosswhite, "The Spectra of the Doubly and Triply Ionized Rare Earths," *Appl. Opt.*, vol. 2, p. 675, July 1963.

[91] R. T. Wegh, A. Meijerink, and R.-J. Lamminmäki, "Extending Dieke's diagram," *J. Lumin.*, vol. 87-89, pp. 1002–1004, May 2000.

[92] M. Saad, "Heavy metal fluoride glass fibers and their applications," in *Proc. SPIE 8307, Passiv. Components Fiber-Based Devices VIII* (B. P. Pal, ed.), vol. 8307, p. 83070N, Nov. 2011.

[93] O. Henderson-sapir, J. Munch, and D. J. Ottaway, "Mid-infrared fiber lasers at and beyond 3.5 μm using dual-wavelength pumping," *Opt. Lett.*, vol. 39, no. 3, pp. 493–496, 2014.

[94] D. Hudson, E. Magi, L. Gomes, and S. Jackson, "1W diode-pumped tunable Ho3+, Pr3+-doped fluoride glass fibre laser," *Electron. Lett.*, vol. 47, no. 17, p. 985, 2011.

[95] T. Sumiyoshi, H. Sekita, T. Arai, S. Sato, M. Ishihara, and M. Kikuchi, "High-power continuous-wave 3- and 2-μm cascade Ho3+:ZBLAN fiber laser and its medical applications," *IEEE J. Sel. Top. Quantum Electron.*, vol. 5, no. 4, pp. 936–943, 1999.

[96] J. Li, L. Gomes, and S. D. Jackson, "Numerical Modeling of Holmium-Doped Fluoride Fiber Lasers," *IEEE J. Quantum Electron.*, vol. 48, pp. 596–607, May 2012.

[97] N. Iwanus, D. D. Hudson, T. Hu, and S. D. Jackson, "Aim at the bottom: directly exciting the lower level of a laser transition for additional functionality.," *Opt. Lett.*, vol. 39, no. 5, pp. 1153–1156, 2014.

[98] S. D. Jackson, "Single-transverse-mode 2.5-W holmium-doped fluoride fiber laser operating at 2.86 μm," *Opt. Lett.*, vol. 29, no. 4, p. 334, 2004.

[99] S. D. Jackson, "High-power and highly efficient diode-cladding-pumped holmium-doped fluoride fiber laser operating at 294 μm," *Opt. Lett.*, vol. 34, p. 2327, July 2009.

[100] J. Li and S. D. Jackson, "Numerical Modeling and Optimization of Diode Pumped Heavily-Erbium-Doped Fluoride Fiber Lasers," *IEEE J. Quantum Electron.*, vol. 48, pp. 454–464, Apr. 2012.

[101] X. Zhu and R. Jain, "10-W-level diode-pumped compact 2.78 μm ZBLAN fiber laser," *Opt. Lett.*, vol. 32, p. 26, Apr. 2007.

[102] L. E. Hargrove, R. L. Fork, and M. a. Pollack, "Locking of He-Ne laser modes induced by synchronous intravacity modulation," *Appl. Phys. Lett.*, vol. 5, no. 1, p. 4, 1964.

[103] J. A. Armstrong, "Measurement of Picosecond Laser Pulse Widths," *Appl. Phys. Lett.*, vol. 10, no. 1, p. 16, 1967.

[104] D. Kuizenga and A. Siegman, "FM and AM mode locking of the homogeneous laser - Part I: Theory," *IEEE J. Quantum Electron.*, vol. 6, pp. 694–708, Nov. 1970.

[105] H. W. Mocker and R. J. Collins, "Mode Competition and Self-Locking Effects in a Q-Switched Ruby Laser," *Appl. Phys. Lett.*, vol. 7, no. 10, p. 270, 1965.

[106] I. S. Ruddock and D. J. Bradley, "Bandwidth-limited subpicosecond pulse generation in mode-locked cw dye lasers," *Appl. Phys. Lett.*, vol. 29, no. 5, p. 296, 1976.

[107] F. Druon, F. Balembois, P. Georges, A. Brun, A. Courjaud, C. Hönninger, F. Salin, A. Aron, F. Mougel, G. Aka, and D. Vivien, "Generation of 90-fs pulses from a mode-locked diode-pumped Yb3+:Ca4GdO(BO3)3 laser," *Opt. Lett.*, vol. 25, p. 423, Mar. 2000.

[108] Y. Zaouter, J. Didierjean, F. Balembois, G. L. Leclin, F. Druon, P. Georges, J. Petit, P. Goldner, and B. Viana, "47-fs diode-pumped Yb3+:CaGdAlO4 laser," *Opt. Lett.*, vol. 31, no. 1, p. 119, 2006.

[109] S. Set, H. Yaguchi, Y. Tanaka, and M. Jablonski, "Laser Mode Locking Using a Saturable Absorber Incorporating Carbon Nanotubes," *J. Light. Technol.*, vol. 22, pp. 51–56, Jan. 2004.

[110] Q. Bao, H. Zhang, Y. Wang, Z. Ni, Y. Yan, Z. X. Shen, K. P. Loh, and D. Y. Tang, "Atomic-Layer Graphene as a Saturable Absorber for Ultrafast Pulsed Lasers," *Adv. Funct. Mater.*, vol. 19, pp. 3077–3083, Oct. 2009.

[111] D. Richardson, R. Laming, D. Payne, V. Matsas, and M. Phillips, "Selfstarting, passively modelocked erbium fibre ring laser based on the amplifying Sagnac switch," *Electron. Lett.*, vol. 27, no. 6, p. 542, 1991.

[112] I. Duling, "Subpicosecond all-fibre erbium laser," *Electron. Lett.*, vol. 27, no. 6, p. 544, 1991.

[113] D. E. Spence, P. N. Kean, and W. Sibbett, "60-fsec pulse generation from a self-mode-locked Ti:sapphire laser," *Opt. Lett.*, vol. 16, p. 42, Jan. 1991.

[114] N. Akhmediev and A. Ankiewicz, *Solitons: Nonlinear pulses and beams.* Chapman & Hall, London, 1997.

[115] N. Akhmediev, J. M. Soto-Crespo, and G. Town, "Pulsating solitons, chaotic solitons, period doubling, and pulse coexistence in mode-locked lasers: Complex Ginzburg-Landau equation approach," *Phys. Rev. E*, vol. 63, p. 056602, Apr. 2001.

[116] F. O. Ilday, J. R. Buckley, W. G. Clark, and F. W. Wise, "Self-Similar Evolution of Parabolic Pulses in a Laser," *Phys. Rev. Lett.*, vol. 92, p. 213902, May 2004.

[117] D. Anderson, M. Desaix, M. Karlsson, M. Lisak, and M. L. Quiroga-Teixeiro, "Wave-breaking-free pulses in nonlinear-optical fibers," *J. Opt. Soc. Am. B*, vol. 10, p. 1185, July 1993.

[118] F. O. Ilday, J. R. Buckley, and F. W. Wise, "Similariton Laser," in *Conf. Lasers Electro-Optics*, no. Figure 2, pp. 1–3, 2003.

[119] J. M. Dudley, C. Finot, D. J. Richardson, and G. Millot, "Self-similarity in ultrafast nonlinear optics," *Nat. Phys.*, vol. 3, pp. 597–603, Sept. 2007.

[120] J. R. Buckley, F. W. Wise, F. O. Ilday, and T. Sosnowski, "Femtosecond fiber lasers with pulse energies above 10 nJ," *Opt. Lett.*, vol. 30, pp. 1888–1890, July 2005.

[121] A. Chong, J. Buckley, W. Renninger, and F. Wise, "All-normal-dispersion femtosecond fiber laser," *Opt. Express*, vol. 14, no. 21, pp. 660–662, 2006.

[122] A. Chong, W. H. Renninger, and F. W. Wise, "All-normal-dispersion femtosecond fiber laser with pulse energy above 20 nJ," *Opt. Lett.*, vol. 32, no. 16, pp. 2408–2410, 2007.

[123] A. Chong, W. H. Renninger, and F. W. Wise, "Properties of normal-dispersion femtosecond fiber lasers," *J. Opt. Soc. Am. B*, vol. 25, no. 2, p. 140, 2008.

[124] R. Trebino, "Short course notes: Introduction to Ultrafast Optics," in *CLEO 2014 - Laser Sci. to Photonic Appl.*, p. 3, 2014.

[125] "Finisar Corporation - 70 GHz balanced photodetector - https://www.finisar.com/optical-components/bpdv3120r-0," *Finisar*, pp. 1–2, 2014.

[126] T. Hirayama and M. Sheik-Bahae, "Real-time chirp diagnostic for ultrashort laser pulses," *Opt. Lett.*, vol. 27, p. 860, May 2002.

[127] R. Trebino, *Frequency-resolved Optical Gating: The measurement of Ultrashort Laser Pulses:*. Springer Science & Business Media, 2000, illustrate ed., 2000.

[128] M. Rhodes, G. Steinmeyer, and R. Trebino, "Standards for ultrashort-laser-pulse-measurement techniques and their consideration for self-referenced spectral interferometry.," *Appl. Opt.*, vol. 53, pp. D1–11, June 2014.

[129] J. Peatross and A. Rundquist, "Temporal decorrelation of short laser pulses," *J. Opt. Soc. Am. B*, vol. 15, p. 216, Jan. 1998.

[130] J.-H. Chung and A. Weiner, "Ambiguity of ultrashort pulse shapes retrieved from the intensity autocorrelation and the power spectrum," *IEEE J. Sel. Top. Quantum Electron.*, vol. 7, no. 4, pp. 656–666, 2001.

[131] D. Kane and R. Trebino, "Characterization of arbitrary femtosecond pulses using frequency-resolved optical gating," *IEEE J. Quantum Electron.*, vol. 29, no. 2, pp. 571–579, 1993.

[132] A. Baltuska, M. Pshenichnikov, and D. Wiersma, "Second-harmonic generation frequency-resolved optical gating in the single-cycle regime," *IEEE J. Quantum Electron.*, vol. 35, pp. 459–478, Apr. 1999.

[133] H. Stark, *Image recovery - theory and application.* University of Michigan: Academic Press, 1987, 1987.

[134] J. Ratner, G. Steinmeyer, T. C. Wong, R. Bartels, and R. Trebino, "Coherent artifact in modern pulse measurements.," *Opt. Lett.*, vol. 37, pp. 2874–6, July 2012.

[135] G. Taft, A. Rundquist, M. Murnane, I. Christov, H. Kapteyn, K. DeLong, D. Fittinghoff, M. Krumbugel, J. Sweetser, and R. Trebino, "Measurement of 10-fs laser pulses," *IEEE J. Sel. Top. Quantum Electron.*, vol. 2, no. 3, pp. 575–585, 1996.

[136] J. Dudley, X. Gu, L. Xu, M. Kimmel, E. Zeek, P. O'Shea, R. Trebino, S. Coen, and R. Windeler, "Cross-correlation frequency resolved optical gating analysis of broadband continuum generation in photonic crystal fiber: simulations and experiments," *Opt. Express*, vol. 10, p. 1215, Oct. 2002.

[137] L. Xu, D. J. Kane, and R. Trebino, "Amplitude ambiguities in second-harmonic-generation frequency-resolved optical gating: comment," *Opt. Lett.*, vol. 34, p. 2602; discussion 2603, Sept. 2009.

[138] T. Hu, D. D. Hudson, and S. D. Jackson, "Actively Q-switched 2.9 μm Ho3+Pr3+-doped fluoride fiber laser," *Opt. Lett.*, vol. 37, no. 11, pp. 2145–2147, 2012.

[139] T. Hu, D. D. Hudson, and S. D. Jackson, "High peak power actively Q-switched Ho3+, Pr3+-co-doped fluoride fibre laser," *Electron. Lett.*, vol. 49, pp. 766–767, June 2013.

[140] F. J. McClung and R. W. Hellwarth, "Giant Optical Pulsations from Ruby," *J. Appl. Phys.*, vol. 33, no. 3, p. 828, 1962.

[141] R. J. Collins and P. Kisliuk, "Control of Population Inversion in Pulsed Optical Masers by Feedback Modulation," *J. Appl. Phys.*, vol. 33, no. 6, p. 2009, 1962.

[142] R. Scheps and J. F. Myers, "Performance of a diode-pumped laser repetitively Q-switched with a mechanical shutter," *Appl. Opt.*, vol. 33, no. 6, pp. 969–978, 1994.

[143] R. Daly and S. D. Sims, "An Improved Method of Mechanical Q-Switching Using Total Internal Reflection," *Appl. Opt.*, vol. 3, p. 1063, Sept. 1964.

[144] C. A. Ebbers and S. P. Velsko, "High average power KTiOPO4 electro-optic Q-switch," *Appl. Phys. Lett.*, vol. 67, no. 5, p. 593, 1995.

[145] H. Bürger, W. Vogel, and V. Kozhukharov, "IR transmission and properties of glasses in the TeO2 -[RnOm, RnXm, Rn(SO4)m, Rn(PO3)m and B2O3] systems," *Infrared Phys.*, vol. 25, pp. 395–409, Feb. 1985.

[146] M. Eichhorn and S. D. Jackson, "High-pulse-energy, actively Q-switched Tm3+,Ho3+-codoped silica 2 μm fiber laser," *Opt. Lett.*, vol. 33, p. 1044, May 2008.

[147] T. Hu, D. D. Hudson, and S. D. Jackson, "Stable, self-starting, passively mode-locked fiber ring laser of the 3 μm class.," *Opt. Lett.*, vol. 39, no. 7, pp. 2133–6, 2014.

[148] J. Li, D. D. Hudson, Y. Liu, and S. D. Jackson, "Efficient 2.87 μm fiber laser passively switched using a semiconductor saturable absorber mirror," *Opt. Lett.*, vol. 37, no. 18, pp. 3747–3749, 2012.

[149] C. Wei, X. Zhu, R. A. Norwood, and N. Peyghambarian, "Passively continuous-wave mode-locked Er(3+)-doped ZBLAN fiber laser at 2.8 μm.," *Opt. Lett.*, vol. 37, pp. 3849–51, Sept. 2012.

[150] A. Haboucha, V. Fortin, M. Bernier, J. Genest, Y. Messaddeq, and R. Vallée, "Fiber Bragg grating stabilization of a passively mode-locked 2.8 μm Er: fluoride glass fiber laser.," *Opt. Lett.*, vol. 39, pp. 3294–7, June 2014.

[151] K. G. Wilcox and A. C. Tropper, "Comment on SESAM-free mode-locked semiconductor disk laser," *Laser Photon. Rev.*, vol. 7, pp. 422–423, May 2013.

[152] B. Braun, K. J. Weingarten, F. X. Kartner, and U. Keller, "Continuous-wave mode-locked solid-state lasers with enhanced spatial hole burning," *Appl. Phys. B Lasers Opt.*, vol. 61, pp. 429–437, Nov. 1995.

[153] J.-C. M. Diels, J. J. Fontaine, I. C. McMichael, and F. Simoni, "Control and measurement of ultrashort pulse shapes (in amplitude and phase) with femtosecond accuracy," *Appl. Opt.*, vol. 24, p. 1270, May 1985.

[154] F. Gan, "Optical properties of fluoride glasses: a review," *J. Non. Cryst. Solids*, vol. 184, pp. 9–20, May 1995.

[155] C. Hönninger, R. Paschotta, F. Morier-Genoud, M. Moser, and U. Keller, "Q-switching stability limits of continuous-wave passive mode locking," *J. Opt. Soc. Am. B*, vol. 16, p. 46, Jan. 1999.

[156] Q. Wang, J. Geng, T. Luo, and S. Jiang, "Mode-locked 2 μm laser with highly thulium-doped silicate fiber.," *Opt. Lett.*, vol. 34, pp. 3616–8, Dec. 2009.

[157] R. C. Sharp, D. E. Spock, N. Pan, and J. Elliot, "190-fs Passively Mode-Locked Thulium Fiber Laser With a Low Threshold," *Opt. Lett.*, vol. 21, p. 881, June 1996.

[158] C. Frerichs and U. B. Unrau, "Passive Q-Switching and Mode-Locking of Erbium-Doped Fluoride Fiber Lasers at 2.7 μm," *Opt. Fiber Technol.*, vol. 2, pp. 358–366, Oct. 1996.

[159] D. E. Spence and W. Sibbett, "Femtosecond pulse generation by a dispersion-compensated, coupled-cavity, mode-locked Ti:sapphire laser," *J. Opt. Soc. Am. B*, vol. 8, p. 2053, Oct. 1991.

[160] F. Qamar and T. King, "Self pulsations and self Q-switching in Ho3+, Pr3+:ZBLAN fibre lasers at 2.87μm," *Appl. Phys. B*, vol. 81, pp. 821–826, Sept. 2005.

[161] D. D. Hudson, "Invited paper: Short pulse generation in mid-IR fiber lasers," *Opt. Fiber Technol.*, vol. 20, pp. 631–641, Dec. 2014.

[162] T. Hu, S. D. Jackson, and D. D. Hudson, "Ultrafast pulses from a mid-infrared fiber laser," *Opt. Lett.*, vol. 40, p. 4226, Sept. 2015.

[163] C. Wei, X. Zhu, R. a. Norwood, K. Kieu, and N. Peyghambarian, "Picosecond passively mode-locked mid-infrared fiber laser," vol. 8601, p. 86011G, Feb. 2013.

[164] S. Tokita, M. Murakami, S. Shimizu, M. Hashida, and S. Sakabe, "Graphene Q-switching of a 3 μm Er : ZBLAN fiber laser," in *Adv. Solid-State Lasers Congr.*, pp. 3–5, 2013.

[165] N. Vukovic, N. Healy, F. H. Suhailin, P. Mehta, T. D. Day, J. V. Badding, and a. C. Peacock, "Ultrafast optical control using the Kerr nonlinearity in hydrogenated amorphous silicon microcylindrical resonators.," *Sci. Rep.*, vol. 3, p. 2885, Jan. 2013.

[166] P. Maker, R. Terhune, and C. Savage, "Intensity-Dependent Changes in the Refractive Index of Liquids," *Phys. Rev. Lett.*, vol. 12, pp. 507–509, May 1964.

[167] R. H. Stolen, J. Botineau, and A. Ashkin, "Intensity discrimination of optical pulses with birefringent fibers," *Opt. Lett.*, vol. 7, p. 512, Oct. 1982.

[168] M. Dennis and I. Duling, "Experimental study of sideband generation in femtosecond fiber lasers," *IEEE J. Quantum Electron.*, vol. 30, pp. 1469–1477, June 1994.

[169] E. Takaoka and K. Kato, "Thermo-optic Dispersion Formula for AgGaS_2," *Appl. Opt.*, vol. 38, p. 4577, July 1999.

[170] N. Caron, M. Bernier, D. Faucher, and R. Vallée, "Understanding the fiber tip thermal runaway present in 3 μm fluoride glass fiber lasers.," *Opt. Express*, vol. 20, pp. 22188–94, Sept. 2012.

[171] U. Mø ller, Y. Yu, I. Kubat, C. R. Petersen, X. Gai, L. Brilland, D. Méchin, C. Caillaud, J. Troles, B. Luther-Davies, and O. Bang, "Multi-milliwatt mid-infrared supercontinuum generation in a suspended core chalcogenide fiber," *Opt. Express*, vol. 23, p. 3282, Feb. 2015.

[172] D. D. Hudson, S. A. Dekker, E. C. Mägi, A. C. Judge, S. D. Jackson, E. Li, J. S. Sanghera, L. B. Shaw, I. D. Aggarwal, and B. J. Eggleton, "Octave spanning supercontinuum in an As2S2 taper using ultralow pump pulse energy.," *Opt. Lett.*, vol. 36, pp. 1122–4, Apr. 2011.

[173] D. D. Hudson, E. C. Mägi, A. C. Judge, S. a. Dekker, and B. J. Eggleton, "Highly nonlinear chalcogenide glass micro/nanofiber devices: Design, theory, and octave-spanning spectral generation," *Opt. Commun.*, vol. 285, pp. 4660–4669, Oct. 2012.

[174] O. Sinkin, R. Holzlohner, J. Zweck, and C. Menyuk, "Optimization of the split-step fourier method in modeling optical-fiber communications systems," *J. Light. Technol.*, vol. 21, pp. 61–68, Jan. 2003.

[175] J. M. Dudley and S. Coen, "Coherence properties of supercontinuum spectra generated in photonic crystal and tapered optical fibers," *Opt. Lett.*, vol. 27, p. 1180, July 2002.